Turbulence Parameterisation in Hydrobiological Models for Natural Waters

Vom Fachbereich Mechanik
der Technischen Universität Darmstadt
zur Erlangung des akademischen Grades eines
Doktors der Ingenieurwissenschaften
genehmigte Dissertation

von

Dipl.-Ing. Lars Umlauf
aus Rüsselsheim

Referent: Prof. K. Hutter, Ph.D./Cornell Univ.
Korreferent: Prof. M. Oberlack
Tag der Einreichung: 18. April 2001
Tag der mündlichen Prüfung: 4. Juli 2001

Darmstadt, 2001
Darmstädter Dissertationen D 17

Herstellung: Books on Demand Schweiz GmbH
ISBN: 3-8311-2627-0

Adresse:

Lars Umlauf
Laboratoire des Recheres Hydrauliques
Dept. de Génie Civil
Ecole Polytechnique de Lausanne
CH-1015 Lausanne

Zusammenfassung

In dieser Arbeit werden verschiedene Turbulenzmodelle auf ihre Anwendbarkeit in ozeanographischen und limnologischen Problemen untersucht. Der Schwerpunkt liegt dabei auf Zweigleichungsmodellen für rotierende, dichtegeschichtete Strömungen. Nach einer kurzen Einführung in Kapitel 1 werden in Kapitel 2 die Transportgleichungen für die turbulenten Flüsse von Impuls, Wärme und der Varianz der Temperaturfluktuationen in rotierenden, dichtegeschichteten Flüssigkeiten hergeleitet. Zur Schließung dieser Gleichungen werden mehrere Parametrisierungen für die Druck-Streckungs-Korrelation und die Druck-Temperaturgradienten-Korrelation vorgestellt. Die geschlossenen Transportgleichungen werden anschließend algebraisiert und in der sogenannten Grenzschichtapproximation angeschrieben. In dieser Approximation lassen sich die essentiellen Eigenschaften der Turbulenzmodelle in Form sogenannter Stabilitätsfunktionen darstellen. Das Kapitel schließt mit der Präsentation einiger aus der Literatur bekannter oder neu hergeleiteter Stabilitätsfunktionen.

In Kapitel 3 werden zunächst kurz die Eigenschaften von integrierten und differentiellen Turbulenzmodellen für geophysikalische Anwendungen verglichen. Verschiedene Zweigleichungsmodelle (insbesondere das k-ϵ Modell, das k-ω Modell von Wilcox [293, 294] und das Modell von Mellor und Yamada [169]) werden anschließend formuliert und in einigen Standardsituationen vergleichend getestet. Die Tests umfassen folgende Spezialfälle: Das logarithmische Wandgesetz, das Abklingen homogener Turbulenz, homogen geschichtete und gescherte homogene Turbulenz im *vollen Gleichgewicht* und im *strukturellen Gleichgewicht* und das Gleichgewicht zwischen turbulentem Transport von turbulenter kinetischer Energie und ihrer Dissipationsrate. Folgende Resultate werden vorgestellt:

1. Erstmalig wird ein für dichtegeschichtete, rotierende Strömungen erweitertes k-ω Modell vorgestellt.

2. Für das strukturelle Gleichgewicht werden die Stabilitätsfunktionen erstmalig als Funktionen der Richardsonzahl allein dargestellt. Entsprechende Ausdrücke für die turbulente Prandtlzahl und die Verhältnisse verschiedener turbulenter Längenskalen werden abgeleitet. Obwohl die untersuchten Zweigleichungsmodelle im strukturellen Gleichgewicht isomorph sind, reagieren sie sensibel in Bezug auf unterschiedliche Werte der Modellparameter. Die besten Ergebnisse werden mit dem k-ω Modell erzielt.

3. Analytische Lösungen (in Übereinstimmung mit numerischen Berechnungen) für die betrachteten Zweigleichungsmodelle im Gleichgewicht von turbulentem Transport turbulenter kinetischer Energie und ihrer Dissipationsrate werden vorgestellt. Es wird gezeigt, daß das k-ϵ Modell für verschiedene physikalisch sinnvolle Parameterkonstellationen eine Singularität aufweist und daß das Modell von Mellor und Yamada [169] nur ohne seine obligatorische Wandfunktion im Einklang mit den Messungen steht. Lediglich das k-ω Modell berechnet das experimentell gegebene Abklingverhalten in allen Situationen zufriedenstellend.

Kapitel 4 beschäftigt sich mit Anwendungen verschiedener Zweigleichungsmodelle im Bereich der Limnologie und Ozeanographie. Hauptergebnisse sind die folgenden:

1. Die Mischungstiefe und damit die Temperatur der Mischungsschicht in Scherströmungen werden durch die stationäre Richardsonzahl der Modelle bestimmt. Diese durch Modellparameter justierbare Grösse ist damit entscheidend für biologische Modellkomponenten, die in der Regel sehr sensibel auf Temperaturunterschiede reagieren.

2. Die durch interne Schwingungen induzierte turbulente Bodengrenzschicht im Alpnacher See (Schweiz) konnte in Übereinstimmung mit allen wesentlichen Messergebnissen modelliert werden. Lediglich die Phasenverschiebung zwischen der turbulenten Dissipationsrate und der Stromscherung wurde von den Modellen unterschätzt. Dieser Teil der Arbeit entstammt einer Zusammenarbeit mit der schweizerischen EAWAG und stellt den ersten Vergleich von kontinuierlichen Messungen turbulenter Grössen und ihrer Modellierung in einer solchen Grenzschicht dar.

3. Mit einem gekoppelten Sauerstoff-Turbulenz Modell konnten gemessene Sauerstoffprofile im Ammersee zufriedenstellend nachgebildet werden.

In Kapitel 5 wird das numerische Finite-Volumen Verfahren vorgestellt. Die Eigenschaften einer neuen Diskretisierungstechnik für die Randvolumina werden diskutiert. Dieses Kapitel schließt mit einigen numerischen Tests bezüglich der Robustheit von Zweigleichungsmodellen. Im Gegensatz zu traditionellen Computerprogrammen zur Berechnung turbulenter Strömungen, beruht die in Kapitel 6 vorgestellte Programmarchitektur auf einer objektorientierten Technik. Es wird erstmalig gezeigt, wie sich Turbulenzmodelle im abstrakten Vokabular einer objektorientierten Sprache ausdrücken lassen, die an Klarheit, Zuverlässigkeit und Erweiterbarkeit strukturellen Sprachen überlegen ist.

Abstract

In this thesis different turbulence models are tested with respect to their applicability to oceanographical and limnological problems. Two-equation models for rotating stratified flows are emphasized.

After a short introduction in Chapter 1, the transport equations for the turbulent fluxes of momentum, heat and the variance of the temperature fluctuations are derived in Chapter 2. Several closure models for the pressure-strain correlation and the pressure-temperature-gradient correlation are introduced. After their algebraization, the closed transport equations are presented in the so-called boundary layer approximation. With this approximation it is possible to describe the essential features of turbulence models in terms of so-called stability functions. The chapter closes with the presentation of some stability functions, new or already known in the literature.

In Chapter 3 the relative merits of integrated and differential turbulence models for geophysical applications are briefly discussed. Then, different two-equation models (in particular the k-ϵ model, the k-ω model of Wilcox [293, 294] and the model of Mellor and Yamada [169]) are formulated and compared in some standard situations. Considered are: The logarithmic law-of-the-wall, the decay of homogeneous turbulence, homogeneously stratified and sheared homogeneous turbulence in *full equilibrium* and in *structural equilibrium*, and the balance between turbulent transport of turbulent kinetic energy and its rate of dissipation. The following results are presented:

1. For the first time, a k-ω model extended to rotating stratified flows is introduced.

2. Stability functions for the *structural equilibrium*, depending *only* on the Richardson number, are introduced. Analogous expressions for the turbulent Prandtl number and for the ratios of different length-scales are derived. Even though the two-equation models investigated are isomorphic in structural equilibrium, they are sensible with respect to different values of the model parameters. The best results are achieved with the k-ω model.

3. Analytical solutions (in agreement with numerical computations) of two-equation models for the balance between turbulent transport of turbulent kinetic energy and its dissipation are derived. It is demonstrated that the k-ϵ model exhibits a singularity for physically reasonable parameters and that the model of Mellor and

YAMADA [169] is in accordance with the measurements only without its compulsory wall function. Only the k-ω model reproduces the experimental decay satisfactorily in all situations.

Chapter 4 is concerned with applications of two-equation models to problems in limnology and oceanography. The main results are as follows:

1. The mixed layer depth and hence the temperature of the mixed layer in shear-driven entrainment situations is determined by the steady-state Richardson number, an intrinsic property of the models. This quantity, which can be adjusted by parameter calibration, is thus crucial for biological sub-models generally being very sensible with respect to temperature differences.

2. The turbulent bottom boundary layer in Lake Alpnach (Switzerland), induced by internal oscillations, could be modelled in agreement with all significant measurements. However, the phase-lag between the rate of dissipation and the current shear was underestimated by all models. This part of the work was based on a cooperation with the EAWAG (Switzerland) and includes the first reported comparison of continuous turbulence measurements and models in such a boundary layer.

3. A coupled oxygen-turbulence model is suggested that reproduces the measured oxygen profiles in Lake Ammer (Germany) adequately.

In Chapter 5 the numerical Finite-Volume method is introduced. The properties of a new discretization of the boundary volumes are discussed. This chapter closes with some tests of the numerical robustness of two-equation models.

In contrast to traditional program codes for the computation of turbulent flows, the program architecture suggested in Chapter 6 is based on an object-oriented technique. It is illustrated how turbulence models can be expressed by the abstract vocabulary of an object-oriented language, superior in terms of clarity, reliability, and extendibility compared to structural languages.

Acknowledgements

During the creation of this thesis I enjoyed a lot of advice, help, encouragement, and many other nice things from my colleagues, my friends and my family. Without them, I would not have enjoyed my time at our group in Darmstadt as much as I did. This is a good opportunity to say a little "danke schön" to all of them.

In the first place, I want to express my thanks to Prof. K. Hutter, the "father" of this dissertation, who also provided the necessary financial support making my work at all possible. I appreciated very much his comments and hints to parts of the manuscript and the numerous helpful and clarifying discussions with him. Without the great freedom he gave to me in all respects, my work would have been much less satisfying for me than it was.

I want to thank also Prof. M. Oberlack, for his careful examination of my dissertation as a co-referee, for his interest in my work, and for a number of discussions that gave me new insight in some of my results from a different angle of view.

I'm also very grateful to Klaus Jöhnk from Konstanz, a former member of our group, who partly supervised my work, guided my first steps, and with whom I had many fruitful discussions about water quality modelling in lakes. He taught me most I know about the coupling of physical and biological models in aquatic systems.

A very special thank I want to express to Hans Burchard from Hamburg, from whom I learned a lot about turbulence modelling and the modelling community. His helpful, cooperative and uncomplicated way made working with him always a pleasure. I'm very much looking forward to our future projects, parts of which have already started.

Thanks to Alfred Wüest and Andreas Lorke from the EAWAG, Switzerland, for many thrilling conversations about lakes and other things at the numerous workshops we met. I'm indebted to them for generously making their recently measured data in Lake Alpnach available to me. This fact gave birth to a new section of this thesis, enriching it considerably.

Thanks go also to Erich Bäuerle from Konstanz for trying to explain me the secrets of internal oscillations in lakes, for unforgettable hard-core hikes (including philosophical pitfalls) at the Lake Baikal Conference, for enlightening conversations about the abysses

of science, and simply for being the example of an unconventional scientist.

I want to express a big "thank you" also to the members of our group at the Mechanics Department in Darmstadt, who all together created a great atmosphere that I will miss a lot (along with the legendary international cake palette at our tea hours). There is a number people in this group I want to mention explicitly. Here is an extra "thanks" to

> Magnus Weis for being a very likeable office neighbour, who spent more than once his spare time to save my life in solving unsolvable computer problems. Who else could have answered questions like: "If you have a virtual multiple inheritance template base class iterator pointing to a static obscure class member, which is also an iterator ... yeah, what then?" My humble reverence to the Master of Computer-Universe!
>
> Yongqui Wang for our joint work with the three-dimensional lake model, in which he was always a perfectly cooperative and reliable colleague.
>
> Joachim Weis for many interesting discussions about turbulence modelling and other strange topics, for giving helpful comments to parts of the manuscript, and for not getting upset when I *again* grabbed interestingly looking books from his desk. ("Lars, do you have the Wilcox book again?!")
>
> Sergio Faria for the cordial atmosphere in our office, for bearing the misery of my sticky and spinose plants next to his writing desk, for supplying me with the most incredible authentic Brasilian jokes (all levels of taste), and for saving my family life with remarks like "Go home now. You should really go home now!"

I thank the most loving creatures in my life, my wife Susanne and my little daughter Mira, who missed me at many evenings and weekends, for their love, patience, and encouragement. Their steady support was crucial for the completion of my work. Also thank you to Marion and Markus, who share our apartment and are part of the "family", for suffering patiently under my neglected domestic duties during the last months of writing. I hereby promise to clean the whole flat twice, as soon as I'm finished.

Darmstadt, July 2001 Lars Umlauf

Contents

Chapter 1

Introduction

> *He looked into the water and saw that it was made up of a thousand thousand thousand and one different currents, each one a different colour, weaving in and out of one another like a liquid tapestry of breathtaking complexity; and Iff explained that these were the Streams of Story, that each coloured strand represented and contained a single tale. (...) And because the stories were held here in fluid form, they retained the ability to change, to become new versions of themselves, to join up with other stories and so become yet other stories; so that unlike a library of books, the Ocean of the Streams of Story was much more than a storeroom of yarns. It was not dead but alive.*
>
> *from: Salman Rushdie, "Haroun and the Sea of Stories"*

On March, 22nd 2000, the UNESCO announced the "world day for water". In an excellent documentation of this event[1], the UNESCO had to state that "it is already clear that in the first half of the 21st century water issues will be the most important, even among other global problems facing humankind such as adequate food and power production". It is evident that this problem, its roots being mainly political and educational grievances, will not be solved with engineering tools alone. Nevertheless, the prediction of the distribution and quality of water is vital for the correct political decision making in order to satisfy the pressing needs for the "blue gold" in many regions. This fact is the link to the present study, which addresses the aspects of water motion and water quality in natural waters.

Hydrobiological models, suited for the prediction of water quality, have to take into account numerous interactions between biogeochemical and physical factors. In some cases, biological parameters may have an important influence on physical quantities, either di-

[1] see the internet location `http://www.unesco.org/science/waterday2000/`

rectly (as, e.g., in the case of bio-convection) or indirectly (e.g., in stabilizing the water column by enhanced light absorption of algae). However, since biogeochemical variables behave in most cases like passive tracers, many processes are dominated by the hydrodynamical properties of the system. It is in particular the effect of turbulence, described so beautifully by Salman Rushdie with the metaphor of a "liquid tapestry of breathtaking complexity", that makes the prediction of water quality such a puzzling problem. Since turbulence directly affects the environment perceived by particles, including biota, detritus and suspended sediment, in many cases the understanding of biological processes presumes the understanding of turbulence[2]. For this reason, the major part of this study is devoted to the problem of turbulence modelling in natural waters.

The cornerstones for modern second-order turbulence models, as those discussed in the following chapters, were set more than half a century ago. Nevertheless, their properties in buoyancy affected, rotating flows are still not completely understood. Even though today one can dare to say, that these models did not fulfil their promise for a "general" description of all turbulent flows (and probably never will), particularly in stably stratified flows, a number of encouraging results were obtained during the last decade. Above all, the question, to which situations of geophysical interest the simple and yet powerful so-called Algebraic Stress Models can faithfully be applied, could be answered to some extent, and this work will be in line with such earlier attempts to answer this question completely.

Due to the effect of gravity, both, physical and biological parameters are structured predominantly in the vertical direction, and valuable insight can be gained with one-dimensional models, and inspired by this idea only such models are considered here (apart from a few exceptions). One-dimensional models may be regarded solely as test versions for the implementation of turbulence schemes and water quality modules in existing three-dimensional circulation models. They can, however, also be considered as a self-contained class of models, resulting from the horizontal integration of transport equations in a closed basin. Both points of view will be adopted in the following, depending on their suitability to a particular situation.

Even though the largest part of this dissertation is devoted to turbulence and its description, biological parameterizations are also treated in detail. A whole section is concerned with the interaction of a complex Algebraic Closure Model of turbulence with a biogeochemical model of the oxygen budget in a lake. Also addressed in great detail is the structure of the turbulent boundary layers at the surface and the bottom of natural wa-

[2]Also in oceanography, recent research projects focus on these interactions (see e.g. the European Community's joint project "PROVESS", `http://www.pol.ac.uk/provess/`).

ters, which is perceived as the "skin" of the water body, through which all exchange of physical and chemical properties takes place.

One may object, that many physical processes in natural waters cannot be adequately described by one-dimensional water-column models. In fact, a few Algebraic Stress Models have been successfully implemented in existing three-dimensional circulation models of lakes, some of them also including biological compartments. Soon, however, it became apparent that atmospheric parameters, like the wind field over the lake, exert an influence on the results that dominates the differences induced by different turbulence models by far. As long as the wind field cannot be reasonably well resolved, one should not expect much more information from a three-dimensional model than the correct prediction of the principal internal and external wave modes. At present, it seems that neither the spectrum of these internal waves nor their combined effect on the nutrient paths in the water body can be predicted with any accuracy by such models.

Thus, even though a three-dimensional model was available, in this study only simple, but fundamental, situations were emphasized, in which a one-dimensional representation of both, physical and biological processes, could be faithfully applied. The good agreement with laboratory and field measurements were an encouraging result and a little step forward towards the development of a general water quality model of lakes and reservoirs.

Chapter 2

Turbulence Models

Turbulence is ubiquitous in geophysical flows. There are hardly any situations in the dynamics of natural waters and the atmosphere that do not involve turbulent effects at some point, and only little insight can be gained in the dominant processes, if turbulence is not taken into account. Thus, the modelling of this phenomenon has attracted a great many researchers and more and more advanced models, suitable to the description of a large variety of geophysical flows, evolved over the last decades.

The beauty of turbulence (Fig. 2.1), however, is alloyed with its outstanding complexity. A general model embracing all aspects of turbulence is still out of reach. Nevertheless, there has been an enormous progress in the understanding of turbulence in the past. Particularly, the availability of powerful computers made it possible to apply and extend the theories developed in the first half of the 20th century. More recently, Direct Numerical Simulations (DNS) and Large Eddy Simulations (LES) provided data that were up to then only available by high-precision laboratory setups (or not at all) and had a large impact on the development of new turbulence models. It seems likely that, especially in oceanography and meteorology, LES will take a position equitable to the ensemble averaged methods in the near future. At present, however, LES is too expensive for standard simulations of geophysical interest. Therefore, the models used in this work are based on the Reynolds Averaged Navier-Stokes Equations (RANS) and closures for the single-point correlations of different order. The most advanced models of this type (see, e.g., Canuto et al. [38]) have been shown to reproduce many of the features observed in sheared, buoyancy affected or convective turbulent flows. In this chapter a rational derivation of the governing equations will be presented and some ideas developed in the last years will be shortly discussed. Also, the simplifications leading to advanced Algebraic

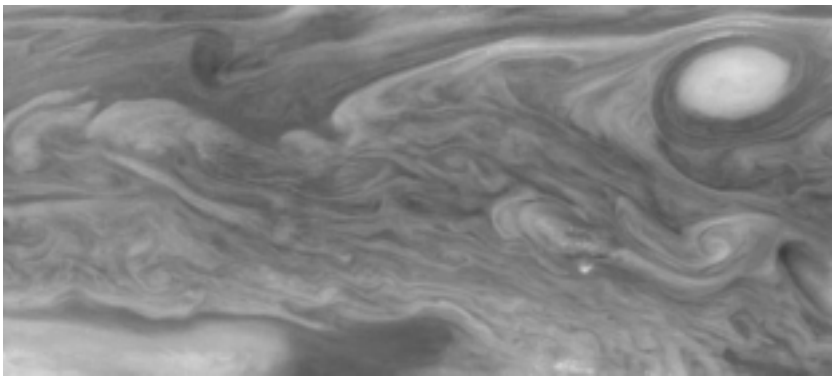

Figure 2.1: Atmospheric turbulence in Jupiter's equatorial region. Image taken on December 17, 1996, at a range of 1.5 million kilometres by the Galileo probe. (Source: NASA's Jet Propulsion Laboratory.)

Stress Models (ASMs) will be motivated. Finally, the concept of stability functions used throughout this work will be established. The chapter closes with the introduction of some recently suggested stability functions.

2.1 Reynolds Averaged Navier-Stokes Equations in the Boussinesq Approximation

For a variable $\tilde{\Phi}$ it is assumed that there exists a well-defined ensemble averaged mean value. A Reynolds decomposition into a mean value, Φ, and a fluctuating part, Φ', is assumed to have the properties

$$\tilde{\Phi} = \Phi + \Phi' \,, \quad \langle\tilde{\Phi}\rangle = \Phi \quad \text{and} \quad \langle\Phi'\rangle = 0 \,, \tag{2.1}$$

where $\langle(\cdot)\rangle$ denotes the averaging procedure.

The presence of different wave phenomena is frequently observed in geophysical situations. Fluctuations in statistical quantities caused by a random wave field and by turbulence are often hard to discern. However, statistical properties scale in fundamentally different ways, depending whether waves or turbulence dominate and turbulence closures seldom account for this fact. Moreover, it is well-known that waves can extract energy from the mean flow or from turbulence at one point and dissipate it (again via turbulence) at other points. This property is in serious contradiction to the assumption of locality used at times below. It should be noted that extended decompositions of the flow into a mean

part, an oscillating part due to waves, and a part attributed to turbulent fluctuations in analogy to (2.1) have been suggested (HUSSAIN AND REYNOLDS [112, 113]). EINAUDI AND FINNIGAN [67] applied such a decomposition to the atmospheric turbulent boundary layer. They concluded that the coupling of turbulence and stratospheric internal waves is an important factor. But they also pointed out, that for a reasonable decomposition of the flow field very regular and long-lasting records are necessary that were only available to them in a special situation.

Here, the classical Reynolds decomposition is used throughout and waves can be thought as being absorbed in the fluctuating parts. This idea expresses the hope that the turbulent closures include, at least partly, an appropriate model for the wave effects. In situations in which this is not the case, an additional wave parameterization must be sought for.

The decomposition (2.1) is inserted in the standard statements of the balances of mass, momentum, heat, and a passive tracer for a linearly viscous heat conducting fluid and the equations are then averaged. The Boussinesq assumption is invoked, i.e. the density, ρ, is assumed to be a constant, ρ_0, except in the buoyancy term. This assumption reduces the averaged local balance of mass to[1]

$$\frac{\partial u_i}{\partial x_i} = 0 \,, \tag{2.2}$$

u_i being the components of the mean velocity vector in a Cartesian system. The Reynolds Averaged Navier-Stokes Equations on the rotating Earth become (in the Boussinesq approximation)

$$\frac{\partial u_i}{\partial t} + u_l \frac{\partial u_i}{\partial x_l} + f_{il} u_l = -\frac{1}{\rho_0}\frac{\partial p}{\partial x_i} + \frac{\partial}{\partial x_l}\left(\nu \frac{\partial u_i}{\partial x_l} - \langle u_i' u_l' \rangle\right) - \frac{\rho}{\rho_0} g \delta_{i3} \,, \tag{2.3}$$

where p is the mean pressure, ν the kinematic viscosity, g the gravity acceleration of the Earth, and δ_{ij} the Kronecker symbol. The matrix of the Coriolis parameters f_{ij} introduced in (2.3) is defined as

$$f_{ij} = \begin{pmatrix} 0 & -f & \tilde{f} \\ f & 0 & 0 \\ -\tilde{f} & 0 & 0 \end{pmatrix} \quad . \tag{2.4}$$

The components are defined as $f = 2\Omega \sin\phi$ and $\tilde{f} = 2\Omega \cos\phi$, where Ω stands for the magnitude of the angular velocity of the Earth and ϕ for the angle of latitude.

[1] Cartesian tensor notation is used and Einstein's summation convention is applied over repeated indices.

The averaged energy balance becomes

$$\frac{\partial \theta}{\partial t} + u_l \frac{\partial \theta}{\partial x_l} = \frac{\partial}{\partial x_l}\left(\frac{\lambda}{\rho_0 c_v}\frac{\partial \theta}{\partial x_l} - \langle \theta' u_l' \rangle\right) + \frac{1}{c_v}\mathcal{R} \ , \tag{2.5}$$

where θ is the temperature, λ the molecular conductivity of water and $\mathcal{R}$ a radiative heat production term. In the derivation of (2.5) the production of heat by dissipation has been neglected and the specific heat, c_v, was assumed to be a constant.

An equation of state of the form

$$\rho = \hat{\rho}(\theta, s, p) \tag{2.6}$$

must be supplied. However, the dependence on salinity, s, and pressure, p, was found to be very small and a pure dependence on the temperature, θ, as suggested by Chen and Millero [43] suitable for relatively shallow waters was implemented instead.

Completely analogously to (2.5), an equation for the transport of a passive tracer, c, can be derived:

$$\frac{\partial c}{\partial t} + u_l \frac{\partial c}{\partial x_l} = \frac{\partial}{\partial x_l}\left(D_c \frac{\partial c}{\partial x_l} - \langle c' u_l' \rangle\right) + \frac{1}{\rho_0}\mathcal{S} \ , \tag{2.7}$$

where D_c is the molecular diffusivity of the tracer, c, and $\mathcal{S}$ a general source term.

2.2 Transport of Turbulent Quantities

The Reynolds Averaged Equations for the mean quantities contain the unknown correlations $\langle u_i' u_j' \rangle$, $\langle \theta' u_i' \rangle$, and $\langle c' u_i' \rangle$. Numerous methods have been suggested to express these correlations as functionals of known mean flow parameters and thus to close the system (2.2)–(2.7). Formally, well-known equations for their transport can be derived in a purely mathematical way (see, e.g., TENNEKES AND LUMLEY [258]).

2.2.1 Second-Order Equations

A transport equation for the Reynolds stress tensor, $\langle u_i' u_j' \rangle$, can be derived by multiplying (2.3) for u_i with u_j' and (2.3) for u_j with u_i' . If the resulting equations are averaged, added, and re-arranged somewhat, the transport of the single-point correlations can be written down as

$$\begin{aligned}
&\underbrace{\frac{\partial \langle u_i' u_j' \rangle}{\partial t}}_{\text{local change}} + \underbrace{u_l \frac{\partial \langle u_i' u_j' \rangle}{\partial x_l}}_{\text{convective change}} = \underbrace{-\langle u_j' u_l' \rangle \frac{\partial u_i}{\partial x_l} - \langle u_i' u_l' \rangle \frac{\partial u_j}{\partial x_l}}_{P_{ij}} \\
&+ \underbrace{g\delta_{i3}\alpha \langle \theta' u_j' \rangle + g\delta_{j3}\alpha \langle \theta' u_i' \rangle}_{G_{ij}} \quad \underbrace{-f_{il}\langle u_j' u_l' \rangle - f_{jl}\langle u_i' u_l' \rangle}_{F_{ij}} \\
&+ \underbrace{\frac{1}{\rho_0}\langle p' \left(\frac{\partial u_i'}{\partial x_j} + \frac{\partial u_j'}{\partial x_i} \right) \rangle}_{\phi_{ij}} \underbrace{-\frac{\partial \langle u_i' u_j' u_l' \rangle}{\partial x_l}}_{\text{turbulent diffusion}} \underbrace{-\frac{1}{\rho_0} \left(\frac{\partial \langle u_i' p' \rangle}{\partial x_j} + \frac{\partial \langle u_j' p' \rangle}{\partial x_i} \right)}_{\text{pressure diffusion}} \\
&+ \underbrace{\nu \frac{\partial^2 \langle u_i' u_j' \rangle}{\partial {x_l}^2}}_{\text{viscous diffusion}} \underbrace{- 2\nu \langle \frac{\partial u_i'}{\partial x_l} \frac{\partial u_j'}{\partial x_l} \rangle}_{\epsilon_{ij}} \quad .
\end{aligned} \tag{2.8}$$

Here, the density fluctuations, ρ', have been replaced by a linearized version of the equation of state $\rho'/\rho_0 = -\alpha\theta'$ (suitable for fresh water) using the thermal expansion coefficient, α. P_{ij}, G_{ij}, and F_{ij} are defined as the production of Reynolds stresses by mean shear, buoyancy, and Coriolis forces, respectively. ϕ_{ij} is usually referred to as the *pressure-strain* correlations and ϵ_{ij} stands for the rate of dissipation of the Reynolds stresses[2].

[2]Note, that the true rate of dissipation is defined as $\tilde{\epsilon} = 2\nu {S'}_{ij} {S'}_{ij}$, where ${S'}_{ij}$ is the fluctuating part of the symmetric velocity gradient defined in $(2.17)_1$. $\tilde{\epsilon}$ is different from ϵ obtained by half the trace of ϵ_{ij}. Nevertheless, the difference between ϵ and $\tilde{\epsilon}$ is known to be small and the form used here is in agreement with most authors.

Analogously, an equation for the turbulent heat flux, $\langle\theta' u_i'\rangle$, appearing in (2.5) is derived:

$$\begin{aligned}
\underbrace{\frac{\partial\langle\theta' u_i'\rangle}{\partial t}}_{\text{local change}} + \underbrace{u_l\frac{\partial\langle\theta' u_i'\rangle}{\partial x_l}}_{\text{convective change}} &= \underbrace{-\langle u_i' u_l'\rangle\frac{\partial\theta}{\partial x_l}}_{P_i^{\theta u1}} \underbrace{-\langle\theta' u_l'\rangle\frac{\partial u_i}{\partial x_l}}_{P_i^{\theta u2}} \\
&+ \underbrace{g\delta_{i3}\,\alpha\langle\theta'^2\rangle}_{G_i^{\theta u}} \underbrace{-f_{il}\langle\theta' u_l'\rangle}_{F_i^{\theta u}} \\
&+ \underbrace{\frac{1}{\rho_0}\langle p'\frac{\partial\theta'}{\partial x_i}\rangle}_{\phi_i^{\theta u}} - \underbrace{\frac{\partial\langle\theta' u_i' u_l'\rangle}{\partial x_l}}_{\text{turbulent diffusion}} - \underbrace{\frac{1}{\rho_0}\frac{\partial\langle p'\theta'\rangle}{\partial x_i}}_{\text{pressure diffusion}} \\
&+ \underbrace{\frac{\partial}{\partial x_l}\left(\frac{\lambda}{\rho_0 c_v}\langle u_i'\frac{\partial\theta'}{\partial x_l}\rangle + \nu\langle\theta'\frac{\partial u_i'}{\partial x_l}\rangle\right)}_{\text{viscous diffusion}} \underbrace{-\left(\frac{\lambda}{\rho_0 c_v}+\nu\right)\langle\frac{\partial u_i'}{\partial x_l}\frac{\partial\theta'}{\partial x_l}\rangle}_{\epsilon_i^{\theta u}} \quad .
\end{aligned} \tag{2.9}$$

$P_i^{\theta u1}$, $P_i^{\theta u2}$, and $F_i^{\theta u}$ are production terms due to the presence of gradients in the mean temperature field, in the mean velocity field, and due to the Coriolis force, respectively. Similarly to (2.8), a pressure redistribution term, $\phi_i^{\theta u}$, and a dissipation term, $\epsilon_i^{\theta u}$, appear. The buoyancy production term, $G_i^{\theta u}$, introduces the variance of the temperature fluctuations, $\langle\theta'^2\rangle$, into the equations. A transport equation for this term is found by multiplying the balance of heat (2.5) with θ' and averaging. After re-arranging, the result can be written as

$$\begin{aligned}
\underbrace{\frac{\partial\langle\theta'^2\rangle}{\partial t}}_{\text{local change}} + \underbrace{u_l\frac{\partial\langle\theta'^2\rangle}{\partial x_l}}_{\text{convective change}} &= \underbrace{-2\langle u_l'\theta'\rangle\frac{\partial\theta}{\partial x_l}}_{P^\theta} \\
- \underbrace{\frac{\partial\langle u_l'\theta'^2\rangle}{\partial x_l}}_{\text{turbulent diffusion}} &+ \underbrace{\frac{\partial}{\partial x_l}\left(\frac{\lambda}{\rho_0 c_v}\frac{\partial\langle\theta'^2\rangle}{\partial x_l}\right)}_{\text{viscous diffusion}} \underbrace{-2\frac{\lambda}{\rho_0 c_v}\langle\frac{\partial\theta'}{\partial x_l}\frac{\partial\theta'}{\partial x_l}\rangle}_{\chi} \quad .
\end{aligned} \tag{2.10}$$

Temperature variance can only be produced by mean temperature gradients through the production term, P^θ. The letter χ is conventionally used for the dissipation of temperature variance.

(2.8) can be contracted to yield an equation for the turbulent kinetic energy defined as $k := \frac{1}{2}\langle u_i' u_i' \rangle$:

$$\underbrace{\frac{\partial k}{\partial t}}_{\text{local change}} + \underbrace{u_l \frac{\partial k}{\partial x_l}}_{\text{convective change}} = \underbrace{-\langle u_i' u_l' \rangle \frac{\partial u_i}{\partial x_l}}_{P}$$

$$- \underbrace{\frac{\partial \langle u_l' \frac{1}{2} u_i' u_i' \rangle}{\partial x_l}}_{\text{turbulent diffusion}} + \underbrace{\nu \frac{\partial^2 k}{\partial {x_l}^2}}_{\text{viscous diffusion}} - \underbrace{\frac{1}{\rho_0} \frac{\partial \langle u_i' p' \rangle}{\partial x_i}}_{\text{pressure diffusion}} \tag{2.11}$$

$$\underbrace{+ g \delta_{i3} \, \alpha \langle \theta' u_i' \rangle}_{G} - \underbrace{\nu \langle \frac{\partial u_i'}{\partial x_l} \frac{\partial u_i'}{\partial x_l} \rangle}_{\epsilon} \quad .$$

The traces of the power of the Coriolis forces and the pressure-strain power are zero. Only viscous and turbulent transport terms, a shear production term, P, a buoyancy production term, G, and the dissipation, ϵ, are retained.

More equations describing the turbulent transport of different types of tracers can be constructed by derivation from (2.7) (see Frey [79]). However, they introduce new unknown correlations and the number of equations easily increases beyond a manageable limit. Besides this, there are hardly any experimental data available for modelling the new terms. Thus, in accordance with most other authors, similarity of the transport of a passive tracer and of heat will be assumed.

2.2.2 Modelling the Turbulent Transport Equations

To arrive at a balance between the number of unknowns and the number of equations describing the transport of the turbulent fluxes, approximations for the unknown correlations in terms of known flow properties have to be devised. Chou [46], Prandtl [193, 194], and Rotta [209, 210] were among the first who suggested closure assumptions for the most important terms in (2.8). Many of their pioneering suggestions have been seized and extended in more recent references (see Lumley [154], Speziale [237], Cambon and Scott [34]). The most advanced ideas with respect to geophysical and astrophysical modeling are discussed, e.g., by Canuto and co-workers [35, 36, 37, 40, 38] and in a carefully written review article by Sander [215], who classifies recent modelling approaches with respect to geophysical applications.

All closure schemes presume the knowledge of a number of turbulent length-scales. There are different ways to obtain estimates of these scales. Some authors (Canuto and

Minotti [39] and Cheng and Canuto [45]) obtain them analytically as functions of local flow parameters such as the turbulent Froude number, Fr, or the shear number, Sh. This approach works particularly well for the sub-grid scale models used in advanced LES, because the filter size, Δ, sets a convenient reference scale needed in these models. In ensemble averaged models there is no obvious choice for such a reference scale[3].

An alternative approach is to obtain the length-scales from the solution of differential equations. In simple models of this type all scales are assumed to be proportional to a so-called *master length-scale*, l. In that case, a differential equation can be formulated either directly for l or indirectly for a related quantity such as the rate of dissipation, ϵ, or a turbulent frequency ω, or for the product kl. The different possibilities will be discussed in great detail below.

All closure models introduced in the following sections will be formulated in terms of the turbulent kinetic energy, k, and the rate of dissipation, ϵ, as the variable that determines the master length-scale. This choice was made since in all numerical codes, no matter what length-scale related variable is actually used, ϵ has to be calculated at some point for insertion into the budgets (2.8) or (2.11). Hence, there is no extra cost, if ϵ is also used in the closure models. Without any loss of generality, of course, a conversion to other pairs of variables is possible. Mellor and Yamada [169] formulated directly in terms of k and l, and Wilcox [294] in terms of k and ω.

2.2.3 The Pressure Redistribution Terms

Because of their importance, the pressure-strain term, ϕ_{ij}, and pressure-temperature-gradient term, $\phi_i^{\theta u}$, have received the greatest amount of attention by turbulence modellers. Guided by the ideas of Rotta [209], almost all authors distinguish between a "slow" part describing the return to isotropy in the absence of mean velocity gradients and buoyancy, and a complementary "rapid" part. For both contributions non-linear formulations have been introduced. However, for reasons discussed below, in this chapter only the most important linear parts are retained.

[3]Much simpler algebraic forms like the formulations of Blackadar [14] and Mellor and Yamada [168] are also still in use. Their predictive power, however, is assumed to be small.

The Pressure-Strain Term

Among the most popular linear models for the pressure-strain correlation is the model of Launder, Reece and Rodi [147] that has been extended to include the effects of buoyancy by Launder [146] and Gibson and Launder [87, 88]. This model is usually formulated as

$$\begin{aligned}\phi_{ij} &= \underbrace{-c_1\tau_p^{-1}\left(\langle u_i'u_j'\rangle - \delta_{ij}\frac{2}{3}k\right)}_{\text{slow pressure-strain}} \\ &- \underbrace{c_2\left(P_{ij}-\frac{2}{3}\delta_{ij}P\right) - c_3\left(G_{ij}-\frac{2}{3}\delta_{ij}G\right)}_{\text{rapid pressure-strain I}} \\ &- \underbrace{c_4\left(D_{ij}-\frac{2}{3}\delta_{ij}D\right) - c_5 kS_{ij}}_{\text{rapid pressure-strain II}} ,\end{aligned} \tag{2.12}$$

where τ_p is the so-called *return-to-isotropy* time-scale. Quantities appearing in (2.12) that have not been defined yet, are explained in the context of (2.15).

Recently, Shih and Shabbir [223] compared different closure schemes for the pressure-strain term and suggested a more general shape also including non-linear terms. After their ideas Canuto [37] and Canuto et al. [38] constructed a turbulent closure for the pressure-strain term, of which the linear part can be written as

$$\begin{aligned}\phi_{ij} &= -c_1\tau_p^{-1}\left(\langle u_i'u_j'\rangle - \delta_{ij}\frac{2}{3}k\right) + \frac{4}{5}kS_{ij} \\ &+ \alpha_1\Sigma_{ij} + \alpha_2 Z_{ij} - (1-\beta_5)\left(G_{ij}-\frac{2}{3}\delta_{ij}G\right) ,\end{aligned} \tag{2.13}$$

using the notation of these authors. The new tensors Σ_{ij} and Z_{ij} are defined in (2.15).

In the presence of stratification, τ_p has been suggested to be of the form

$$\tau_p = \begin{cases} \tau & \text{if } N^2 \le 0, \\ \frac{\tau}{1+hN^2\tau^2} & \text{if } N^2 > 0, \end{cases} \tag{2.14}$$

where $N^2 = -\frac{g}{\rho}\frac{\partial\rho}{\partial z}$ is the square of the buoyancy frequency, $\tau = k/\epsilon$ a typical time-scale of turbulence, and h an additional model constant (Weinstock [290, 291], Canuto [37], and Canuto et al. [40]). The latter authors found that (2.14) considerably improves the behaviour of all quantities near the inversion layer in a simulation of free convection

of the atmospheric boundary layer. The effect of this paramerization will be studied in detail below. For flows that are not affected by stable stratification, the slow part of the pressure-strain correlation obviously reduces to the classical proposal of Rotta [209].

The "anisotropic production" tensors appearing in (2.12) and (2.13) are defined as

$$\begin{aligned} D_{ij} &= -\langle u_i' u_l' \rangle \frac{\partial u_l}{\partial x_j} - \langle u_j' u_l' \rangle \frac{\partial u_l}{\partial x_i} \ , \\ \Sigma_{ij} &= S_{il} b_{lj} + S_{jl} b_{li} - \frac{2}{3} \delta_{ij} S_{lm} b_{lm} \\ Z_{ij} &= W_{il}^* b_{lj} + W_{jl}^* b_{li} \quad \text{and} \\ D &= P = \frac{1}{2} D_{ll} = \frac{1}{2} P_{ll} \ , \end{aligned} \tag{2.15}$$

where

$$b_{ij} = \langle u_i' u_j' \rangle - \frac{2}{3} \delta_{ij} k \tag{2.16}$$

defines the anisotropic part of the Reynolds stress tensor. The symmetric and skew-symmetric parts of the velocity gradient have been denoted by

$$\begin{aligned} S_{ij} &= \frac{1}{2} \left(\frac{\partial u_i}{\partial x_j} + \frac{\partial u_j}{\partial x_i} \right) , \\ W_{ij} &= \frac{1}{2} \left(\frac{\partial u_i}{\partial x_j} - \frac{\partial u_j}{\partial x_i} \right) , \quad \text{and} \\ W_{ij}^* &= W_{ij} + \epsilon_{ilj} \Omega_l = W_{ij} + \frac{1}{2} f_{ij} \quad . \end{aligned} \tag{2.17}$$

The topics of frame dependence and form invariance of second-order models have been addressed by several authors (cf. Lumley [155], Speziale [232, 233, 234, 236]). Some of their results were recently extended by Sadiki and Hutter [213], who stated that second-order turbulent closures are *form invariant* (i.e. all balance equations retain the same functional form for different observers), but remain *frame dependent* through the emergence of (in general frame dependent) body forces. Speziale [236] and Canuto et al. [37, 38] pointed out that the *implicit* influence of the frame dependence can only appear via the Coriolis forces in combination with the skew-symmetric part of the velocity gradient according to $(2.17)_3$. Thus, the form of the pressure-strain model in rotating flows is completely determined by its non-rotating form (Speziale [236]).

It is demonstrated in Appendix A.3 that the new pressure-strain model (2.13) and the

traditional model (2.12) are isomorphic for non-rotational flows [4]. This somewhat surprising result contradicts BURCHARD AND BODLING [28], who claimed that the tensor Z_{ij} extends the classical model (2.12) in non-rotating flows. This fact leads to two important conclusions:

- The different behaviour of the new Canuto et al. [37, 38] model in non-rotating flows as compared to other models and as discussed in detail in the following sections, cannot be attributed to the different *form* of the model, as suggested by the authors. Largely different values of some model constants are likely the main reason for the different model performance (see below).

- The pressure-strain model in the form (2.13) exhibits a very advantageous property in rotating flows: It extracts the part of the pressure-strain model, which depends explicitly on the skew-symmetric part of the velocity gradient, thus allowing for a straightforward substitution of $(2.17)_3$. In contrast, (2.12) does not distinguish between the symmetric and skew-symmetric parts of the velocity gradient. Only if the velocity gradient is split in symmetric and skew-symmetric parts it is obvious, in which way rotational terms should enter in (2.12). In its original form suggested by GIBSON AND LAUNDER [87], however , this model cannot be expected to behave correctly in rotating flows, even though it is consistent in non-rotating flows by its isomorphism to (2.13).

	c_1	c_2	c_3	c_4	c_5
MELLOR AND YAMADA [169]	3.0	0	0	0	−0.32
KANTHA AND CLAYSON [135]	3.0	0	0	0	−0.32
LAUNDER ET AL. [147]	1.5	0.764	0	0.109	0.364
GIBSON AND LAUNDER [87]	2.2	0.55	0.55	0	0
GIBSON AND LAUNDER [88]	1.8	0.6	0.5	0	0
LUYTEN ET AL. [156]	1.5	0.777	0.5	0.218	0.527
CANUTO [38]	2.5	0.776	0.4	0.2	0.512

Table 2.1: Model coefficients for the pressure-strain model (2.12) used by different authors.

Remarkably, the rapid pressure-strain model of LAUNDER ET AL. [147] for unstratified

[4] As shown in Appendix A.3, in rotational flows (2.12) and (2.13) are isomorphic only if the factor $\alpha_2 F_{ij} = (c_2 - c_4)F_{ij}$ is added to the right hand side of (2.12).

flows depends only on a single model coefficient, c:

$$c_2 = \frac{8+c}{11}\,, \quad c_4 = \frac{8c-2}{11} \quad \text{and} \quad c_5 = 2\frac{30c-2}{55} \quad . \tag{2.18}$$

Model values used by these authors and others are compiled in Tab. 2.1.

	c_1^θ	c_2^θ	c_3^θ	c_4^θ	c^θ
Mellor and Yamada [169]	3.74	0	0	0	1.217
Kantha and Clayson [135]	3.74	0.7	0.7	0.2	1.217
Gibson and Launder [87]	3.2	0.5	0.5	0.5	1.6
Gibson and Launder [88]	3.0	0.33	0.33	0.33	1.6
Luyten et al. [156]	3.0	0.33	0.33	0.33	1.6
Canuto [38]	5.97	0.6	1	0.33	1.44

Table 2.2: Model coefficients for the pressure-temperature-gradient model (2.19) used by different authors.

The Pressure-Temperature-Gradient Term

The pressure temperature gradient correlation is modelled in a way suggested by Gibson and Launder [88]. However, following the recommendation of Canuto et al. [37, 38], an extension of the Gibson and Launder [88] model is introduced by splitting the mean shear production in two parts, depending on the symmetric and the skew-symmetric part of the velocity gradient (for the derivation, see Appendix A.3). Note, that in non-rotating flows this splitting is the only *structural* difference between the Gibson and Launder [88] and the Canuto et al. [37, 38] model families in the form presented here. The pressure-temperature-gradient correlation can be expressed according to:

$$\phi_i^\theta = -c_1^\theta \tau_p^{-1} \langle \theta' u_i' \rangle + c_2^\theta S_{ij} \langle \theta' u_j' \rangle + c_3^\theta W_{ij}^* \langle \theta' u_j' \rangle - c_4^\theta G_i^{\theta u} \quad . \tag{2.19}$$

Gibson and Launder [88] used in their model $c_2^\theta = c_3^\theta$ and W_{ij} instead of W_{ij}^*. For this fact it must be considered inconsistent in rotating flows. Tab. 2.2 displays coefficients used in some well-known models. Tab. 2.1 and Tab. 2.2 also demonstrate that the different behaviour of the Canuto et al. [37, 38] model is likely caused by the comparably high values of c_1, c_1^θ, and c_3^θ.

Discussion of the Pressure Redistribution Model

Many derivations of the redistribution models introduced above have been used. The most well-known models with respect to geophysical applications shall be very briefly reviewed here.

A linear pressure-strain model identical to that of LAUNDER ET AL. [147] for unstratified flows has been adopted in the so-called *Stress-ω model*, recently published by WILCOX [294]. The coefficients are given values very similar to those chosen by LAUNDER ET AL. [147]. However, to my knowledge, no generalization of the Stress-ω model for buoyancy affected flows has been attempted until now. It will be an important part of this work to discuss the relative merits of a new, buoyancy extended, Stress-ω model.

Some reduced redistribution models have already been applied to oceanographic situations. The term multiplied by the factor c_2 in the rapid pressure-strain part of (2.12) was found to be dominant in many situations (LAUNDER ET AL. [147]). As an extension of their suggestion, RODI [206] recommended $c_2 = c_3$ and $c_4 = c_5 = 0$ as a good approximation. This simplified model with $c_2^\theta = c_3^\theta = c_4^\theta$ (however, with an additional wall reflection term) has been used by BURCHARD AND BAUMERT [27] in their one-dimensional ocean turbulence model.

The models of MELLOR [163] and MELLOR AND YAMADA [168, 169], which are up to now very popular in geophysical applications, implement an even more reduced pressure-strain relation: These authors retain only the slow pressure-strain term of ROTTA [209] and the term multiplied by the factor c_5 in (2.12). Moreover, they set $c_2^\theta = c_3^\theta = c_4^\theta = 0$ in (2.19). RODI [206] remarks that these simplifications are not entirely clear and doubts that the model performs as well as the full pressure-strain model in free shear layers. A slightly improved model has been introduced by KANTHA AND CLAYSON [135] allowing $c_2^\theta = c_3^\theta \neq 0$ and $c_4^\theta \neq 0$.

Following a proposal of SHIR [225], some authors (e.g., GIBSON AND LAUNDER [88]) added to their pressure-strain models a so-called "wall reflection term" that involves a surface damping function accounting for the anisotropy of the normal Reynolds stresses close to a rigid wall . This procedure has been shown by CELIK AND RODI [42] also to simulate suitably the influence of a free surface. For the following reasons this approach is not adopted here: First, WILCOX [294] pointed out that his Stress-ω model – despite all its similarity to the model of Launder, Reece and Rodi [147] – does not require a "wall reflection term" to achieve a satisfactory channel flow solution. He concludes that

the large "wall reflection term" term is only needed to accommodate a deficiency of the modelled ϵ equation. Second, ABID AND SPEZIALE [1] showed that models that perform satisfactorily in homogeneous shear flows also compute a reasonable solution in the logarithmic boundary layer, provided the coefficient c_1 in Rotta's model is not too large. They demonstrated that, if this is not the case, a "wall reflection term" can be used to remedy the model deficiency at the boundary. However, they also pointed out that the most common "wall reflection terms" are not applicable for general geometries and, moreover, may influence the flow even far from the wall. From a practical point of view, the wall reflection term seems to be unimportant in oceanographic applications: BURCHARD AND BAUMERT [27] compared two versions of the k-ϵ model (one with and one without a "wall reflection term") for a stably stratified mixing layer setup in the North Sea. They were not able to decide, which model is superior. The above arguments indicate that there is no objective advantage gained by including a "wall reflection term" for the modelling of flows considered here.

As remarked above, all pressure redistribution models discussed above are linear models[5]. However, a wealth of experience has also been gained with non-linear formulations (see, e.g., SHIH AND SHABBIR [223], CANUTO [35, 36, 37]). CRAFT ET AL. [50] summarize the benefits of the non-linear type of models for buoyancy affected flows. Though the authors themselves remark that the new models may seem "intimidatingly bulky", they also claim a somewhat wider range of applicability. Interestingly, they also show that the non-linear terms are, at least partly, capable of replacing the "wall reflection term", indicating once more that the physical importance of this term is questionable.

For the following reasons the non-linear approach was found to be inappropriate in the context of this work. As shown below, the differential equations describing the evolution of turbulent correlations can be simplified to yield an Algebraic Stress Model. The resulting set of equations can then be solved for the turbulent fluxes by simple matrix inversion only, if the pressure-strain model (and hence the system) is linear. Second, in the context of mixing in the atmosphere, in oceans or in lakes, there seem to be many other effects (mixing by internal waves, boundary mixing) that still cannot sufficiently be parameterized. It is likely, these effects (and the insecurity of their description) by far out-weigh the relatively small non-linear contribution to the pressure-strain model.

[5]Linearity in this context denotes a linear dependence of the pressure-strain term and the pressure-temperature-gradient term on (parts of) the velocity gradient and on the correlations of fluctuating quantities.

2.2.4 Rate of Dissipation

To model the tensor of viscous dissipation of the Reynolds stresses, ϵ_{ij}, most authors follow KOLMOGOROV [139] and assume local isotropy:

$$\epsilon_{ij} := 2\nu\langle\frac{\partial u_i'}{\partial x_l}\frac{\partial u_j'}{\partial x_l}\rangle \stackrel{!}{=} \frac{2}{3}\delta_{ij}\epsilon \tag{2.20}$$

The idea of local isotropy can also be used for the dissipation of the turbulent heat fluxes leading to

$$\epsilon_i^{\theta u} := (\nu+\lambda)\langle\frac{\partial u_i'}{\partial x_l}\frac{\partial \theta'}{\partial x_l}\rangle \stackrel{!}{=} 0\ , \tag{2.21}$$

since there is no isotropic vector function in three dimensions. (2.21) can also be viewed as the statement that the spectra of the temperature and velocity gradient fluctuations peak at different wave-numbers. The destruction of temperature variance is modelled by assuming a balance with production in (2.10), i.e.

$$\chi := 2\frac{\lambda}{\rho_0 c_v}\langle\frac{\partial \theta'}{\partial x_j}\frac{\partial \theta'}{\partial x_j}\rangle \stackrel{!}{=} \frac{2}{c^\theta}\tau^{-1}\langle\theta'^2\rangle\ , \tag{2.22}$$

with dimensionless c^θ. (2.20) is merely a statement of isotropy and does not specify how ϵ should be derived. In contrast to that (2.22) is a more stringent, local statement. Some authors relaxed it and formulated a differential equation also for χ (ZEMAN AND LUMLEY [301, 302]).

2.2.5 Turbulent Transport

The turbulent transport of the Reynolds stresses, the turbulent heat fluxes, and the temperature variance are modelled by many authors as down-gradient diffusion processes. It is clear that such a simple parameterization is one of the main drawbacks for an appropriate description of counter-gradient fluxes known to appear in free convection (WILLIS AND DEARDORFF [295], DEARDORFF AND WILLIS [57]). They have also been observed in stably stratified shear flows (KOMORI ET AL. [140]). Some authors (ZEMAN AND LUMLEY [301], CANUTO ET AL. [40], D'ALESSIO ET AL. [56]) emphasized that for an appropriate description of this phenomenon transport equations for the third-order moments have to be solved, at least to some degree. (However, see discussion in SCHUMANN [218]).

Since the turbulent transport terms will be neglected by the simplifications that lead to an Algebraic Stress Model (ASM), there will definitely be model deficiencies in describing

situations in which counter-gradient terms are important. Turbulent transport terms are only retained in the transport equation of the turbulent kinetic energy:

$$-\langle u_l' \frac{1}{2} u_i' u_i' \rangle - \frac{1}{\rho_0} \langle u_l' p' \rangle = \nu_k \frac{\partial k}{\partial x_l} \ , \tag{2.23}$$

where the turbulent diffusivity of k, ν_k, can be related to the turbulent diffusivity of momentum via a turbulent Schmidt number as in $(3.7)_3$ and $(3.14)_2$ below.

2.2.6 The Full Model

With all model assumptions inserted into (2.8), (2.9) and (2.10), the complete transport equations read

$$\begin{aligned}\frac{\partial\langle u_i'u_j'\rangle}{\partial t}+u_l\frac{\partial\langle u_i'u_j'\rangle}{\partial x_l} &= \mathcal{D}_{ij}+P_{ij}+G_{ij}+(1-c_2+c_4)F_{ij}\\ &- c_1\tau_p^{-1}\left(\langle u_i'u_j'\rangle-\frac{2}{3}\delta_{ij}k\right)\\ &- c_2\left(P_{ij}-\frac{2}{3}\delta_{ij}P\right)-c_3\left(G_{ij}-\frac{2}{3}\delta_{ij}G\right)\\ &- c_4\left(D_{ij}-\frac{2}{3}\delta_{ij}P\right)-c_5kS_{ij}-\frac{2}{3}\delta_{ij}\epsilon\ ,\end{aligned} \tag{2.24}$$

$$\begin{aligned}\frac{\partial\langle\theta'u_i'\rangle}{\partial t}+u_l\frac{\partial\langle\theta'u_i'\rangle}{\partial x_l} &= \mathcal{D}_i^{\theta u}+P_i^{\theta u1}-c_1^\theta\tau_p^{-1}\langle\theta'u_i'\rangle\\ &- (1-c_2^\theta)S_{il}\langle\theta u_l'\rangle-(1-c_3^\theta)\overline{W}_{il}\langle\theta u_l'\rangle+(1-c_4^\theta)G_i^{\theta u}.\end{aligned} \tag{2.25}$$

and

$$\frac{\partial\langle\theta'^2\rangle}{\partial t}+u_l\frac{\partial\langle\theta'^2\rangle}{\partial x_l} = \mathcal{D}^\theta+P^\theta-\frac{2}{c^\theta}\tau^{-1}\langle\theta'^2\rangle\quad . \tag{2.26}$$

The tensor $\overline{W}_{ij}$ appearing in (2.25) is defined in (A.44) (as derived in Appendix A.3). In non-rotating flows it reduces to the skew-symmetric part of the velocity gradient, W_{ij}. The terms $\mathcal{D}_{ij}$, $\mathcal{D}_i^{\theta_u}$ and $\mathcal{D}^\theta$ summarize the turbulent and viscous transport of the Reynolds stresses, the turbulent heat fluxes and the temperature variance, respectively. These terms are defined implicitly in (2.8), (2.9), and (2.10), respectively.

The terms involving the implicit and explicit Coriolis effect require extra comments: Galperin et al. [81] used a model of the Rotta type with an extension for rotational flows suggested by Zeman and Tennekes [303]. This model yields implicit Coriolis terms of the form $-c_FF_{ij}$, hence reducing the effect of the explicit terms F_{ij} by the factor $(1-c_F)$. Unfortunately, the model of Zeman and Tennekes [303] is in-objective and therefore inconsistent in rotating flows. Nevertheless, the reduction of the explicit Coriolis terms is analogous to the present model, where the term $(-c_2+c_4)F_{ij}$ reduces the explicit terms, F_{ij}, since $(-c_2+c_4)$ is positive for all models. Galperin et al. [81] showed that, if rotation does not enter the model equations at any other place (see discussion below), then their effect in stably stratified fluids is small. With the above analogy, their arguments apply equally well to the present case.

The modelled transport equation for the turbulent kinetic energy, k, must be the contraction of (2.24); with the use of (2.23) this yields

$$\frac{\partial k}{\partial t} + u_l \frac{\partial k}{\partial x_l} = \frac{\partial}{\partial x_l}\left(\nu_k \frac{\partial k}{\partial x_l}\right) + P + G - \epsilon \quad . \tag{2.27}$$

The system (2.24)–(2.26) can only be solved if the time-scales τ and τ_p are prescribed.

2.3 Algebraic Stress Models

Simple models based on the so-called Boussinesq hypothesis represent a tensorial equivalent to Prandtl's mixing-length model. They can be formulated as

$$\langle u_i' u_j' \rangle = \frac{2}{3}\delta_{ij} k - \nu_t \left(\frac{\partial u_i}{\partial x_j} + \frac{\partial u_j}{\partial x_i}\right) \quad . \tag{2.28}$$

(2.28) provides a good description of many flows of engineering and geophysical interest, especially for thin boundary layers, where it reduces to the scalar form of the mixing-length model. Nevertheless, there are numerous applications for which the predicted flow properties differ greatly from corresponding measurements. Among the most noteworthy types of applications in physical limnology and oceanography, where (2.28) is questionable are:

- primarily flows, where buoyancy effects induce differences among the longitudinal Reynolds stresses (referred to as anisotropies),
- flows with sudden changes in the mean strain rate,
- flows over irregular topography,
- flows in rotating fluids.

Explicit Models

One approach to achieve a more appropriate description of the Reynolds stress tensor without introducing any additional differential equations is to assume that the Boussinesq approximation [6] is simply the leading term in a series expansion of functionals in terms

[6] Here (2.28) is meant to be the Boussinesq approximation.

of the rate of strain and vorticity tensors. According to this idea, SPEZIALE [235] derived an explicit quadratic model that improved predictions for the secondary motions induced by the anisotropy of the longitudinal Reynolds stresses in a rectangular duct. However, the model still fails to improve predictions for flows with sudden changes in the mean strain rate and flows with curved streamlines. Even cubic models of this type have been published (see CRAFT ET AL. [51]). A critical evaluation of the existing explicit models (also including models for buoyancy affected flows) with respect to their conformance with the second law of thermodynamics has been recently presented by SADIKI ET AL. [212, 214].

Implicit Models

A second, at first glance very different method to derive algebraic equations for the Reynolds stresses was given by RODI [205]. He assumed that the convective and turbulent transport can be taken approximately proportional to the Reynolds stress component considered, i.e.

$$\begin{aligned} \frac{\partial \langle u_i' u_j' \rangle}{\partial t} \quad &+ \quad u_l \frac{\partial \langle u_i' u_j' \rangle}{\partial x_l} - \mathcal{D}_{ij} \\ &= \quad \frac{\langle u_i' u_j' \rangle}{k} \left(\frac{\partial k}{\partial t} + u_l \frac{\partial k}{\partial x_l} - \mathcal{D}_k \right) = \frac{\langle u_i' u_j' \rangle}{k} (P + G - \epsilon) \quad . \end{aligned} \tag{2.29}$$

An impression of the applicability of RODI'S [205] assumption can be gained, if the material derivative, denoted as $\dot{(\ )}$, of the Reynolds stress tensor is expressed in terms of the non-dimensional anisotropy tensor a_{ij}, defined via the equation

$$\langle u_i' u_j' \rangle = \left(\frac{2}{3} \delta_{ij} + a_{ij} \right) k \quad . \tag{2.30}$$

The chain rule then yields

$$\dot{\langle u_i' u_j' \rangle} = \dot{k} \frac{\langle u_i' u_j' \rangle}{k} + \dot{a}_{ij} k \quad . \tag{2.31}$$

If the turbulent diffusion terms, $\mathcal{D}_{ij}$ and $\mathcal{D}_k$, are neglected, comparison with (2.29) reveals that RODI'S [205] assumption amounts to the statement

$$\dot{a}_{ij} = 0 \quad . \tag{2.32}$$

An important case where the turbulent diffusion terms are negligible and where (2.32) agrees very well with measurements are homogeneously sheared (and possibly stratified) flows (see JACOBITZ ET AL. [126]). In this case the results of an algebraic model according to (2.29) and a full Reynolds stress closure coincide (see discussion in Section 3.4.5).

GIBSON AND LAUNDER [87] generalized the method of RODI [205] later in a completely analogous way for the convective and turbulent transport terms in (2.25) that simplify according to

$$\frac{\partial\langle u_i'\theta'\rangle}{\partial t} + u_l\frac{\partial\langle u_i'\theta'\rangle}{\partial x_l} - \mathcal{D}_i^{\theta u} = \frac{\langle u_i'\theta'\rangle}{2k}(P+G-\epsilon) \quad . \tag{2.33}$$

GATSKI AND SPEZIALE [84] solved the implicit three-dimensional system (2.24) (with Rodi's assumption (2.29)) for the general form of the pressure-strain model of LAUDNER ET AL. [147] without buoyancy effects. According to them, an algebraic stress model can be interpreted as a special case of an *explicit* non-linear model for the Reynolds stresses (see also SPEZIALE [238]).

ASMs derived as outlined above can deal reasonably well with many situations where a standard two-equation model fails (WILCOX [294]). However, any ASM with a slow pressure-strain parameterization of the ROTTA [209] type will fail to predict flows with a sudden change in the mean strain rate like that realized by TUCKER AND REYNOLDS [271]. It is not clear, to what extent such cases are important in an oceanographical or meteorological context. This model deficiency seems to be a relatively small price compared to the advantages gained by converting a system of differential equations to algebraic equations.

A different approach for simplifying the turbulent transport equations has been used by MELLOR AND YAMADA [168, 169]. Briefly, it involves scaling all terms in (2.24) by powers of the non-dimensional anisotropy tensor a_{ij}. All terms of order a_{ij}^2 are then neglected. Similar arguments can be applied to (2.25) and (2.26). GALPERIN ET AL. [80] reviewed this procedure and found a slight inconsistency in the scaling arguments of MELLOR AND YAMADA [168, 169]. Essentially, the scaling suggested by GALPERIN ET AL. [80] amounts to using the equilibrium assumption, $P+G=\epsilon$, only in the equations for the second moments, but retaining the full transport equations for k, thereby creating the notation of a "quasi-equilibrium".

Using the scaling arguments of MELLOR AND YAMADA [168, 169] and applying the "quasi-equilibrium" concept once, (2.24)-(2.26) can be written as

$$\begin{aligned}\langle u_i'u_j'\rangle &= \frac{2}{3}\delta_{ij}k + \frac{\tau_p}{c_1}\Big[(1-c_2+c_4)F_{ij} + (1-c_2)\,P_{ij} + (1-c_3)\,G_{ij} \\ &- c_4D_{ij} - c_5kS_{ij} + \frac{2}{3}\delta_{ij}\left((c_2+c_4)\,P + c_3G - \epsilon\right)\Big]\,,\end{aligned} \tag{2.34}$$

$$\langle\theta'u_i'\rangle = \frac{\tau_p}{c_1^\theta}\left[P_i^{\theta u1} - (1-c_2^\theta)S_{il}\langle\theta'u_l'\rangle - (1-c_3^\theta)\overline{W}_{il}\langle\theta'u_l'\rangle + (1-c_4^\theta)G_i^{\theta u}\right]\,, \tag{2.35}$$

and

$$\langle \theta'^2 \rangle = \frac{c^\theta}{2} \tau P^\theta \quad . \tag{2.36}$$

The simple form of (2.36) is supported by some measurements in the ocean and in lakes by DILLON [65], who concludes "that the rate of decay of temperature variance in most cases cannot be an important term". In situations of counter-gradient heat fluxes, however, the simple form of (2.36) is known to be one of the main reasons for an inaccurate description of this phenomenon (SCHUMANN [218]). If one considers adding an additional differential equation, an extension of (2.36) would probably be the most interesting candidate.

The Coriolis terms will be neglected from now on. They seem to be of some importance at least in free convection with rotation as shown very recently by the LES of MIRONOV ET AL. [170]. In stably stratified flows there is currently no agreement about their importance. GALPERIN ET AL. [81] concluded that due to the effect of stable stratification, rotation is only marginally important and thus does not require any additional modelling. On the other hand, CANUTO ET AL. [38] claimed that rotation must also exert an influence at other places (e.g. in the equation for the rate of dissipation, ϵ) and reached the opposite conclusion with their second-order closure. Besides this, SPEZIALE AND MAC GIOLLA MHUIRIS [239] compared the performance of the model of LAUNDER ET AL. [147], a model of the Rotta-Kolmogorov type (i.e. a model similar to the MELLOR AND YAMADA [169] model), and some other models for the case of homogeneous rotating turbulence with plane shear and no stratification. They found that none of the models yielded sufficient predictions for the time evolution of turbulent quantities. As long as the situtation is so unclear, there is little gained by including rotational terms in the model. Then, the tensor F_{ij} drops out, and the tensor $\overline{W}_{ij}$ simplifies to W_{ij}.

Several other models of geophysical interest can be recovered from (2.34)–(2.36). The model of LUYTEN ET AL. [156] is exactly recovered for $c_2^\theta = c_3^\theta = c_4^\theta$, if the production, P, is replaced by $\epsilon - G$ in (2.34) (P. J. LUYTEN, pers. com., for the model coefficients see Tab. 2.1 and Tab. 2.2). This assumption is consistent with the "quasi-equilibrium" concept of GALPERIN ET AL. [80].

If it is assumed that $c_2 = c_3 = c_4 = 0$ and $c_2^\theta = c_3^\theta = c_4^\theta = 0$ the famous model of MELLOR AND YAMADA [169] with the modifications suggested by GALPERING ET AL. [80] is recovered. FREY [79] used the same assumptions in his model.

BURCHARD AND BAUMERT [27] set $c_2 = c_3$ and $c_4 = c_5 = 0$ as suggested by RODI [206] and also applied $c_2^\theta = c_3^\theta = c_4^\theta$. In addition, they modelled the time rate and transport terms according to RODI [205] and GIBSON AND LAUNDER [87] as discussed in the context

of (2.29) and (2.33). However, they were not able to show a clear superiority of this slightly more complex model.

2.3.1 The Boundary Layer Approximation

If it is assumed that all variables except the pressure are horizontally homogeneous, (2.2), (2.3) and (2.5) simplify considerably[7]. The horizontal pressure-gradient has to be retained as one of the driving forces of the system. However, it cannot be determined as a solution of the boundary layer equations, but is imposed from the outer flow. Its effect (in lakes mainly due to wind set-up and internal and external oscillations) has to be parameterized, if desired. In the so-called boundary layer approximation the balance equations of mass, momentum and energy, (2.2), (2.3) and (2.5) reduce to

$$\begin{aligned} \frac{\partial u}{\partial t} - fv &= -\frac{1}{\rho_0}\frac{\partial p}{\partial x} + \frac{\partial}{\partial z}\left(\nu\frac{\partial u}{\partial z} - \langle u'w'\rangle\right), \\ \frac{\partial v}{\partial t} + fu &= -\frac{1}{\rho_0}\frac{\partial p}{\partial y} + \frac{\partial}{\partial z}\left(\nu\frac{\partial v}{\partial z} - \langle v'w'\rangle\right), \end{aligned} \tag{2.37}$$

and

$$\frac{\partial \theta}{\partial t} = \frac{\partial}{\partial z}\left(\frac{\lambda}{\rho_0 c_v}\frac{\partial \theta}{\partial z} - \langle \theta'w'\rangle\right) + \frac{1}{c_v}\mathcal{R} \quad . \tag{2.38}$$

Since $u = u(z,t)$ and $v = v(z,t)$ the balance of mass yields $w = 0$, if the vertical velocity is zero at the boundaries. The vertical balance of momentum reduces to a hydrostatic pressure balance.

The equations describing the transport of variances and covariances of the turbulent variables are also very advantageously affected by the boundary layer approximation. Using the expressions derived in Appendix A.2, (2.34)–(2.36) reduce to

$$\langle u'v'\rangle = \frac{\tau_p}{c_1}\left[-(1-c_2)\left(\langle v'w'\rangle\frac{\partial u}{\partial z} + \langle u'w'\rangle\frac{\partial v}{\partial z}\right)\right], \tag{2.39}$$

$$\begin{aligned} \langle u'w'\rangle &= \frac{\tau_p}{c_1}\Bigg[-(1-c_2)\langle w'^2\rangle\frac{\partial u}{\partial z} + (1-c_3)g\alpha^\theta\langle\theta'u'\rangle \\ &+ c_4\left(\langle u'^2\rangle\frac{\partial u}{\partial z} + \langle u'v'\rangle\frac{\partial v}{\partial z}\right) - \frac{c_5}{2}k\frac{\partial u}{\partial z}\Bigg], \end{aligned} \tag{2.40}$$

[7] In what follows x and y are the horizontal coordinates and the z-axis is taken anti-parallel to the acceleration of gravity.

$$\begin{aligned}\langle v'w'\rangle &= \frac{\tau_p}{c_1}\Big[-(1-c_2)\langle w'^2\rangle\frac{\partial v}{\partial z}+(1-c_3)g\alpha^\theta\langle\theta'v'\rangle \\ &+ c_4\left(\langle v'^2\rangle\frac{\partial v}{\partial z}+\langle u'v'\rangle\frac{\partial u}{\partial z}\right)-\frac{c_5}{2}k\frac{\partial v}{\partial z}\Big],\end{aligned} \tag{2.41}$$

$$\begin{aligned}\langle u'^2\rangle &= \frac{2}{3}k+\frac{\tau_p}{c_1}\Big[-2(1-c_2)\langle u'w'\rangle\frac{\partial u}{\partial z} \\ &+ \frac{2}{3}\left((c_2+c_4)P+c_3\,g\alpha^\theta\langle\theta'w'\rangle-\epsilon\right)\Big],\end{aligned} \tag{2.42}$$

$$\begin{aligned}\langle v'^2\rangle &= \frac{2}{3}k+\frac{\tau_p}{c_1}\Big[-2(1-c_2)\langle v'w'\rangle\frac{\partial v}{\partial z} \\ &+ \frac{2}{3}\left((c_2+c_4)P+c_3\,g\alpha^\theta\langle\theta'w'\rangle-\epsilon\right)\Big],\end{aligned} \tag{2.43}$$

$$\begin{aligned}\langle w'^2\rangle &= \frac{2}{3}k+\frac{\tau_p}{c_1}\Big[2(1-c_3)g\alpha_\theta\langle\theta w\rangle-2c_4P \\ &+ \frac{2}{3}\left((c_2+c_4)P+c_3\,g\alpha^\theta\langle\theta'w'\rangle-\epsilon\right)\Big],\end{aligned} \tag{2.44}$$

$$\langle\theta'u'\rangle=\frac{\tau_p}{c_1^\theta}\left[-\langle u'w'\rangle\frac{\partial\theta}{\partial z}+\frac{c_2^\theta+c_3^\theta-2}{2}\langle\theta'w'\rangle\frac{\partial u}{\partial z}\right], \tag{2.45}$$

$$\langle\theta'v'\rangle=\frac{\tau_p}{c_1^\theta}\left[-\langle v'w'\rangle\frac{\partial\theta}{\partial z}+\frac{c_2^\theta+c_3^\theta-2}{2}\langle\theta'w'\rangle\frac{\partial v}{\partial z}\right], \tag{2.46}$$

$$\begin{aligned}\langle\theta'w'\rangle &= \frac{\tau_p}{c_1^\theta}\Big[-\langle w'^2\rangle\frac{\partial\theta}{\partial z}+\frac{c_2^\theta-c_3^\theta}{2}\left(\frac{\partial u}{\partial z}\langle\theta'u'\rangle+\frac{\partial v}{\partial z}\langle\theta'v'\rangle\right) \\ &+ (1-c_4^\theta)g\alpha^\theta\langle\theta'^2\rangle\Big],\end{aligned} \tag{2.47}$$

$$\langle\theta'^2\rangle=-c^\theta\tau\langle\theta'w'\rangle\frac{\partial\theta}{\partial z}\quad. \tag{2.48}$$

As remarked above, the Coriolis terms have been ignored. It is nevertheless straightforward to retain them. The tensors of the Coriolis production, F_{ij} and $F_i^{\theta u}$, valid for boundary layers are derived in Appendix A.2.

(2.39)–(2.48) constitute a linear system that can be solved for the turbulent fluxes as functions of k, ϵ, and gradients of the mean field variables. Alternatively, it would of course be possible to embed this ASM directly in a time stepping scheme and solve it numerically.

2.3.2 Stability Functions

It turns out that the solution for the vertical turbulent momentum and heat fluxes can be written *in analogy* with the Boussinesq approximation (2.28) as

$$\begin{aligned} \langle u'w' \rangle &= -c_\mu^\epsilon(k,\epsilon,N^2,M^2)\frac{k^2}{\epsilon}\frac{\partial u}{\partial z} \,, \\ \langle v'w' \rangle &= -c_\mu^\epsilon(k,\epsilon,N^2,M^2)\frac{k^2}{\epsilon}\frac{\partial v}{\partial z} \,, \\ \langle \theta'w' \rangle &= -c_\mu^{\epsilon\,\prime}(k,\epsilon,N^2,M^2)\frac{k^2}{\epsilon}\frac{\partial \theta}{\partial z} \,, \end{aligned} \tag{2.49}$$

where

$$N^2 = -\frac{g}{\rho_0}\frac{\partial \rho}{\partial z} \tag{2.50}$$

is the buoyancy or Brunt-Väisälä frequency and

$$M^2 = \left(\frac{\partial u}{\partial z}\right)^2 + \left(\frac{\partial v}{\partial z}\right)^2 \tag{2.51}$$

the shear frequency. Note, that (2.49) only *resembles* the form of the Boussinesq assumption (2.28). This does by no means imply that the Boussinesq approximation has been assumed. In fact, it is the purpose of the ASM introduced above to exactly *avoid* the application of the Boussinesq assumption. If the boundary layer assumption is not used, the Reynolds shear stresses cannot be expressed in a simple form analogous to (2.49). The stability functions, c_μ^ϵ and $c_\mu^{\epsilon\,\prime}$, contain the essential information of the ASM (2.39)–(2.48). They make it possible to implement full ASMs efficiently in existing three-dimensional numerical codes for the hydrostatic Reynolds Averaged Navier-Stokes Equations. In such codes the turbulent fluxes are most often expressed in terms of a mean field gradient times diffusivity, as stated in (2.49), if $c_\mu^\epsilon\, k^2/\epsilon$ is interpreted as a turbulent diffusivity.

Generally, a turbulent diffusivity can be defined in terms of k and any other length-scale determining variable, e.g.,

$$\nu_t^\omega = c_\mu^\omega \frac{k}{\omega} \,, \quad \nu_t^l = c_\mu^l k^{\frac{1}{2}} l \,, \quad \nu_t^\epsilon = c_\mu^\epsilon \frac{k^2}{\epsilon} \quad . \tag{2.52}$$

In each case, the stability functions themselves can be expressed in terms of the non-dimensional parameters α_N and α_M describing the influence of shear and stratification, respectively. They read

$$c_\mu^\varphi = \bar{c}_\mu^\varphi(\bar{\alpha}_N,\bar{\alpha}_M) = \tilde{c}_\mu^\varphi(\tilde{\alpha}_N,\tilde{\alpha}_M) = \hat{c}_\mu^\varphi(\hat{\alpha}_N,\hat{\alpha}_M) \,, \tag{2.53}$$

where φ stands for any of the variables ω, l, or ϵ. The non-dimensional parameters introduced in (2.53) are defined as

$$\bar{\alpha}_N = \frac{l^2}{k} N^2 \ , \quad \tilde{\alpha}_N = \frac{k^2}{\epsilon^2} N^2 \ , \quad \hat{\alpha}_N = \frac{1}{\omega^2} N^2 \ , \tag{2.54}$$

and

$$\bar{\alpha}_M = \frac{l^2}{k} M^2 \ , \quad \tilde{\alpha}_M = \frac{k^2}{\epsilon^2} M^2 \ , \quad \hat{\alpha}_M = \frac{1}{\omega^2} M^2 \quad . \tag{2.55}$$

They relate to well-known non-dimensional numbers resulting from the analysis of stratified shear flows. $\sqrt{\bar{\alpha}_N}$ is proportional to an inverse turbulent Froude number, F_i, and $\sqrt{\tilde{\alpha}_M}$ is equal to the so-called shear number, $M\frac{k}{\epsilon}$, both important parameters in homogeneously stratified shear flows.

Instability Exhibited by the Non-Equilibrium Stability Functions

Numerical difficulties with the stability functions introduced above have been encountered by several authors, first of all by Mellor and Yamada [169] themselves, who stated that "for some model simulations a discontinuity in the velocity could develop and persist".

Deleersnijder [58] and Deleersnijder and Luyten [59] showed that the problem is serious: The original stability functions of Mellor and Yamada [169] resulted in almost useless, extremely jittery diffusivity profiles. They analyzed the problem and found regions of *de*creasing (normalized) stability functions within regions of *in*creasing non-dimensional shear α_M, a behaviour that leads to a fatal positive feedback. Deleersnijder [58] pointed out that the problem did not appear if the quasi-equilibrium concept of Galperin et al. [80] is used, since the shear dependency in the resulting stability functions drops out. Unfortunately, along with the omission of α_M as an independent variable, all related information of the ASM is lost: In the unstratified case the models reduce to the standard forms with constant coefficients.

Very recently, however, Canuto et al. [38] introduced a new set of non-equilibrium stability functions that resulted from the rather complete ASM also used in this work. It came somewhat as a surprise that, even though the authors did not use the quasi-equilibrium concept and thus retained the dependency on α_M, their stability functions proved to yield stable solutions. This fact led Burchard and Deleersnijder [29] to re-analyse the stability problem. They confirmed the findings of Deleersnijder [58] and Deleersnijder and Luyten [59] and stated quite clearly that the Mellor-Yamada stability functions are " not at all useful neither in their original nor in the modified form".

The reason for the stability of the new CANUTO ET AL. [38] functions was found to be an increase of the (normalized) stability functions for increasing non-dimensional shear, α_M, in conditions close to equilibrium. The MELLOR AND YAMADA [169] functions showed just the opposite behaviour. CANUTO ET AL.'S [38] stability functions appear to be the only stable set of non-equilibrium stability functions available at present.

Conversion Relations

As remarked above, the ASM (in form of stability functions) has to be supplemented by prescriptions of the turbulent kinetic energy, k, and a length-scale related variable. If a two-equation model is used, the most popular choices for the length-scale related (second) equation are an equation for the turbulent frequency, ω, for the product of k and l, kl, and for the dissipation of turbulent kinetic energy, ϵ. Since stability functions are usually derived only for one kind of length-scale related variable (ϵ was used here), a generalization presumes the knowledge of conversion relations.

It will be shown in Section 3.4 below, that the variables determining the length-scale are not independent of each other. From (3.7) and (3.11) below the following conversion relations for the non-dimensional stratification and shear and for the stability functions can be derived:

$$\begin{aligned} &\bar{\alpha}_N = (c_\mu^0)^6 \tilde{\alpha}_N \;, \qquad \hat{\alpha}_N = (c_\mu^0)^8 \tilde{\alpha}_N \;, \qquad \hat{\alpha}_N = (c_\mu^0)^2 \bar{\alpha}_N \;, \\ &c_\mu^l = \frac{1}{(c_\mu^0)^3} c_\mu^\epsilon \;, \qquad c_\mu^\omega = \frac{1}{(c_\mu^0)^4} c_\mu^\epsilon \;, \qquad c_\mu^\omega = \frac{1}{c_\mu^0} c_\mu^l \;, \end{aligned} \tag{2.56}$$

where c_μ^0 is conventionally the value of c_μ^l for zero stratification. All stability functions introduced in this work are generally given in k-ϵ notation. As mentioned above, this choice has not been made because the k-ϵ model is considered to be somehow superior (in fact, the opposite will be shown in the following sections); it has been made because in *any* two-equation model the rate of dissipation, ϵ, needs to be computed at some point since it is a crucial quantity in the budget of k. Thus, there is no extra computational effort, but probably some extra storage will be needed, if the second variable is not ϵ. If this is to be avoided, the stability functions can be converted to whatever notation is preferred using the relations (2.56). The resulting code will, however, become less generic then.

For simplicity, from now on the variables α_N and α_M will replace $\tilde{\alpha}_N$ and $\tilde{\alpha}_M$, respectively.

Presentation of Some Stability Functions

Computation of stability functions from the ASM (2.39)–(2.48) requires the analytical inversion matrices. Only in very simple cases this task can be achieved by hand. The relations presented here have been derived by means of a symbolic mathematical tool. Model constants as given in Tab. 2.1 and Tab. 2.2 have been inserted in (2.39)–(2.48) after inversion. Clearly, it would have been possible then to present the stability functions (and also the auto- and cross-correlations) analytically in terms of the model parameters. The corresponding expressions, however, turn out to be rather lengthy in some cases and no advantage was felt in writing them down here. Readers, who are interested in the pure analytical form of the stability functions can obtain a symbolic notebook from the author to compute their own relations[8].

Galperin et al. [80] (GKHR) applied the quasi-equilibrium assumption to the model of Mellor and Yamada [169] to obtain their stability functions. If their model equations are converted to k-ϵ notation (see Appendix A.4) and the corresponding linear system is solved, the stability functions can be written down as

$$\text{(GKHR):} \qquad \begin{aligned} c_\mu^\epsilon &= \frac{0.0948 + 0.0108\alpha_N}{1 + 0.592\alpha_N + 0.0448\alpha_N^2} \,, \\ c_\mu^{\epsilon\,\prime} &= \frac{0.119}{1 + 0.503\alpha_N} \quad . \end{aligned} \tag{2.57}$$

This result could also have been obtained by simply converting the stability functions given in Galperin et al. [80] by means of (2.56).

Kantha and Clayson [135] (KC) extended the pressure-temperature-gradient model of Galperin et al. [80] slightly by introducing terms analogous to (2.19). Using again the relations derived in Appendix A.4, their stability functions can be translated to

$$\text{(KC):} \qquad \begin{aligned} c_\mu^\epsilon &= \frac{0.0948 + 0.012\alpha_N}{1 + 0.527\alpha_N + 0.039\alpha_N^2} \,, \\ c_\mu^{\epsilon\,\prime} &= \frac{0.119}{1 + 0.438\alpha_N} \quad . \end{aligned} \tag{2.58}$$

Making use of (2.56), for both sets of stability functions a value of $c_\mu^0 = 0.5549$ can be computed. Recall, that c_μ^0 was defined as a convention for c_μ^l in the unstratified equilibrium $P = \epsilon$. It is related to the more popular quantity $c_\mu^{\epsilon\,0}$ via the equation $c_\mu^{\epsilon\,0} = (c_\mu^0)^4$ following from (2.56).

[8] Complete analytical expression for some of the stability functions used here can also be found in a recent publication of Burchard and Bolding [28].

The model of Luyten et al. [156] (LDOR) includes the full pressure-strain model auf Launder et al. [147] with model constants as given in Tab. 2.1 and Tab. 2.2. Its quasi-equilibrium version was computed to be

$$\text{(LDOR):} \qquad \begin{aligned} c_\mu^\epsilon &= \frac{0.091 + 0.023\alpha_N}{1 + 0.714\alpha_N + 0.067\alpha_N^2}\,, \\ c_\mu^{\epsilon\,\prime} &= \frac{0.125}{1 + 0.603\alpha_N}\quad . \end{aligned} \tag{2.59}$$

A value of $c_\mu^0 = 0.5492$ was obtained, only slightly different from the value of Galperin et al. [80] and Kantha and Clayson [135].

As remarked above, Canuto et al. [38] (CHCD) very recently developed two new sets of non-equilibrium stability functions. They are considered (by the authors) the state-of-the-art of this type of ASMs. If they are converted to k-ϵ notation (see Burchard and Bolding [28]) they read

$$\begin{aligned} c_\mu^\epsilon &= \frac{0.1070 + 0.01741\alpha_N - 0.00012\alpha_M}{1 + 0.256\alpha_N + 0.0287\alpha_M + 0.00868\alpha_N^2 + 0.0052\alpha_N\alpha_M - 0.0000337\alpha_M^2}, \\ c_\mu^{\epsilon\,\prime} &= \frac{0.1120 + 0.004519\alpha_N + 0.00088\alpha_M}{1 + 0.256\alpha_N + 0.0287\alpha_M + 0.00868\alpha_N^2 + 0.0052\alpha_N\alpha_M - 0.0000337\alpha_M^2}, \end{aligned} \tag{2.60}$$

with $c_\mu^0 = 0.5268$, and

$$\begin{aligned} c_\mu^\epsilon &= \frac{0.1270 + 0.01526\alpha_N - 0.00016\alpha_M}{1 + 0.198\alpha_N + 0.0315\alpha_M + 0.00583\alpha_N^2 + 0.00417\alpha_N\alpha_M - 0.000042\alpha_M^2}, \\ c_\mu^{\epsilon\,\prime} &= \frac{0.1190 + 0.004294\alpha_N - 0.00066\alpha_M}{1 + 0.198\alpha_N + 0.0315\alpha_M + 0.00583\alpha_N^2 + 0.00417\alpha_N\alpha_M - 0.000042\alpha_M^2}. \end{aligned} \tag{2.61}$$

They will be referred to as the stability functions "A" and "B" of Canuto et al. [38], respectively. Their differences are based on slightly different model assumptions discussed in the original paper.

In an earlier publication, Canuto [37] and Canuto et al. [40] used the return-to-isotropy time-scale, τ_p, as defined in (2.14). They suggested a value $h = 0.04$ for the new model parameter introduced with (2.14). Since it is not clear to what extent this parameterization is valid for other types of models it is interesting to derive stability functions that retain the parameter h explicitly. This was done here by introducing τ_p to the model of Kantha and Clayson [135], a model of intermediate complexity. After solving the corresponding linear system, it turns out that the stability functions become

considerably more complex, but still can be written in the form (2.53). They read

$$
\begin{aligned}
c_\mu^\epsilon &= \frac{\mathcal{N}}{\mathcal{D}}\,, \qquad \text{where} \\
\\
\mathcal{N} &= 0.0948 + (0.012 + 0.358h)\alpha_N \\
&+ (0.054 + 0.432h)h\alpha_N^2) + (0.044 + 0.168h)h^2\alpha_N^3\,, \\
\mathcal{D} &= 1 + (0.527 + 4h)\alpha_N + (0.039 + 1.315h + 6h^2)\alpha_N^2 \\
&+ (0.023 + 1.05h + 4h^2)h\alpha_N^3 + (0.26 + h)h^3\alpha_N^4\,, \\
\\
c_\mu^{\epsilon\,\prime} &= \frac{0.119 + 0.178h\alpha_N}{1 + (0.438 + 2h)\alpha_N + (0.26 + h)h\alpha_N^2}\,.
\end{aligned}
\tag{2.62}
$$

Clearly, for $h \to 0$, the return-to-isotropy time-scale τ_p approaches τ and the stability functions of KANTHA AND CLAYSON [135] in the form (2.58) are recovered.

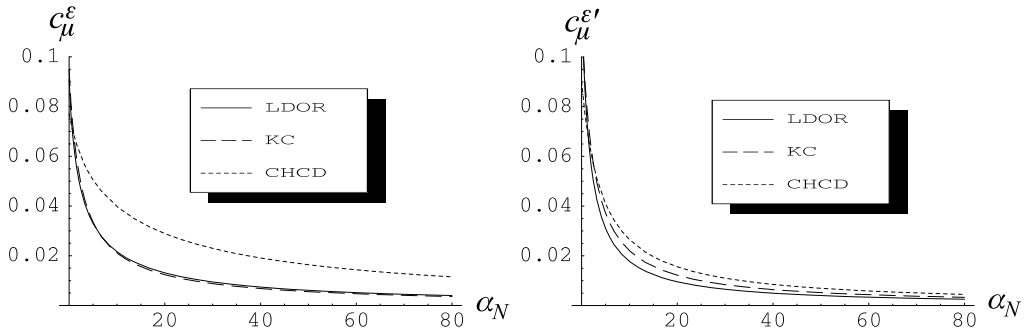

Figure 2.2: The quasi-equilibrium stability functions of LUYTEN ET AL. [156] (LDOR), KANTHA AND CLAYSON [135] (KC), and CANUTO ET AL. [38] (CHCD) in k-ϵ notation.

Fig. 2.2 illustrates the difference of three sets of quasi-equilibrium stability functions converted to k-ϵ notation. The quasi-equilibrium version of the "A" stability functions of CANUTO ET AL. [38] has been derived by applying the quasi-equilibrium concept as explained above.

It is obvious that the differences between the KANTHA AND CLAYSON [135] and the LUYTEN ET AL. [156] stability functions are only marginal, even though the latter authors use a much more elaborate model for the pressure redistribution terms. However, the different model parameters used by CANUTO ET AL. [38] and possibly also the slightly different model for the pressure-temperature-gradient correlations have a large effect. The full non-equilibrium set of the stability functions of CANUTO ET AL. [38] is displayed in Fig. 2.3.

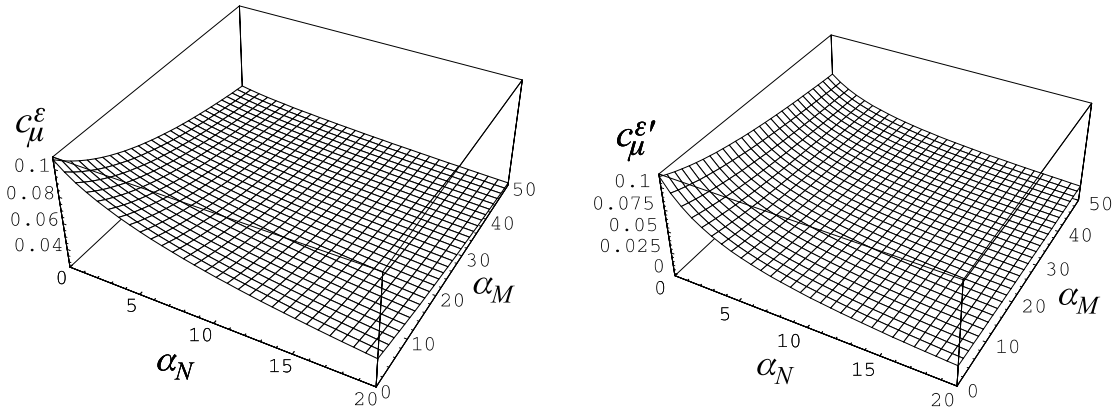

Figure 2.3: The non-equilibrium stability functions of CANUTO ET AL.'S [38] "A" model in k-ϵ notation.

A puzzling behaviour is exhibited by the stability functions expressed in (2.62). First of all, Fig. 2.4 reveals that for very small values of the parameter h the original model of KANTHA AND CLAYSON [135] is recovered. However, also for quite large values of h the extended model becomes very similar to the original model. Only for some intermediate

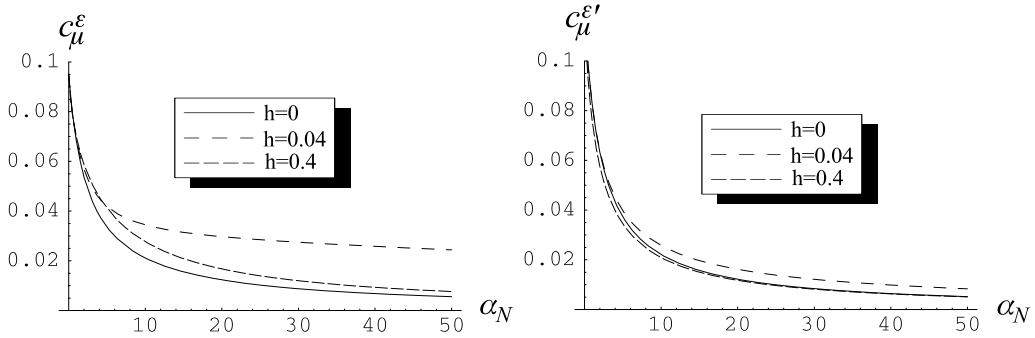

Figure 2.4: The quasi-equilibrium stability functions of (2.62) for different values of the model parameter h in k-ϵ notation.

values, e.g. $h \approx 0.04$, the stability functions are very different from their original form, especially for strongly stable stratification. $h = 0.04$ corresponds to the original proposal of CANUTO [37]. It is obvious that the parameter h dominates the overall behaviour of the stability functions in this case. Obviously, details in the pressure redistribution model are completely overshadowed by the influence of the parameter h. Without a thorough comparison to experimental data it is difficult to decide whether differences in the return-to-isotropy time-scale can really have such a large influence. Hence, this set of stability functions is excluded from further consideration.

Chapter 3

Analysis of Two-Equation Models for Geophysical Applications

Turbulence in the atmosphere and in natural waters is extremely rich in scales and processes. Its modelling is notoriously difficult and even the most advanced second- and third-order closures are known to have their deficiencies (Canuto [37], Sander [215]). In spite of this fact, most of the three-dimensional models used in oceanography and physical limnology implement much simpler one- or two-equation turbulence closures, only extended by ASMs of a structure outlined in the preceeding chapter. Naturally, the question arises in what situations these models are at all useful and give a reasonable description of the processes occurring in the real world. This chapter is devoted to the answer of this question.

Before the attention is concentrated on two-equation models, current modelling approaches for buoyancy affected turbulence are very briefly reviewed. Since bulk integrated turbulence models are still the ones most frequently used in physical limnology, it seemed necessary to continue with a short summary of their properties and to show some recent developments. The relative merits of bulk integrated and differential models will be addressed. The main part of this chapter then starts with the comparison of some well-known two-equation models. For the first time, a buoyancy extended version of the Wilcox [293, 294] k-ω model is suggested and systematically explored (Umlauf and Hutter [280]). The interrelations of two-equation models with some well-known ASMs are discussed and in this context the new concept of the "structural equilibrium" stability functions, an extension of the Galperin et al. [80] "quasi-equilibrium" stability functions, will be established (Umlauf [278]). Then, this new concept is applied to anal-

yse characteristic turbulent length-scales of turbulence in structural equilibrium and to compare the results to some recently published experimental and DNS data. The chapter closes with an investigation of the turbulence models in a state of equilibrium between diffusive transport and dissipation of turbulent kinetic energy, a balance that is known to be of some importance in geophysical applications.

3.1 Modelling Approaches for Turbulence in Natural Waters and in the Atmosphere

Turbulence phenomena of geophysical interest are most often affected by the buoyancy of the fluid. Buoyancy introduces the notion of potential energy to the budget equations. This fact inherently complicates the description of turbulence: At first, potential energy can be converted to kinetic energy in free convection. Next, in stable situations potential energy can be gained from kinetic energy and a parallel energy cascade ending with the destruction of temperature fluctuations by thermal conduction is opened up. It is known that there exists also an alternative route for a backward flow of potential energy toward larger scales (Schumann [218], Canuto and Minotti [39]). Besides this, the situation is further complicated by the fact that non-locally acting internal waves with properties completely different from turbulence can also contribute significantly to the fluctuating potential energy.

3.1.1 Free Convection

In unstable situations, potential energy converted to turbulent kinetic energy can lead to vigorous mixing. The statistics of this process are complicated (Willis and Deardorff [295], Deardorff and Willis [57]) and need a careful and expensive modelling. Canuto et al. [35, 36, 39, 37, 40] and the references therein give an extensive summary of geo- and astrophysical modelling approaches to convection with second-order closures and LES. Free convection is known to be a pitfall for two-equation models: Burchard and Bolding [28] tested the k-ϵ model with the most advanced ASMs and concluded that the height of the entrainment layer is not met very well and that, because of the inability to model counter-gradient fluxes, the predicted temperature profiles are principally different from the observed ones. They pointed out that the diffusion term for the turbulent kinetic energy, which is underestimated by a factor of approximately 2, might

be the main reason for the model's misbehaviour.

3.1.2 Stably Stratified and Sheared Flows

Stably stratified situations are of great importance for mixing in the atmosphere (Nieuwstadt [182]) and in the ocean (Gregg [93]). The particularities of stratified turbulence in lakes have been addressed by Imboden and Wüest [122]. Stable stratification complicates the situation additionally by introducing two types of fluctuating potential energy: A turbulent part and a part related to the (possibly random) motion of internal waves. This is a particularly difficult topic because internal waves cause mixing by either overturning or by contributing to the instability of the water column by wave shear (Woods [297]). On the other hand turbulence itself may degenerate to random wavy motions and so-called two-dimensional turbulence may develop under strongly stable stratification (Hopfinger [110]).

Remote from boundaries of lakes and oceans, currents are weak and the mean Richardson number is large. Mixing is thought to be generated by random instability of a random internal wave field (Gregg [93]). In such cases the turbulent dissipation can be estimated by considering the energy flux to high wave numbers and equating with the rate of dissipation, ϵ (Gregg [94]). The turbulence closures considered here are not applicable to such high Richardson number flows. However, when the scales of internal waves become much larger than any of the turbulent scales, internal waves can in principle be considered as part of the mean flow and two-equation models can be applied with success. An example is given in Section 4.2.

Transferring the above conclusions to the situation in lakes, there seem to be only a few regimes in which two-equation models are a promising modelling tool:

- The surface mixed layer in regions of moderate to small Richardson number if convection is not the dominant process.
- The seiche induced (perhaps stratified) bottom boundary layer if the breaking of internal waves is not the dominant mixing process.
- Gravity-driven down-slope currents with density stratification, if shear is the main turbulence generating agent.

In Section 4 applications of two-equation models for the first two cases will be discussed.

3.2 Bulk Models

Stimulated by numerous observations of well mixed layers on top of a sharp, step-like thermocline in the ocean, models able to reproduce the dynamics of such a configuration were looked for. Attention was soon focused upon a category of models called *bulk integrated models* that trace back to the work of KRAUS AND TURNER [274, 141]. These models were based on the idea that quantities do not change much across a well-mixed layer and thus vertical integrals of the balance equations for mean and turbulent variables provide a useful representation of the system[1].

Bulk models have undergone a considerable evolution in the past 30 years and are still in use with great success. Because of their omnipresence in physical limnology (IMBERGER AND PATTERSON [120], SPIGEL ET AL. [240]) and also in physical-biological coupled modelling (HAMILTON AND SCHLADOW [97, 216], FRANKE ET AL. [77]), a brief review of this branch of modelling seems worthwhile.

The one-dimensional vertically integrated balance equation for the turbulent kinetic energy, k, requires some closure assumptions, as does its differential counterpart. The classical entrainment experiments, which were hoped to mimic the entrainment across a thermocline as it occurs in lakes and in the ocean, were considered to provide some of the information needed to close the bulk models.

These experiments suggested a functional dependence of the entrainment velocity of the interface, u_e, on a bulk Richardson number, Ri_b, as in

$$\frac{u_e}{U} = E(Ri_b) = E(\frac{g\Delta\rho h}{\rho_0 U^2}) \, , \tag{3.1}$$

where E is the entrainment function, h the mixed layer depth, $\Delta\rho$ the density difference across the interface, U an unknown velocity scale, and ρ_0 a reference density. The form of (3.1) is compulsory by dimensional arguments. However, there was (and still is) a controversy about the proper choice of the scaling velocity U. Many scales seem to be at least plausible:

- The friction velocity, $u_* = \sqrt{\tau/\rho_0}$, which is known to be the right scaling in the law-of-the-wall regions of shear driven boundary layers;

[1] Under certain conditions bulk models can compute appropriate results even if the upper layer is not well mixed and the profiles of the variables are not homogeneous (see Section 4.1.3).

- the velocity difference across the interface, ΔU, which is a controlling parameter for shear instabilities across the interface;
- the variance of the velocity fluctuations close to the interface. This scaling is physically the most reasonable one, but it marks already the limits of bulk models: Entrainment laws formulated in terms of interface quantities must refer to a local Richardson number, which can in general not be determined from bulk parameters.

Different authors prefer distinct scalings: In their classical paper, Turner and Kraus [274] scaled with the friction velocity u_*. In contrast to that, some of the classical shear layer experiments were scaled with ΔU (e.g. Ellison and Turner [69], Moore and Long [176]), whereas others preferred u_* (Kato and Phillips [137], Kantha et al. [136]). Pollard et al. [192] claimed that shear instability at the bottom of the mixed layer does most significantly contribute to entrainment and suggested to scale generally with ΔU.

Niiler [183] clarified the situation somewhat by showing that models of the Kraus-Turner type, which use a u_* scaling (like the models of Turner and Kraus [274] and Denman [60]) can be used with benefit for the long term prediction of thermocline erosion, if large time-steps are used. However, for the prediction of the short term reaction to wind forcing, these models do not capture the right physics and lead to inaccurate results. Niiler [183] suggested a combination of the model of Denman [60] and of a ΔU scaled model like that of Pollard et al. [192].

Motivated by observations in the ocean (see Price et al. [196]) exhibiting strong evidence for the entrainment scaled with ΔU rather than u_*, Price [195] could show that the differences between the classical experiments of Kato and Phillips [137] and Kantha et al. [136] were mainly due to the wrong scaling. Using ΔU as the most appropriate scale (and correcting for the influence of the side-wall drag), Price [195] was able to collapse the two experiments and also the buoyant jet data of Ellison and Turner [69] for a small range of bulk Richardson numbers.

Albeit there is up to the present day no agreement about the functional form of the entrainment law (and hence about the most crucial closure assumption of bulk models), numerous successful applications of these models in limnological situations have been reported. One of the most advanced bulk-integrated models, DYRESM, is described in Imberger and Patterson [120]. It uses a synthesis of the entrainment models of Niiler [183] and Zeman and Tennekes [304] as described in a review article of Sherman et al. [222]. Spigel et al. [240] and Imberger [116] extended the model

further to retain the average mixed layer turbulent kinetic energy as an explicit variable. This, and the inclusion of a parameterization of Kelvin-Helmholtz billowing using the results of some experiments by THORPE [263, 264, 265, 266], were shown to be important if time-steps shorter than a day are used and the forcing varies strongly.

HAMILTON AND SCHLADOW [97, 216] claim that DYRESM is a model free of calibration and use it as the hydrodynamic component of their water quality model. A much simpler model of the Kraus-Turner type with u_* scaling has been implemented by FRANKE ET AL. [77] in their coupled model. However, since time-steps of much less than a day were used and also periods of strongly varying winds were modelled (both cases in which standard Kraus-Turner type models are strictly not applicable), it is not clear, if the physics is sufficiently represented in that case.

Bulk integrated or mixed layer models have also been implemented in three-dimensional models of the ocean (CHEN ET AL. [44] and STERL AND KATTENBERG [246]) and of lakes (see the very recent publication by HODGES ET AL. [108]).

3.3 Differential Models

A different class of models was also applied with great success in meteorology, oceanography and later in physical limnology. EKMAN [68] can be considered the pioneer of the so-called *differential models* used in oceanography. In contrast to their integrated counterparts, these models try to resolve the structure of the mixed (better: mixing) layer and describe it by differential equations. MUNK AND ANDERSON [180] generalized the results of EKMAN [68] by suggesting a dependence of the vertical turbulent diffusivity on the Richardson number, an approach that is used until today in numerous models with some success (see, e.g., PACANOWSKI AND PHILANDER [187]).

However, a much more powerful family of differential turbulence closures applied in oceanography and atmospheric sciences evolved together with the rapid success in second-order turbulence modelling during the seventies of the last century. It was not surprising that early applications in oceanography (e.g., MELLOR AND DURBIN [165]) and physical limnology (SVENSSON [249, 250]) emanated from the institutes dominating turbulence research at that time, namely Princeton and the Imperial College in London.

Today, there is an almost uncountable list of successful geophysical applications of differential models. However, since differential methods have often been critisized by the

advocators of integral methods until very recently (e.g., HODGES ET AL. [108]), it seems necessary to review some of the arguments to clarify the relative merits of both types of models:

- The exact prediction of the mixed layer depth is one of the main purposes of turbulence models for the mixed layer. The capabilities of bulk integrated models in simulating the depth of the mixed layer has been demonstrated many times (e.g. SPIGEL ET AL. [240]). However, also differential models have been shown to compare excellently to the entrainment experiments mentioned above (BURCHARD AND BOLDING [28], LUYTEN ET AL. [156]). In spite of this, differential models are known to yield too shallow mixed layer depths in real-world simulations (MARTIN [160], LARGE AND CRAWFORD [145]). This problem has been recognized by MELLOR [164], who very recently suggested a modification of the Mellor-Yamada model that partly removed this deficiency.

- Local turbulent variables of a differential model can be integrated to yield bulk parameters, but no local values can be derived from the integrated models. This means that differential models can be verified with both, measured bulk parameters and local turbulent parameters obtained from measurements. Since it is now widely accepted that turbulence in stratified fluids scales with local parameters (see IVEY AND IMBERGER [125, 118], NIEUWSTADT [182]), a tremendous amount of data recently obtained from measurements and from DNS can be used to compare and calibrate differential models.

- Differential one- and two-equation models are known to be in accordance with the similarity theory of MONIN AND OBUKHOV [175], a cornerstone of turbulence theory (MELLOR AND YAMADA [169], KANTHA AND CLAYSON [135], BURCHARD AND PETERSEN [30]). Besides this, LUYTEN ET AL. [156] showed that at least the k-ϵ model does also reproduce the self-similar structure exhibited in entrainment experiments as suggested by KUNDU [143] and MELLOR AND STRUB [167]. It is shown in Section 4.1.3 that these findings can also be extended to the k-ω model. Bulk models cannot be tested in terms of self-similarity.

- For the three-dimensional modelling of lakes, computing power has increased so far that, together with an adaptable and topography-following vertical grid, a resolution sufficient for the convergence of differential schemes can be achieved (UMLAUF ET AL. [283]). Nevertheless, in ocean modelling a too coarse vertical resolution must still be considered a problem. (EZER [70] for example resolves a 5550m deep water column in the Atlantic ocean with only 15 levels.)

- Franks [78] reviewed physical-biological coupled models and found that both, mixed-layer and differential models have been used with some success in the past. However, a new interesting branch of coupled modelling that focuses on the interaction between small-scale turbulence and biology has started to develop (Capblancq [41], Denman and Gargett [61] and Reynolds [199]). Only the differential models are able to resolve the turbulent parameters required by the biological model and thus can be used as the physical component.

3.4 Two-Equation Models of Turbulence

In view of a widely applicable description of the turbulent length-scale, l, models were developed that use a differential transport equation for l or a related quantity. Two-equation models that use two differential transport equations for both, the turbulent kinetic energy, k, and a length-scale determining variable have proven to be an excellent compromise between accuracy and computational effort. Alternatives to the formulation of a second differential equation have also been suggested. In fact, there has been an enormous development of powerful analytical descriptions for the turbulent length-scales in stratified flows in the last years. These descriptions are usually formulated in terms of local non-dimensional parameters, some of which are conveniently available only in sub-grid models of LES, and thus their applicability to ensemble averaged models is very restricted (Schumann [219], Canuto and Minotti [39], Cheng and Canuto [45]). Very simple analytical formulae like the one of Blackadar [14] or that suggested for the zero- or one-equation models of Mellor and Yamada [168] are also still in use. Their predictions, however, are often not satisfactory.

Among the most well-known two-equation models used in geophysics is the "model of the level 2.5" from the hierarchy of closure schemes successively developed by Mellor and Herring [166], Mellor [163], and Mellor and Yamada [168, 169]. It will from now on be referred to as the *Mellor-Yamada model*. This model uses a length-scale related equation that describes the evolution of the product kl.

Another model that recently attracted great attention in the geophysical modelling community, describes the evolution of the rate of dissipation of turbulent kinetic energy, ϵ. It has originally been developed by Hanjalić and Launder [101], Jones and Launder [132], and Launder and Spalding [148]. Rodi [206] described some geophysical applications of this model that is usually called the k-ϵ model.

There have been numerous applications of one-dimensional versions of the Mellor-Yamada model (e.g., Martin [160], Price et al. [196], Large and Crawford [145], Richardson et al. [201]) and of the k-ϵ model (e.g., Svensson [249, 250], Kundu [142], Omstedt et al. [185], Rodi [206], Baumert and Radach [12], Burchard and Baumert [27], Jöhnk [130]). Quasi-one-dimensional models of both types have also been implemented and tested in well-known ocean circulation models (e.g., Blumberg and Mellor [16], Allen et al. [4], Federiuk and Allen [72], Luyten et al. [156], Stansby [242], Ezer [70]). Also for lakes there are some recent examples of three-dimensional implementations (see, e.g., Güting and Hutter [96]). Beletsky et al. [13] recently reported a highly interesting comparison of a three-dimensional implementation of the Mellor-Yamada model and a simple Richardson number dependent model in a simulation of observed Kelvin waves in Lake Michigan.

Driven by a steadily increasing amount of data describing turbulent properties of stratified flows from field measurements, laboratory experiments, LES, and DNS, there appeared a number of works in the last decade investigating the properties of two-equation models in simple, but from a theoretical viewpoint fundamental flows (Baum and Caponi [10], Craig and Banner [53], Burchard and Baumert [27], Baumert and Peters [11], Burchard and Bolding [28]). Unfortunately, only very few authors conducted a systematic comparison of different two-equation models. Moreover, only the k-ϵ and the Mellor-Yamada model have been compared so far (see Burchard et al. [31], Burchard and Petersen [30]). This work is intending to fill the gap.

One model has been largely unnoticed by the geophysical turbulence modelling community: The model of Wilcox [293, 294], which will be referred to as the k-ω model from now on. This model has been shown to be free of many deficiencies of the Mellor-Yamada model (e.g., its non-locality induced by the wall function) and of the k-ϵ model (e.g., its misbehaviour very close to rigid walls), while sharing all the merits of these models in the case of unstratified fluids. However, the k-ω model has, to my knowledge, not been extended to the case of buoyancy affected flows. As a consequence, its applicability to atmospheric and oceanographic flows was extremely restricted. In this work an extension of the k-ω model to stratified flows will be suggested and the properties of the resulting model will be closely examined.

In the following section all three two-equation models will be briefly introduced. Their mathematical properties will then be compared for homogeneous and density stratified flows. All models will be presented in both, the original formulation used by their respective authors and in an unified form that simplifies the identification of model constants

with the same functionality in different models.

3.4.1 The *k*-ω Model

The equations for this relatively recent model are discussed in WILCOX [293] and WILCOX [294]. They are repeated here for reference:

$$\begin{aligned} \frac{\partial k}{\partial t} + u_l \frac{\partial k}{\partial x_l} &= \frac{\partial}{\partial x_l}\left(\sigma^* \nu_t \frac{\partial k}{\partial x_l}\right) + P - \beta^* k\omega \ , \\ \frac{\partial \omega}{\partial t} + u_l \frac{\partial \omega}{\partial x_l} &= \frac{\partial}{\partial x_l}\left(\sigma \nu_t \frac{\partial \omega}{\partial x_l}\right) + \alpha \frac{\omega}{k} P - \beta \omega^2 \ , \end{aligned} \tag{3.2}$$

where the variable ω described by the second equation can be interpreted as a turbulent frequency or an inverse time-scale of the energy containing eddies. β and β^* may be functions of the mean flow and turbulent properties, but σ and σ^* are simply constants. Note, that the original version of the model is not applicable to buoyancy affected flows.

As mentioned above, all models will be converted to a unified notation (borrowed from the standard k-ϵ literature) to simplify the comparison of the model structure. If necessary, constants will be subscripted, e.g., with an ω as in $c_{\omega 1}$ to make it clear that this constant belongs to the k-ω model and plays a role comparable to the constant c_1 in the standard k-ϵ notation.

Translated to unified form, (3.2) reads

$$\begin{aligned} \frac{\partial k}{\partial t} + u_l \frac{\partial k}{\partial x_l} &= \frac{\partial}{\partial x_l}\left(\nu_k^{\omega} \frac{\partial k}{\partial x_l}\right) + P + G - \epsilon \ , \\ \frac{\partial \omega}{\partial t} + u_l \frac{\partial \omega}{\partial x_l} &= \frac{\partial}{\partial x_l}\left(\nu_{\omega} \frac{\partial \omega}{\partial x_l}\right) + \frac{\omega}{k}(c_{\omega_1} P + c_{\omega_3} G - \frac{c_{\omega_2}}{f_{c_\mu}}\epsilon) \quad . \end{aligned} \tag{3.3}$$

The unified model (3.3) contains already the suggested extension to buoyancy affected flows. The extension of the equation for k is straightforward and follows directly from (2.11). The fruitfulness of the extension suggested for the transport equation of ω will be discussed in greater detail below.

The k-ω model in its revised form recently suggested by WILCOX [294] contains the two parameter functions called f_{c_μ} and f_{c_ω} in unified notation. They are defined by

$$\epsilon = (c_\mu^0)^4 f_{c_\mu} k\omega \tag{3.4}$$

$$f_{c_\mu} = \begin{cases} 1 & \chi_k \leq 0 \\ \frac{1+680\chi_k^2}{1+400\chi_k^2} & \chi_k > 0 \end{cases}, \quad \chi_k = \frac{1}{\omega^3}\frac{\partial k}{\partial x_j}\frac{\partial \omega}{\partial x_j} \tag{3.5}$$

$$c_{\omega 2} = c^0_{\omega 2} f_{c_\omega}, \quad f_{c_\omega} = \frac{1+70\chi_\omega}{1+80\chi_\omega}, \quad \chi_\omega = \left|\frac{W^*_{ij}W^*_{jl}S_{li}}{(c^0_\mu)^1 2\omega^3}\right|, \tag{3.6}$$

where S_{ij} and W^*_{ij} as defined in (2.17) have been used [2].

The traditional WILCOX [293] model can be recovered by setting $f_{c_\mu} = f_{c_\omega} = 1$. The function f_{c_μ} was intended by WILCOX [294] to reduce the somewhat too large spreading rate for free shear layers by enhancing the dissipation near the edge of the layer, but leaving the flow close to the boundary almost untouched. f_{c_ω} was introduced to treat the so-called round-jet/plane-jet anomaly known to be a plague for every turbulence model. WILCOX [294] demonstrated convincingly that his new k-ω model retains the superiority of the older version over the k-ϵ model for wall bounded flows and, in addition, is now also better suited for the prediction of standard jet and shear entrainment situations. It will be very interesting to see how this promising model behaves in scenarios of geophysical interest.

If the k-ω and other two-equation models are applied to the logarithmic part of the law-of-the-wall, useful relationships between different model variables and the parameter c^0_μ can be obtained. To derive these relationships, one has to use the well-known asymptotic behaviour of the turbulent variables in the logarithmic boundary layer $P = \epsilon$, $\epsilon = u_*^3/\kappa z$, $\partial U/\partial z = u_*/\kappa z$, $l = \kappa z$, etc., where κ is the von Kármán constant and z the distance perpendicular to the wall. The turbulent length-scale, l, is seen to coincide with the Prandtl mixing length close to a wall. (Note, that the scale l is different from a length-scale with the same name sometimes used in WILCOX [294]). For the constant c^0_μ, usually referred to as Bradshaw's constant, the relation $(c^0_\mu)^2 = u_*^2/k$ can be shown to hold in the logarithmic boundary layer. Its value is known to be about $(c^0_\mu)^2 = 0.3$ from numerous measurements (see TOWNSEND [270]). The following useful relations apply:

$$\begin{aligned} \epsilon &= (c^0_\mu)^4 f_{c_\mu} k\omega, \quad l = \frac{1}{c^0_\mu}\frac{k^{\frac{1}{2}}}{\omega}, \\ \nu_t &= c^\omega_\mu \frac{k}{\omega}, \quad \nu^\omega_k = \frac{\nu_t}{\sigma^\omega_k}, \quad \nu_\omega = \frac{\nu_t}{\sigma_\omega}, \end{aligned} \tag{3.7}$$

where σ^ω_k and σ_ω are the turbulent Schmidt numbers for the diffusivities of k and ω, respectively. The function c^ω_μ results from an ASM as shown above. All model constants can be found in Tab. 3.1.

[2] The original model uses the in-objective tensor W_{ij} in place of W^*_{ij}. As discussed in Chapter 2, such a formulation is inconsistent in rotating flows.

model parameters	c_μ^0	σ_k^ω	σ_ω	$c_{\omega 1}$	$c_{\omega 2}^0$	$c_{\omega 3}$
original parameters	$(\beta_0^*)^{\frac{1}{4}}$	$1/\sigma*$	$1/\sigma$	α	$\beta_0/(c_\mu^0)^4$	—
WILCOX '88 [293]	0.5477	2	2	0.555	0.833	see text
WILCOX '98 [294]	0.5477	2	2	0.52	0.8	see text

Table 3.1: Constants of the k-ω model

3.4.2 The Mellor-Yamada Model

The two-equation version of the Mellor-Yamada models was introduced by MELLOR AND YAMADA [169]. They referred to it as the "level 2.5" of their hierarchy of turbulent closures reaching from simple equilibrium models to a full second-order closure. In its original form it was written as

$$\begin{aligned} \frac{\partial q^2}{\partial t} + u_l \frac{\partial q^2}{\partial x_l} &= \frac{\partial}{\partial x_l}\left(l q S_q \frac{\partial q^2}{\partial x_l} \right) + 2(P + G - \frac{q^3}{B_1 l}) \, , \\ \frac{\partial q^2 l}{\partial t} + u_l \frac{\partial q^2 l}{\partial x_l} &= \frac{\partial}{\partial x_l}\left(l q S_l \frac{\partial q^2 l}{\partial x_l} \right) + l E_1 (P + G) - \frac{F q^3}{B_1} \quad . \end{aligned} \tag{3.8}$$

Noting that $q^2 := 2k$ this model can be transformed to the unified form and re-written as

$$\begin{aligned} \frac{\partial k}{\partial t} + u_l \frac{\partial k}{\partial x_l} &= \frac{\partial}{\partial x_l}\left(\nu_k^l \frac{\partial k}{\partial x_l} \right) + P + G - \epsilon \, , \\ \frac{\partial kl}{\partial t} + u_l \frac{\partial kl}{\partial x_l} &= \frac{\partial}{\partial x_l}\left(\nu_l \frac{\partial kl}{\partial x_l} \right) + l(c_{l1} P + c_{l3} G - c_{l2} F \epsilon) \quad . \end{aligned} \tag{3.9}$$

By inspection of the second equation of (3.8) it is clear that the model constants c_{l1} and c_{l3} are not independent. In fact, for the lack of precise data MELLOR AND YAMADA [169] chose them to be equal. As discussed below this decision has a large negative impact on the model performance in stratified shear flows (see also BURCHARD [24]).

The Mellor-Yamada model only reproduces the logarithmic region of the law-of-the-wall, if the wall damping function, F, is described according to

$$F = 1 + E_2 \left(\frac{l}{\kappa L} \right) \, , \tag{3.10}$$

where the new model constant has been assigned a value $E_2 = 1.33$ by MELLOR AND YAMADA [169]. L is supposed to be a measure of the distance away from the wall that has to converge to $L = z$ as the wall is approached. Of course, the functional choice is otherwise little restricted and there are many alternatives. Unfortunately, different

choices for L may result in considerably different results even at remote distances from walls. BURCHARD ET AL. [31] compared a triangular and a parabolic profile for L and demonstrated that in the simulation of a simple barotropic channel flow the velocities in the middle of the channel could differ as much as 30%. The non-uniqueness and non-locality introduced by the wall damping function has to be considered a large drawback of the Mellor-Yamada model.

The rate of dissipation and the turbulent diffusivities are defined as

$$\begin{aligned} \epsilon &= (c_\mu^0)^3 \frac{k^{\frac{3}{2}}}{l} , \\ \nu_t &= c_\mu^l k^{\frac{1}{2}} l , \quad \nu_k^l = c_k^l k^{\frac{1}{2}} l , \quad \nu_l = c_l k^{\frac{1}{2}} l \quad . \end{aligned} \tag{3.11}$$

The revised model constants of MELLOR AND YAMADA [169] have been converted to the notation used here and are given in Tab. 3.2. Their relation to the original parameters is also displayed.

model parameter	c_μ^0	c_k^l	c_l	c_{l1}	c_{l2}	c_{l3}
original parameters	$2^{\frac{1}{2}} B_1^{-\frac{1}{3}}$	$2^{\frac{1}{2}} S_q$	$2^{\frac{1}{2}} S_l$	$E_1/2$	by insp.	$E_1/2$
MELLOR AND YAMADA [169]	0.5544	0.2828	0.2828	0.9	0.5	0.9

Table 3.2: Constants of the Mellor-Yamada model

3.4.3 The k-ϵ Model

The original k-ϵ model of HANJALIĆ AND LAUNDER [101] is adopted here. However, the triple correlations appearing in the transport equations of k and ϵ are replaced be simple eddy diffusivity formulations also used by RODI [207]. An excellent review of the mathematical properties of the k-ϵ model is given in MOHAMMADI AND PIRONNEAU [171]. This model is usually formulated as

$$\begin{aligned} \frac{\partial k}{\partial t} + u_l \frac{\partial k}{\partial x_l} &= \frac{\partial}{\partial x_l} \left(\frac{\nu_t}{\sigma_k} \frac{\partial k}{\partial x_l} \right) + P + G - \epsilon , \\ \frac{\partial \epsilon}{\partial t} + u_l \frac{\partial \epsilon}{\partial x_l} &= \frac{\partial}{\partial x_l} \left(\frac{\nu_t}{\sigma_\epsilon} \frac{\partial \epsilon}{\partial x_l} \right) + \frac{\epsilon}{k} (c_1 P + c_3 G) - c_2 \frac{\epsilon^2}{k} \quad . \end{aligned} \tag{3.12}$$

The buoyancy term in the transport equation for ϵ is adopted by some authors (RODI [206] and RODI [207]), whereas others refrain from using it (GIBSON AND LAUNDER

[87]). Completely analogous to MELLOR AND YAMADA [169], CRAFT ET AL. [50] set $c_{\epsilon 1} = c_{\epsilon 3}$ and will thus also encounter difficulties in stratified shear flows (see below).

As mentioned above, the unified form is borrowed from the k-ϵ notation, and there is almost no change necessary, and the equations can be re-written as

$$\begin{aligned} \frac{\partial k}{\partial t} + u_l \frac{\partial k}{\partial x_l} &= \frac{\partial}{\partial x_l}\left(\nu_k^\epsilon \frac{\partial k}{\partial x_l}\right) + P + G - \epsilon \,, \\ \frac{\partial \epsilon}{\partial t} + u_l \frac{\partial \epsilon}{\partial x_l} &= \frac{\partial}{\partial x_l}\left(\nu_\epsilon \frac{\partial \epsilon}{\partial x_l}\right) + \frac{\epsilon}{k}(c_{\epsilon 1} P + c_{\epsilon 3} G - c_{\epsilon 2}\epsilon) \end{aligned} \tag{3.13}$$

Again, relations to other model variables can be derived, e.g.,

$$\begin{aligned} l &= (c_\mu^0)^3 \frac{k^{\frac{3}{2}}}{\epsilon} \,, \\ \nu_t &= c_\mu^\epsilon \frac{k^2}{\epsilon} \,, \quad \nu_k^\epsilon = \frac{\nu_t}{\sigma_k^\epsilon} \,, \quad \nu_\epsilon = \frac{\nu_t}{\sigma_\epsilon} \,, \end{aligned} \tag{3.14}$$

where σ_k^ϵ and σ_k denote the Schmidt numbers for k and ϵ, respectively. The relations to the original model parameters given in Tab. 3.3 are trivial. For the constant c_3 there have been numerous suggestions, which will be discussed in the following sections.

model parameters	c_μ^0	σ_k^ϵ	σ_ϵ	$c_{\epsilon 1}$	$c_{\epsilon 2}$	$c_{\epsilon 3}$
original parameters	$(c_\mu^{\text{orig}})^{\frac{1}{4}}$	σ_k	$\sigma_\epsilon^{\text{orig}}$	c_1	c_2	c_3
k-ϵ (RODI [206])	0.5477	1.0	1.3	1.44	1.92	see text

Table 3.3: Constants of the k-ϵ model

3.4.4 Determination of the Model Constants

In this section the impact of the chosen model constants will be analyzed. An application of each model to standard situations like the logarithmic wall layer or the homogeneous decay of turbulence are considered to be indispensable for a thorough comparison. Moreover, useful results will be obtained that can be referred to during the more elaborate evaluations in later sections.

The Constant Stress Layer

The probably best known "dogma" of turbulence theory is the logarithmic velocity profile of a steady-state current close to a rigid wall, where viscous stresses are negligible (see Ap-

pendix A.1). It is the most elementary requirement that a turbulence model reproduces the logarithmic part of the "law-of-the-wall". Thus, it is not surprising that all models introduced above satisfy this requirement. However, it has been pointed out many times that the model of MELLOR AND YAMADA [168, 169] needs a specific wall damping function, F, to yield the logarithmic layer (see $(3.9)_2$). If the standard expressions applying to the logarithmic region ($(c_\mu^0)^2 k = u_*^2$, $\partial U/\partial z = u_*/(\kappa z)$, $l = \kappa z$, etc.) are inserted in the model equations, the turbulent kinetic energy budget always yields $P = \epsilon$. The second equation of each model leads to an important relation between several model constants, which is sometimes referred to as the "compatibility relation" (see e.g. LAUNDER ET AL. [147], ABID AND SPEZIALE [1]). For the k-ω model, for example, the expression

$$\sigma_\omega = \frac{\kappa^2}{(c_\mu^0)^2 (c_{\omega 2}^0 - c_{\omega 1})} \tag{3.15}$$

can be derived. Similar equations follow for the Mellor-Yamada model with

$$c_l = \frac{\left(c_\mu^0\right)^3 \left(c_{l2}\left(1 + E_2\right) - c_{l1}\right)}{\kappa^2} \,, \tag{3.16}$$

and for the k-ϵ model with

$$\sigma_\epsilon = \frac{\kappa^2}{(c_\mu^0)^2 (c_{\epsilon 2} - c_{\epsilon 1})} \quad . \tag{3.17}$$

These equations can be used to determine the value of the von Kármán constant, κ, for the standard model coefficients or, vice versa, the (inverse) turbulent Schmidt number as a function of a selected κ and other model parameters[3]. It should be pointed out that every reasonable model comparison in the turbulent boundary layer requires each model to compute the same value of the von Kármán constant. Here, all models were tuned to the standard value of $\kappa = 0.4$.

The value of the constant c_μ^0 has to be consistent with the ASM used. Tab. 3.4 summarizes some model constants that satisfy the consistency relations. Note, that only the Mellor-Yamada model computes a value of $\kappa = 0.4$ with its standard parameter set.

Homogeneous Decay

Another example of a simple but fundamental turbulent situation is the decay of isotropic, homogeneous turbulence. Data from many experiments are well described by a power law

[3] Even though the compatibility relations must be considered an elementary requirement, ABID AND SPEZIALE [1] found that this constraint "has been ignored in the formulation of some recent second-order closures" and pointed out that it "should be made use of more carefully in the future formulation of models".

	k-ω 1988	k-ω 1998	k-kl	k-ϵ
κ orig.	0.408	0.41	0.4	0.433
$\kappa = 0.4$	$\sigma_\omega = 1.92$	$\sigma_\omega = 1.9$	$c_l = 0.28$	$\sigma_\epsilon = 1.11$

Table 3.4: Model parameters consistent with (3.15)–(3.17). The values have been derived by assuming $c_\mu^0 = 0.548$ for the k-ω and the k–ϵ model and $c_\mu^0 = 0.554$ for the Mellor-Yamada model.

of the form

$$\frac{k}{k_0} = A \left(\frac{t}{\tau_0} \right)^n \ , \tag{3.18}$$

with the initial values of the kinetic energy, k_0, and the *eddy turnover time*, τ_0. The decay rates, n, have been thoroughly documented. Experiments (Bradshaw [20], Townsend [270]) suggest that n is in the range $-1.7 < n < -1.1$, with a consensus for a value near -1.2. DNS, generally conducted at low Reynolds numbers, produce consistently higher values. Briggs et al. [21], e.g., obtain a value near -1.5 from their DNS.

For homogeneous decay, two-equation models simplify to a system of two ordinary differential equations describing the homogeneous decay. They can easily be solved by hand or with the help of a symbolic mathematics tool. The k-ω model reduces to the system

$$\frac{\mathrm{d}k}{\mathrm{d}t} = -(c_\mu^0)^4 \, k\omega \ , \quad \frac{\mathrm{d}\omega}{\mathrm{d}t} = -(c_\mu^0)^4 \, c_{\omega 2}^0 \, \omega^2 \ , \tag{3.19}$$

which has the simple solutions

$$k = k_0 \, (\omega_0 \, c_{\omega 2}^0 (c_\mu^0)^4 \, t + 1)^{-\frac{1}{c_{\omega 2}}} \ , \quad \omega = \omega_0 \, (\omega_0 \, c_{\omega 2}^0 (c_\mu^0)^4 \, t + 1)^{-1} \ , \tag{3.20}$$

where ω_0 defines the value of ω at $t = 0$.

In homogeneous turbulence, the wall damping function, F, of the Mellor-Yamada model reduces to unity, and the model equations simplify according to

$$\frac{\mathrm{d}k}{\mathrm{d}t} = -\frac{1}{(c_\mu^0)^3} \frac{k^{\frac{3}{2}}}{l} \ , \quad \frac{\mathrm{d}kl}{\mathrm{d}t} = -\frac{c_{l2}}{(c_\mu^0)^3} k^{\frac{3}{2}} \ , \tag{3.21}$$

for which a solution of the form

$$k = k_0 \left(\frac{(3 - 2c_{l2}) \, k_0^{\frac{1}{2}}}{2(c_\mu^0)^3 \, l_0} \, t + 1 \right)^{-\frac{2}{3-2c_{l2}}} \ , \quad l = l_0 \left(\frac{(3 - 2c_{l2}) \, k_0^{\frac{1}{2}}}{2(c_\mu^0)^3 \, l_0} \, t + 1 \right)^{-\frac{2(c_{l2}-1)}{3-2c_{l2}}} \tag{3.22}$$

can be computed. If a value of $c_{l2} = 0.5$ (which can be obtained by inspection from the original model, see Tab. 3.2) is inserted in (3.22), the solution simplifies further to

$$k = k_0 \left(\frac{k_0^{\frac{1}{2}}}{(c_\mu^0)^3 \, l_0} \, t + 1 \right)^{-1} , \quad l = l_0 \left(\frac{k_0^{\frac{1}{2}}}{(c_\mu^0)^3 \, l_0} \, t + 1 \right)^{\frac{1}{2}} . \tag{3.23}$$

Analogously, the k-ϵ model reduces to

$$\frac{\mathrm{d}k}{\mathrm{d}t} = -\epsilon , \quad \frac{\mathrm{d}\epsilon}{\mathrm{d}t} = -c_{\epsilon 2} \frac{\epsilon^2}{k} , \tag{3.24}$$

with a solution of the form

$$k = k_0 \left(\frac{\epsilon_0}{k_0} \, (c_{\epsilon 2} - 1) \, t + 1 \right)^{\frac{1}{1 - c_{\epsilon 2}}} , \quad \epsilon = \epsilon_0 \left(\frac{\epsilon_0}{k_0} \, (c_{\epsilon 2} - 1) \, t + 1 \right)^{\frac{c_{\epsilon 2}}{1 - c_{\epsilon 2}}} . \tag{3.25}$$

For large times all models predict a decay of the form (3.18). The decay rates for k are summarized in Tab. 3.5. It can be seen that all models compute reasonable results,

	k-ω (1988)	k-ω (1998)	k-kl	k-ϵ
decay rate n	-1.2	-1.25	-1	-1.087

Table 3.5: Decay rates for homogeneous, isotropic, unstratified turbulence as computed by different models

the Mellor-Yamada model exhibiting a decay rate perhaps a bit to slow and the k-ω model being closest to the bulk of the measurements. Note, that in all cases the decay experiments cited above restrict the range of only one model constant, namely $c_{\varphi 2}$ (where φ is either ω, l, or ϵ).

3.4.5 Homogeneously Sheared and Stratified Turbulence

A natural extension of the concept of decaying homogeneous turbulence, be it unstratified as discussed in the previous section or stratified (Dickey and Mellor [64], Lienhard and van Atta [150], Stillinger et al. [247]), is the inclusion of a homogeneous shear and an aligned homogeneous stratification. Since turbulence is still assumed to be homogeneous, the divergence of any turbulent transport terms vanishes and the intricate interplay between the stabilizing effects of stratification and the destabilizing action of shear can be isolated from further complications. Thus, it is not surprising that this highly interesting special case of turbulence has been explored extensively by laboratory experiments (Tavoularis and Courrsin [254, 255], Tavoularis and Karnik [256],

ROHR ET AL. [208]), by Direct Numerical Simulation (GERZ ET AL. [86], HOLT ET AL. [109], JACOBITZ ET AL. [126]) and by Large-Eddy Simulation (KALTENBACH ET AL. [134]).

Naturally, the experimental results also attracted the attention of turbulence modellers seeking for data to verify their closure assumptions. With this idea in mind this section is structured as follows: First, a canonical notation, similar to that used by BAUMERT AND PETERS [11], to which all models can be mapped is introduced. It will be shown that the model coefficients in this notation are subject to simple, but strong restrictions following from analytical reasoning and experiments. Then, the concepts of *Full Equilibrium* (FE) and *Structural Equilibrium* (SE) are developed. The behaviour of different ASMs in form of stability functions will be strictly explored for both cases. From this evaluation emerges the new concept of the "Structural Equilibrium Stability Functions"that is used to show inconsistencies in the theoretical investigations recently published on this topic.

Canonical Representation

Owing to the assumption of homogeneity, the turbulent transport terms vanish and thus exert no influence on the results. Only in this limiting case, all two-equation models considered here are isomorphic. They will be converted to a so-called canonical two-equation model for the variables k and ϵ. This choice was made, since it was felt that most readers are more familiar with the k-ϵ notation than with any other. Apart from this, the choice is completely arbitrary and other pairs of variables could be used.

The k-ω model can be converted to canonical notation after applying the chain rule of differentiation to (3.4) and obtaining

$$\frac{1}{\epsilon}\frac{\mathrm{d}\epsilon}{\mathrm{d}t} = \frac{1}{k}\frac{\mathrm{d}k}{\mathrm{d}t} + \frac{1}{\omega}\frac{\mathrm{d}\omega}{\mathrm{d}t} \quad . \tag{3.26}$$

If the time derivatives on the right hand side of (3.26) are substituted according to (3.3), the canonical form of the k-ω model for homogeneously sheared and stratified turbulence can be written as

$$\begin{aligned} \frac{1}{k}\frac{\mathrm{d}k}{\mathrm{d}t} &= \frac{1}{k}(P+G) - \frac{\epsilon}{k} \,, \\ \frac{1}{\epsilon}\frac{\mathrm{d}\epsilon}{\mathrm{d}t} &= \left[(c_{\omega 1}+1)P + (c_{\omega 3}+1)G\right]\frac{1}{k} - (c^0_{\omega 2}+1)\frac{\epsilon}{k} \quad . \end{aligned} \tag{3.27}$$

With the help of (2.49) the production terms appearing in (3.27) can be conveniently

expressed as

$$P = c_\mu^\epsilon \frac{k^2}{\epsilon} M^2 \quad \text{and} \quad G = -c_\mu^{\epsilon\prime} \frac{k^2}{\epsilon} N^2 \quad . \tag{3.28}$$

Substitution of this result in (3.27) yields

$$\begin{aligned} \frac{1}{k}\frac{\mathrm{d}k}{\mathrm{d}t} &= (c_\mu^\epsilon M^2 - c_\mu^{\epsilon\prime} N^2)\frac{k}{\epsilon} - \frac{\epsilon}{k} \,, \\ \frac{1}{\epsilon}\frac{\mathrm{d}\epsilon}{\mathrm{d}t} &= \left[(c_{\omega 1}+1)c_\mu^\epsilon M^2 - (c_{\omega 3}+1)c_\mu^{\epsilon\prime} N^2\right]\frac{k}{\epsilon} - (c_{\omega 2}^0+1)\frac{\epsilon}{k} \quad . \end{aligned} \tag{3.29}$$

Note that in homogeneous turbulence with plane shear the parameter functions f_{c_μ} and f_{c_ω} appearing in (3.4)–(3.6) are equal to 1.

Applying the chain rule to $(3.11)_1$, an analogous procedure yields the canonical form of the Mellor-Yamada model

$$\begin{aligned} \frac{1}{k}\frac{\mathrm{d}k}{\mathrm{d}t} &= (P+G)\frac{1}{k} - \frac{\epsilon}{k} \,, \\ \frac{1}{\epsilon}\frac{\mathrm{d}\epsilon}{\mathrm{d}t} &= \left[\left(\frac{5}{2}-c_{l1}\right)P + \left(\frac{5}{2}-c_{l3}\right)G\right]\frac{1}{k} - \left(\frac{5}{2}-c_{l2}\right)\frac{\epsilon}{k} \,, \end{aligned} \tag{3.30}$$

which can also be expressed in the form

$$\begin{aligned} \frac{1}{k}\frac{\mathrm{d}k}{\mathrm{d}t} &= (c_\mu^\epsilon M^2 - c_\mu^{\epsilon\prime} N^2)\frac{k}{\epsilon} - \frac{\epsilon}{k} \,, \\ \frac{1}{\epsilon}\frac{\mathrm{d}\epsilon}{\mathrm{d}t} &= \left[\left(\frac{5}{2}-c_{l1}\right)c_\mu^\epsilon M^2 - \left(\frac{5}{2}-c_{l3}\right)c_\mu^{\epsilon\prime} N^2\right]\frac{k}{\epsilon} - \left(\frac{5}{2}-c_{l2}\right)\frac{\epsilon}{k} \,, \end{aligned} \tag{3.31}$$

where the influence of walls has been assumed to be negligible and thus $F = 1$ in (3.9) has been assumed.

The conversion of the k-ϵ model to the canonical notation is obvious and yields

$$\begin{aligned} \frac{1}{k}\frac{\mathrm{d}k}{\mathrm{d}t} &= (P+G)\frac{1}{k} - \frac{\epsilon}{k} \,, \\ \frac{1}{\epsilon}\frac{\mathrm{d}\epsilon}{\mathrm{d}t} &= (c_{\epsilon 1}P + c_{\epsilon 3}G)\frac{1}{k} - c_{\epsilon 2}\frac{\epsilon}{k} \quad . \end{aligned} \tag{3.32}$$

or

$$\begin{aligned} \frac{1}{k}\frac{\mathrm{d}k}{\mathrm{d}t} &= (c_\mu^\epsilon M^2 - c_\mu^{\epsilon\prime} N^2)\frac{k}{\epsilon} - \frac{\epsilon}{k} \,, \\ \frac{1}{\epsilon}\frac{\mathrm{d}\epsilon}{\mathrm{d}t} &= (c_{\epsilon 1}c_\mu^\epsilon M^2 - c_{\epsilon 3}c_\mu^{\epsilon\prime} N^2)\frac{k}{\epsilon} - c_{\epsilon 2}\frac{\epsilon}{k} \quad . \end{aligned} \tag{3.33}$$

Comparison with (3.29) and (3.31) corroborates that all models are indeed isomorphic. Inspection shows, that model parameters are connected by simple relations summarized in Tab. 3.10 below. *(3.33) will thus be referred to as "the" canonical model from now on.*

TENNEKES [257] used (3.33) and $(3.14)_1$ for the unstratified case to obtain an evolution equation for the turbulent length-scale, l. Generalizing his results for stratified cases one obtains

$$\frac{1}{l}\frac{\mathrm{d}l}{\mathrm{d}t} = (c_{\epsilon 2} - \frac{3}{2})\tau^{-1} + [(\frac{3}{2} - c_{\epsilon 1})c_\mu^\epsilon M^2 - (\frac{3}{2} - c_{\epsilon 3})c_\mu^{\epsilon\prime} N^2]\tau \ , \tag{3.34}$$

where $\tau = k/\epsilon$ can be thought of being related to a typical time-scale of turbulence via the autocorrelation time of the velocity fluctuations

$$\tau \sim \frac{1}{\langle u'^2\rangle}\int_0^\infty \langle u'(t)u'(t+\tilde{t})\rangle \mathrm{d}\tilde{t} \quad . \tag{3.35}$$

Noting that

$$\frac{1}{\tau}\frac{\mathrm{d}\tau}{\mathrm{d}t} = \frac{1}{k}\frac{\mathrm{d}k}{\mathrm{d}t} - \frac{1}{\epsilon}\frac{\mathrm{d}\epsilon}{\mathrm{d}t} \ , \tag{3.36}$$

and using (3.32) it is easy to obtain also an evolution equation for τ,

$$\frac{1}{\tau}\frac{\mathrm{d}\tau}{\mathrm{d}t} = \left((1-c_{\epsilon 1})\,P + (1-c_{\epsilon 3})\,G\right)\frac{1}{k} - (1-c_{\epsilon 2})\,\frac{1}{\tau} \quad . \tag{3.37}$$

With the help of (3.28), this equation can be re-written as

$$\frac{1}{\tau}\frac{\mathrm{d}\tau}{\mathrm{d}t} = \left((1-c_{\epsilon 1})\,c_\mu^\epsilon M^2 - (1-c_{\epsilon 3})\,c_\mu^{\epsilon\prime} N^2\right)\tau - (1-c_{\epsilon 2})\,\frac{1}{\tau} \ , \tag{3.38}$$

which depends only on τ, M^2, and N^2. Alternatively, this equation is expressible as

$$\frac{\mathrm{d}\tau}{\mathrm{d}t} = (1-c_{\epsilon 2})\left(\left(\frac{\tau}{\tau_{SE}}\right)^2 - 1\right) \ , \tag{3.39}$$

with

$$\tau_{SE} = \left(\frac{(1-c_{\epsilon 2})}{(1-c_{\epsilon 1})\,c_\mu^\epsilon M^2 - (1-c_{\epsilon 3})\,c_\mu^{\epsilon\prime} N^2}\right)^{\frac{1}{2}} \quad . \tag{3.40}$$

(3.38) and (3.39) are non-linear ordinary differential equations. Note, that τ_{SE} is a constant only in Structural Equilibrium (see below). In general, it depends on τ via the non-dimensional numbers α_M and α_N introduced by the stability functions, and a particular solution of (3.39) can only be found by numerical integration. Nevertheless, if it is assumed that deviations from Structural Equilibrium are small and τ_{SE} can be assumed to be constant, an analytical solution of the dimensionless form

$$\frac{\tau}{\tau_{SE}} = \frac{\frac{\tau_{SE}+\tau_0}{\tau_{SE}-\tau_0} - \exp\left(-2\,(c_{\epsilon 2}-1)\,\frac{t}{\tau_{SE}}\right)}{\frac{\tau_{SE}+\tau_0}{\tau_{SE}-\tau_0} + \exp\left(-2\,(c_{\epsilon 2}-1)\,\frac{t}{\tau_{SE}}\right)} \tag{3.41}$$

can be derived.

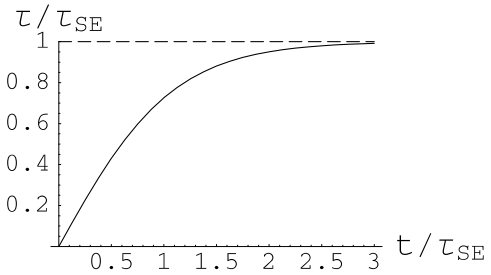

Figure 3.1: Dimensionless solution (3.41) for $\tau_0 = 0$ and $c_{\epsilon 2}$ of the k-ϵ model.

From (3.41) it is seen that the exponential terms approach zero with a time-scale of approximately $\tau_{SE}/2$ *independently of the initial conditions*, since $c_{\epsilon 2} \approx 2$ for all models considered here. From a similar result obtained by a perturbation method, BAUMERT AND PETERS [11] concluded that $\tau \to \tau_{SE}$ with the same time-scale. The exact solution of (3.39) for $\tau_{SE} = \text{const}$ is given by (3.41). If this solution is plotted as in Fig. 3.1 the actual relaxation time-scale is seen to be somewhat larger than $\tau_{SE}/2$. A careful investigation of this topic, including also some numerical results, can be found in BURCHARD [26].

Full Equilibrium in Stably Stratified Flows

Assuming that there is a state of Full Equilibrium (FE) in homogeneous turbulence, i.e., a state of zero growth or decay of any turbulent parameter, the balance equation for the turbulent kinetic energy of the canonical model (3.33) simplifies to

$$\begin{aligned} P + G &= \epsilon \quad \text{or} \\ c_\mu^\epsilon \alpha_M - c_\mu^{\epsilon\,\prime} \alpha_N &= 1 \quad . \end{aligned} \tag{3.42}$$

However, (3.42) is only a necessary condition for FE. In the context of the canonical model, a second constraint is given by requiring that the right hand side of $(3.32)_2$ is also zero in FE. Application of the equilibrium $(3.42)_1$ then yields

$$c_{\epsilon 2} = c_{\epsilon 1} \frac{P}{P+G} + c_{\epsilon 3} \frac{G}{P+G} \; , \tag{3.43}$$

which, using the definitions of the flux Richardson number, R_f, and the gradient Richardson number, Ri,

$$Ri := \frac{N^2}{M^2} = \frac{\alpha_N}{\alpha_M} \quad \text{and} \quad R_f := -\frac{G}{P} = \frac{c_\mu^{\epsilon\,\prime}}{c_\mu^\epsilon} \frac{\alpha_N}{\alpha_M} = \frac{c_\mu^{\epsilon\,\prime}}{c_\mu^\epsilon} Ri \; , \tag{3.44}$$

can be transformed to the simple statements

$$R_f = R_f^{st} = \frac{c_{\epsilon 2} - c_{\epsilon 1}}{c_{\epsilon 2} - c_{\epsilon 3}} \; , \quad Ri = Ri_{st} = \frac{c_\mu^\epsilon}{c_\mu^{\epsilon\,\prime}} \frac{c_{\epsilon 2} - c_{\epsilon 1}}{c_{\epsilon 2} - c_{\epsilon 3}} \quad \text{in FE} \quad . \tag{3.45}$$

Hence, *two-equation models predict FE in homogeneous turbulence only for a single so-called steady-state Richardson number, $Ri = Ri_{st}$.* This is confirmed by the experiments of ROHR ET AL. [208], who observed $Ri_{st} \approx 0.25$. More recent investigations by HOLT ET AL. [109] and PICCARILLO AND VAN ATTA [191], however, showed a systematic dependence of Ri_{st} on the Taylor microscale Reynolds number, Re_λ, an effect that cannot be expected to be captured by the high Reynolds number models used here. A more serious deficiency of two-equation models seems to be the failure of predicting a dependence of Ri_{st} on the initial dimensionless shear number, $\sqrt{\alpha_M}$, introduced in (2.55). Such a dependence is strongly suggested by the recent DNS results of JACOBITZ ET AL. [126]. These authors demonstrated that also all other key quantities in structural equilibrium (e.g., the growth rate and the dimensionless anisotropies) depend on the initial value of $\sqrt{\alpha_M}$ (see next subsection). Unfortunately, there seems to be no obvious way to modify turbulent closures accordingly.

The Structural Equilibrium in Stably Stratified Flows

An important generalization of the FE is the so-called Structural Equilibrium (SE) that is reached, when the left hand sides of (3.38) or (3.39) become zero. Clearly, FE is a special case of SE. The term "Structural Equilibrium" was introduced first in the context of homogeneously sheared, unstratified flows (see e.g. SPEZIALE [239]). In accordance with most other authors, it is used here analogously also for stratified flows, even though flows of this type were realized much earlier without assigning a particular name to them. The basic physics for passively stratified flows in SE have first been successfully described by the experiments of TAVOULARIS AND CORRSIN [254, 255] (also see TAVOULARIS AND KARNIK [256]). Buoyancy affected flows have been produced successfully in the laboratory experiments by ROHR ET AL. [208].

SE is established mathematically by noting that for any constant and homogeneous stratification, N, and shear, M, the value of τ approaches τ_{SE} for large times. As shown above, perturbations to SE relax back exponentially to SE with a time-scale of approximately $2\tau_{SE}$. Thus, in SE (3.37) and (3.38) simplify to

$$\begin{aligned} (1-c_{\epsilon 2}) &= (1-c_{\epsilon 1})\frac{P}{\epsilon} + (1-c_{\epsilon 3})\frac{G}{\epsilon} \qquad \text{or} \\ (1-c_{\epsilon 2}) &= (1-c_{\epsilon 1})c_\mu^\epsilon \alpha_M - (1-c_{\epsilon 3})c_\mu^{\epsilon\prime}\alpha_N \ , \end{aligned} \tag{3.46}$$

respectively.

The Role of the Richardson Number

It is clear that the stability functions in the form (2.53) can be converted to functions of Ri and α_M simply by using the definition (3.44) of the gradient Richardson number, Ri, and writing $\alpha_N = Ri\,\alpha_M$. Along with this idea an interesting question arises: Are there flows described by the models, for which the stability functions reduce to pure functions of Ri, i.e. for which the explicit dependence on the shear number, α_M drops out? That this is indeed the case has been demonstrated more than a decade ago by GALPERIN ET AL. [80] for turbulence in FE. In their derivation (see Section 2.3) the quasi-equilibrium assumption was used extensively and stability functions that can be written solely in terms of Ri emerged. Since in FE the equilibrium $P + G = \epsilon$ necessarily holds, these functions then coincide with the full ASM.

In contrast, for the case of SE, stability functions with a pure Ri dependence have not yet been introduced. Given the importance of homogeneous turbulence in SE, such stability functions should provide a highly interesting analytical tool. In the following, it will be demonstrated, how SE stability functions can be obtained by the use of symbolic algebra.

To derive stability functions for both, FE and SE, one can formally solve $(3.42)_2$ and $(3.46)_2$, respectively, for α_M according to

$$\alpha_M = f_1(\alpha_N)\ , \quad Ri = \frac{\alpha_N}{\alpha_M} = \frac{\alpha_N}{f_1(\alpha_N)} = f_2(\alpha_N)\ , \tag{3.47}$$

since both, c_μ^ϵ and $c_\mu^{\epsilon\prime}$ are only functions of α_N and α_M. Clearly, the functions f_1 and f_2 are different for FE and SE and will depend on the ASM chosen. Moreover, in SE they will also depend on the model constants $c_{\epsilon1}, c_{\epsilon2}$ and $c_{\epsilon3}$ of the canonical model, since these constants appear in $(3.46)_2$. If the relation $(3.47)_2$ is inverted and inserted in $(3.47)_1$ one obtains

$$\alpha_N = f_2^{-1}(Ri) = \check{\alpha}_N(Ri) \quad \text{and} \quad \alpha_M = f_1(\check{\alpha}_N(Ri)) = \check{\alpha}_M(Ri) \quad . \tag{3.48}$$

It follows that not only in FE, but also in SE the stability functions can be expressed in terms of the gradient Richardson number, Ri, without loss of generality. The validity of

$$c_\mu^\epsilon = \check{c}_\mu^\epsilon(Ri) \quad \text{and} \quad c_\mu^{\epsilon\prime} = \check{c}_\mu^{\epsilon\prime}(Ri) \quad . \tag{3.49}$$

in SE is a new result. Note again, that the functional form of (3.49) will change from FE to SE and depends on the model constants $c_{\epsilon1}, c_{\epsilon2}$ and $c_{\epsilon3}$ and the ASM used.

To avoid confusion, at this point it seems worthy to review some of the general properties of the FE and the newly derived SE stability functions and clarify things to the reader.

- Stability functions resulting from the full ASM (2.39)–(2.48) without assuming quasi-equilibrium at any point are referred to as the non-equilibrium stability functions.

- Quasi-equilibrium stability functions can be derived from the ASM (2.39)–(2.48) by assuming the equilibrium $P + G = \epsilon$ in deriving the ASM (in a manner laid out in Section 2.3). However, *the same* quasi-equilibrium stability functions are obtained if one uses $P + G = \epsilon$ in the form $(3.47)_1$ and replaces α_M in the non-equilibrium stability functions by a function of α_N.

- Starting from the quasi-equilibrium functions and assuming quasi-equilibrium once more, α_N appearing in the quasi-equilibrium stability functions can be replaced by a function of Ri according to $(3.48)_1$. The resulting functions will be referred to as the *FE stability functions* from now on. Since the quasi-equilibrium assumption has been invoked anyway, both, the quasi-equilibrium and the FE stability functions contain the same physical information. (However, they will behave differently in different flows, see below!)

- Analogously, (3.48) (now derived for SE!) can be used to replace α_N and α_M in the non-equilibrium stability functions by functions of Ri. The result is referred to as the *SE stability functions*, which then also depend only on Ri.

- Apart from the FE and SE versions, yet another set of stability functions depending only on Ri can be derived: If $(3.48)_1$ (derived for SE!) is used to replace α_N in the quasi-equilibrium functions by a function of Ri, as set of stability functions referred to as the *SEE stability functions* can be obtained.

All in all there are 5 different sets of stability functions now: The non-equilibrium and the quasi-equilibrium versions (which are functions of α_N and, in the former case, also of α_M), and the FE, SE, SEE derivatives of them, which are functions of Ri. Stability functions are used in their Richardson number depending form mostly for theoretical discussions of their properties. In model codes almost exclusively non-equilibrium and quasi-equilibrium versions that depend on α_N and α_M are implemented. The interesting question arises, how these functions are related to each other in the important case of SE. The answer is as follows:

- The SE(Ri) versions describe the behaviour of the non-equilibrium stability functions in SE. This means that in SE they are completely equivalent to the full ASM.

- The SEE(Ri) versions describe the behaviour of the quasi-equilibrium stability functions in SE. Thus, comparing them to the SE versions, an estimate of the error computed by invoking the quasi-equilibrium assumption in SE can be obtained.

- The FE(Ri) versions represent the behaviour of the quasi-equilibrium stability functions in situations where $P + G = \epsilon$. Moreover, in such situations results computed by them coincide with results from the complete ASM (and even from the complete second-order closure). An example of $P + G = \epsilon$ (being of some relevance in oceanography and physical limnology) is given in Fig. 4.7 below, which shows the budget of the turbulent energy equation in a stratified entrainment experiment. In SE, however, the behaviour of the FE(Ri) versions cannot be exactly defined.

The Evaluation of Stability Functions in SE

The ease of using stability functions (in contrast to solving a complete ASM) has attracted many researchers, and it is no wonder that a large number of different stability functions is implemented in oceanographic (and atmospheric) models. Three sets of stability functions, each of them typical of a certain class of models introduced in Section 2.3, will be considered here[4]. The first set consists of the relatively simple stability functions of KANTHA AND CLAYSON [135] (referred to as "KC"), which are a derivative of the original functions of MELLOR AND YAMADA [169]. The second set has been published by LUYTEN ET AL. [156] ("LDOR") and contains the full pressure-strain model of LAUNDER ET AL. [147]. As discussed in Section 2.3, both sets are unstable in their non-equilibrium forms and hence only the quasi-equilibrium versions will be discussed. The third set has been designed by CANUTO ET AL. [38] ("CHCD") and is based on an ASM that constitutes, according to the authors, the state-of-the-art of turbulence models of this type. Apart from this, it seems to be the only available stable set of non-equilibrium stability functions. The three sets are expressed by (2.58), (2.59), and (2.60), respectively.

The traditional approach to analyse stability functions, is to convert their quasi-equilibrium forms to the respective FE forms and display them as functions of the Richardson number, Ri. This idea will be adopted here for the moment, however, only to show its deficiencies. Fig. 3.2 illustrates that in this case the KC and LDOR stability functions behave quite similarly, in spite of the fact that they are based on different model families. The CHCD functions, however, greatly depart from the others. The value attained by them for zero stratification is clearly smaller than the standard value ($c_\mu^\epsilon = 0.09$), but

[4]Model coefficients used in their derivation can be found in Tab. 2.1 and Tab. 2.2.

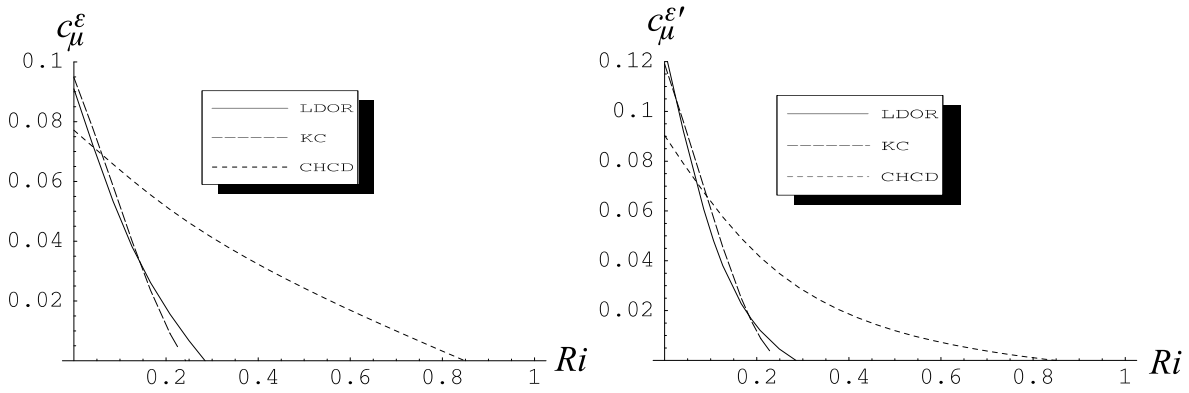

Figure 3.2: The FE stability functions of Luyten et al. [156] (LDOR), Kantha and Clayson [135] (KC), and Canuto et al. [38] (CHCD) as functions of the Richardson number, Ri.

the most remarkable feature is the large value of Ri_{cr}, the critical Richardson number for which the complete extinction of turbulence is predicted. Tab. 3.6 corroborates this fact. It also shows that the LDOR model allows for mixing at a slightly larger Ri_{cr} compared to the KC model.

	LDOR	KC	CHCD
Ri_{cr}	0.284	0.242	0.849

Table 3.6: The traditional critical Richardson number, Ri_{cr}, as predicted by different FE stability functions.

An impression of the behaviour of the new SE version of the CHCD stability functions can be gained by inspection of the left panel of Fig. 3.3, which illustrates the dependence of α_N and α_M on the Richardson number, Ri, as suggested by (3.48). Two points are noticeable: First, as in FE, the existence of a critical Richardson number in SE, Ri_{cr}^{SE}, at which α_N and α_M become infinite and thus all turbulence is damped out, is suggested by the left panel of Fig. 3.3. Second, in the unstratified case, $\alpha_N = 0$, $(3.46)_2$ simplifies to

$$c_\mu^\epsilon(\alpha_M) = \frac{1 - c_{\epsilon 2}}{\alpha_M (1 - c_{\epsilon 1})} \,, \tag{3.50}$$

which is a simple non-linear equation that can be solved for α_M. Hence, the model predicts that SE in the unstratified case occurs only for a single, universal value of the shear number, $M\frac{k}{\epsilon} = \sqrt{\alpha_M}$. This is in accordance with many experiments (see Tavoularis and Karnik [256] and Abid and Speziale [1]). Wilocx [294], pp. 296, summarizes

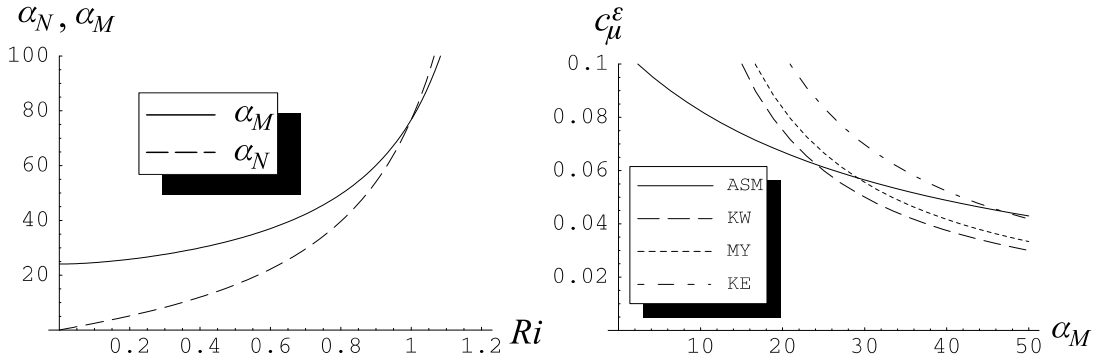

Figure 3.3: Left panel: α_N and α_M as functions of Ri in SE for the CANUTO ET AL. [38] ASM used with the k-ω model. Right panel: Graphical solutions for the SE value of α_M for unstratified flows and different two-equation models. (KW=k-ω, MY= Mellor-Yamada, KE=k-ϵ).

the findings and suggests that the measured value is about $\alpha_M \approx 25$. It is obvious from (3.50) that the value of α_M predicted by the model depends on the model parameters. Tab. 3.7 illustrates that, using the CHCD stability functions, this value is best met with the coefficients of the k-ω model.

	KW88	MY	KE
α_M	25.18	29.1	46.85

Table 3.7: Solutions of (3.50) for $\alpha_M = (M\frac{k}{\epsilon})^2$ for the CHCD stability functions compared for different two-equation models. The experimental value is about $\alpha_M \approx 25$. (KW88=k-ω 1988, MY= Mellor-Yamada, KE=k-ϵ)

It is also instructive to look at a graphical solution of (3.50). To this end, the CHCD stability function c_μ^ϵ for unstratified flows is plotted together with the SE restriction condition (3.50) for different models in the right panel of Fig. 3.3. At the intercept points of the restriction conditions with the stability function, the α_M values of Tab. 3.7 can be recovered. The corresponding values of c_μ^ϵ are in the interval $0.04 \leq c_\mu^\epsilon \leq 0.07$, remote from the value of the standard k-ϵ model, $c_\mu^\epsilon = 0.09$. Fig. 3.3 also illustrates, that the position of the intercept point for the k-ϵ model is very sensitive to small changes in both, the model parameters and the ASM. It is rather unphysical that a slightly different ASM could result in a very different value of α_M, one of the most important parameters in unstratified homogeneous shear flow. Hence, in the unstratified case of SE the ASM of CHCD should be used together with the k-ω model (or the coefficient $c_{\epsilon 2}$ of the k-ϵ model should be modified to yield a reasonable shear number, $\sqrt{\alpha_M}$, in SE).

The steady state Richardson number, Ri_{st}, at which there is neither growth nor decay of stratified turbulence, follows from (3.45). It depends on the model parameters, $c_{\epsilon 1}$, $c_{\epsilon 2}$ and, in particular, on $c_{\epsilon 3}$. In that sense, (3.45) constitutes a means of determining $c_{\epsilon 3}$, once the stability functions, the model parameters $c_{\epsilon 1}$, $c_{\epsilon 2}$ and the steady-state Richardson number, Ri_{st}, have been fixed.

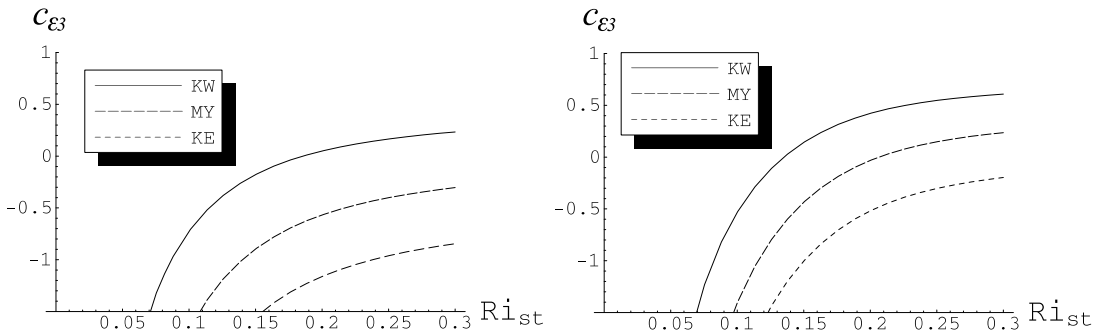

Figure 3.4: Model parameter $c_{\epsilon 3}$ as a function of the steady-state Richardson number, Ri_{st}, for the LDOR (left panel) and the KC (right panel) stability functions and different two-equation models. (KW=k-ω 1988, MY= Mellor-Yamada, KE=k-ϵ)

The dependence of $c_{\epsilon 3}$ on Ri_{st} is displayed in Fig. 3.4 for two ASMs. Precise values for all models considered are given in Tab. 3.8. It is obvious that the value of $c_{\epsilon 3}$ strongly depends on the model parameters $c_{\epsilon 1}$ and $c_{\epsilon 2}$, i.e. on the two-equation model used. This clearly contradicts Baumert and Peters [11], who argued that the canonical values of $c_{\epsilon 1}$ and $c_{\epsilon 2}$ should be very similar for all models and hence a general condition for $c_{\epsilon 3}$, valid for all models, should be derivable. In contrast to them, it is shown here that small differences in $c_{\epsilon 1}$ and $c_{\epsilon 2}$ have an influence on $c_{\epsilon 3}$ that is at least comparable to the influence of the different stability functions themselves. E.g., in the case of the k-ω model the condition $c_{\epsilon 3} < 0$ (equation (78) of Baumert and Peters [11]) excludes the physically most interesting values of Ri_{st} for some sets of stability functions (see Tab. 3.8).

$c_{\epsilon 3}$	LDOR ($Ri_{st} = 0.25$)	LDOR ($Ri_{st} = 0.15$)	KC ($Ri_{st} = 0.20$)	CHCD ($Ri_{st} = 0.25$)	CHCD ($Ri_{st} = 0.15$)
KW88	0.166	−0.178	0.422	0.358	−0.198
MY	−0.401	−0.896	−0.032	−0.124	−0.925
KE	−0.961	−1.556	−0.518	−0.629	−1.589

Table 3.8: Model parameter c_3 in structural equilibrium for different steady-state Richardson numbers, Ri_{st}, and different models. (KW88=k-ω 1988, MY= Mellor-Yamada, KE=k-ϵ)

Note also, that the choice $c_{\epsilon 1} = c_{\epsilon 3} = 1.6$ suggested by MELLOR AND YAMADA [168, 169] yields a model that computes a Ri_{st} far from the physically meaningful range (also see BURCHARD [24]). From the arguments used above it should be clear that the value of the constant c_3 must be carefully re-computed for each model and each ASM in order to assure a well-defined steady-state Richardson number.

The question addressed above, whether in SE, like in FE, there also exists a critical Richardson number, Ri_{cr}^{SE}, at which the model predicts the complete extinction of turbulence, can be answered now, as the values of $c_{\epsilon 3}$ can be determined for all models (if the value of Ri_{st} is fixed). Looking for singularities of the form $\alpha_N, \alpha_M \to \infty$ when $Ri \to Ri_{cr}^{SE}$ in the analytical expressions (3.48) (an illustration of (3.48) is given in the left panel of Fig. 3.3), the values of Ri_{cr}^{SE} compiled in Tab. 3.9 can be derived.

Two facts should be pointed out: First, the values of Ri_{cr}^{SE} are generally higher than the corresponding values of Ri_{cr}. This shows, particularly in the case of the CHCD stability functions, how important it is, to distinguish between FE and SE stability functions: In many situations a model will continue to mix long after the "theoretical" (or better traditional) limit, Ri_{cr}, is exceeded. Second, the values of Ri_{cr}^{SE} depend heavily on the parameters of the two-equation model. For the CHCD stability functions, e.g., the k-ϵ model predicts a complete suppression of turbulence not before the Richardson number reaches $Ri_{cr}^{SE} = 6.9$, a value certainly beyond the physically reasonable range.

Ri_{cr}^{SE}	LDOR ($Ri_{st} = 0.25$)	LDOR ($Ri_{st} = 0.15$)	KC ($Ri_{st} = 0.20$)	CHCD ($Ri_{st} = 0.25$)
KW88	0.289	0.324	0.253	1.353
MY	0.290	0.339	0.257	1.734
KE	0.294	0.387	0.267	6.908

Table 3.9: Critical Richardson number in SE, Ri_{cr}^{SE}, for different steady-state Richardson numbers, Ri_{st}, and different two-equation models. (KW88=k-ω 1988, MY= Mellor-Yamada, KE=k-ϵ)

With the results obtained above, one is now in the position to obtain three versions of stability functions depending only on Ri: The standard FE version, the new SE version introduced in this section, and also the new SEE version, in which the actual behaviour of the quasi-equilibrium version in SE is manifested. Before the actual stability functions are displayed, however, it is instructive to look at the relations (3.48) that form the basis on which the stability functions are built.

The versions of $(3.48)_1$ that can be derived for quasi-equilibrium and thus lead to the

stability functions displayed in Fig. 3.2, are displayed in Fig. 3.5. It is obvious that for the range of α_N displayed, the CHCD model predicts mixing at substantially higher values of Ri. For $\alpha_N \to \infty$, the values of the traditional critical Richardson number, Ri_{cr}, compiled in Tab. 3.6 will be approached. Recall, that these conclusions apply only to turbulence in equilibrium.

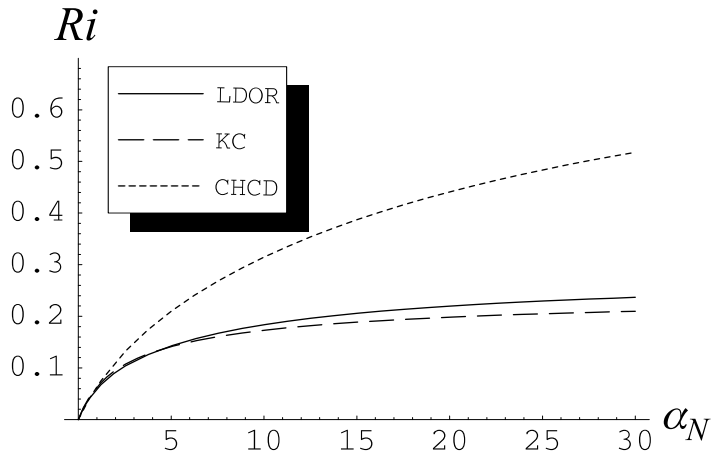

Figure 3.5: Richardson number, Ri, as a function of the buoyancy parameter, α_N, for the FE version of the stability functions.

Since the SE and SEE versions of the stability functions represent the exact behaviour of the non-equilibrium and quasi-equilibrium stability functions in SE, respectively, comparing them to the FE versions leads to an estimate of the error introduced in SE. On the other hand, comparing the SE versions to the SEE versions in situations of SE gives an answer to the interesting question, how large the error between the non-equilibrium and the widely used quasi-equilibrium functions is. This possibility of obtaining error estimates in SE is probably the most interesting application of the newly derived SE stability functions. Up to now, no general statements about the error introduced by the use of different stability functions could be obtained and most authors only conducted numerical case studies of little general relevance.

$(3.48)_1$ for the FE and the SEE versions of the LDOR and the KC stability functions are compared in Fig. 3.6. The SEE versions were computed for model parameters of different two-equation models. This figure illustrates that all versions exhibit only slightly different behaviour, and for the single value of $Ri = Ri_{st}$ they are necessarily equal. For other values of Ri the curves are relatively close to each other and there seems to be no particular need to distinguish between the FE and the SEE versions. Hence, in this particular case there will be little difference between numerical models that evaluate the

quasi-equilibrium versions (depending on α_N), and models that use the FE and SEE versions (both depending only on Ri).

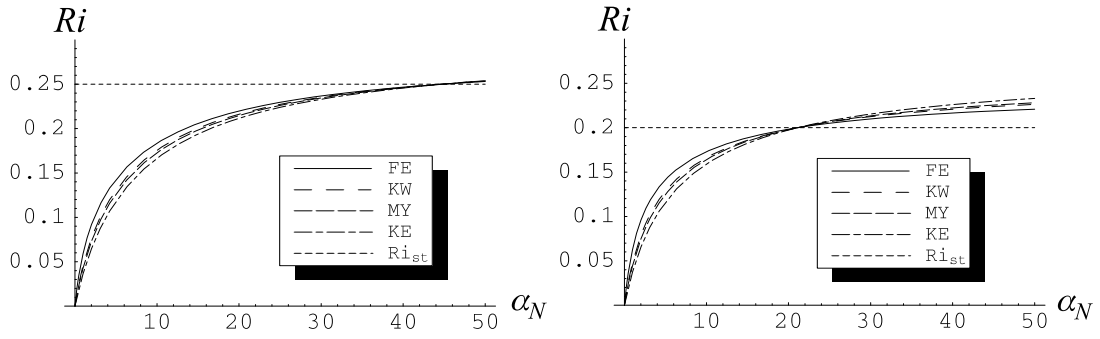

Figure 3.6: Richardson number, Ri, as a function of the buoyancy parameter, α_N, for the FE and the SEE versions of the LDOR (left panel) and the KC (right panel) stability functions. The steady-state Richardson numbers, Ri_{st}, to which the models have been tuned in each case, are marked by horizontal lines. (For the SEE versions: KW88=k-ω 1988, MY= Mellor-Yamada, KE=k-ϵ)

However, Fig. 3.7 demonstrates that care must be observed, if other stability functions are used: For the CHCD stability functions, e.g., the variability induced by using their respective SE/SEE/FE versions (left panel) is exceeded by the variability induced by using different two-equation models (right panel)!

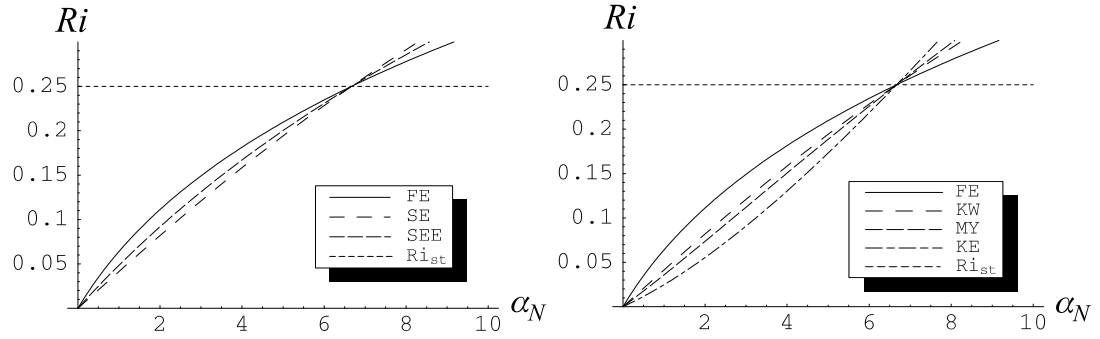

Figure 3.7: Left panel: Richardson number, Ri, as a function of the buoyancy parameter, α_N, for the SE, SEE, and FE versions of the CHCD stability functions. The parameters of the k-ω model have been used. Right panel: Same as left panel, but now only for the FE version and the SE version computed for different two-equation models. (KW88=k-ω 1988, MY= Mellor-Yamada, KE=k-ϵ)

Fig. 3.8 reveals that for high Ri this effect is even more pronounced: For the k-ω model (left panel) all versions of the CHCD stability functions are well behaved, but for the k-ϵ model (displayed together with other two-equation models in the right panel) a completely unrealistic behaviour is computed for $Ri \gtrapprox 0.8$. In this case a value of $Ri_{cr}^{SE} = 6.9$ for

very large α_N can be inferred from Tab. 3.9. Note again, that in all cases the stability functions are equal only for the value $Ri = Ri_{st}$, marked by a horizontal line in all plots. It can be concluded that for the CHCD stability functions there will be large differences in model behaviour depending on what version is implemented in a numerical model. It is recommended here to use the full non-equilibrium version together with the k-ω model.

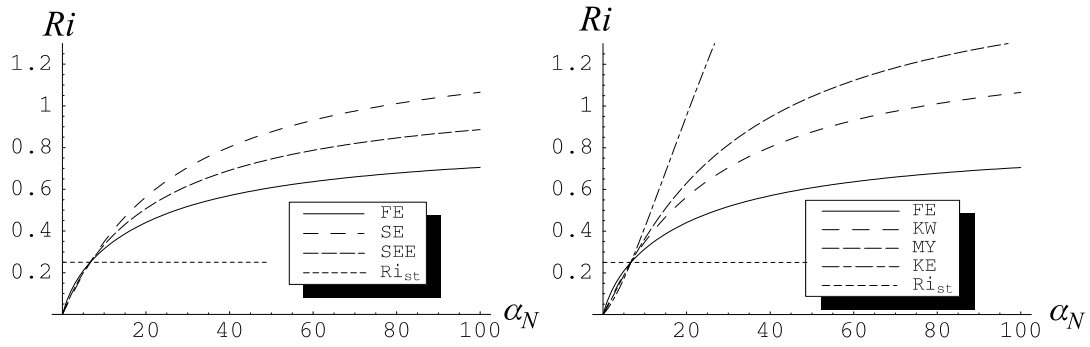

Figure 3.8: Same a Fig. 3.7, but now for a greater range of Richardson numbers.

Corresponding relations for the newly derived, extended form of the KC stability functions of (2.62) are plotted in Fig. 3.9 for different values of the new model parameter h. As already pointed out in the context of (2.62), the overall behaviour is largely determined by the value of h. Fig. 3.9 illustrates that for very small and for large values of h, functions similar to the original KC versions are obtained. However, for intermediate values of h, the functions do not show any similarity to the KC functions. Amazingly, for a value of $h \approx 0.135$, a set of stability functions very similar to the ones suggested by CHCD can be derived (for example the value of Ri_{cr}^{SE} is the same). This picture corroborates the fact that a closer examination of the role of the return-to-isotropy time-scale, τ_p, is necessary, before these stability functions can be used with any confidence.

Fig. 3.10–Fig. 3.13 illustrate, how the features discussed above manifest themselves in the actual stability functions. In these plots, FE and SE/SEE versions of the stability functions are displayed for a moderate range of Richardson numbers. Since the k-ω model has proven to be most advantageous in connection with the stability functions used here, SE and SEE versions are computed for the k-ω model coefficients only. Fig. 3.10 and Fig. 3.11 exemplify, how a different value of Ri_{st} (and hence $c_{\epsilon 3}$) affects the overall behaviour of the stability functions: A decrease of Ri_{st} leads to a small increase of Ri_{cr}^{SE} in this case. FE and SEE versions are only equal for $Ri = Ri_{st}$. For the FE and SEE versions of the KC stability functions shown in Fig. 3.12, a somewhat lower value of $Ri_{st} = 0.2$ had to

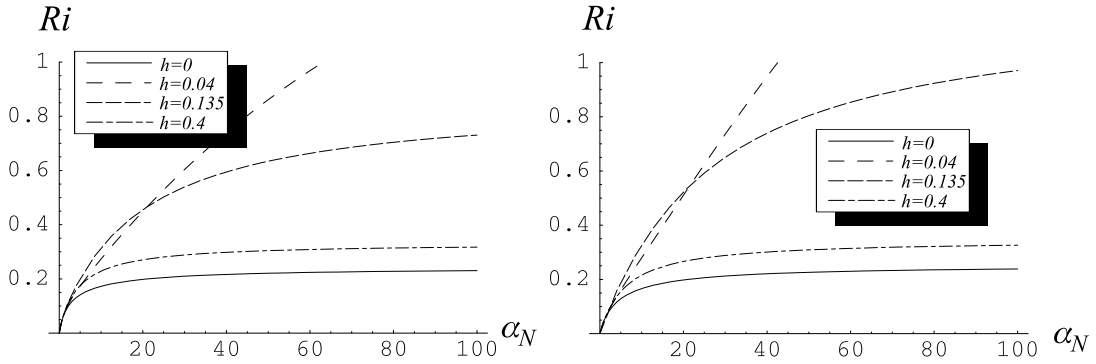

Figure 3.9: Ri as a function of α_N for the FE (left panel) and the SEE (right panel) versions of the modified KC stability functions (see (2.62)). The k-ω model parameters have been used with $c_3 = 0.422$.

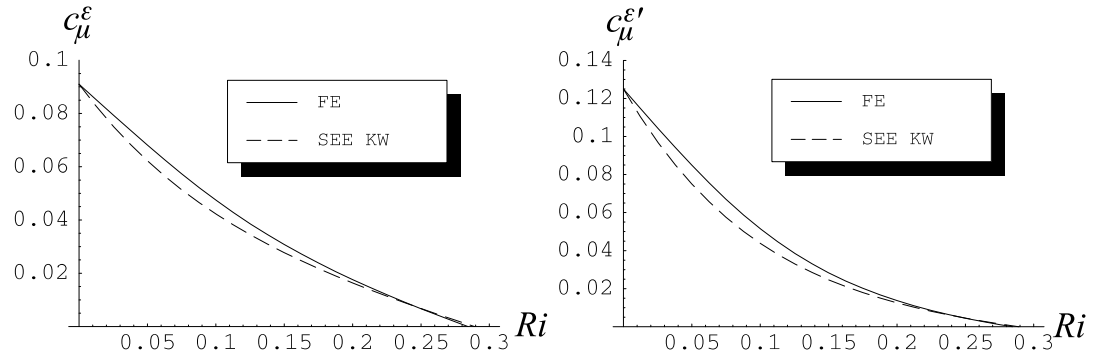

Figure 3.10: FE and SEE versions of c_μ^ϵ (left panel) and $c_\mu^{\epsilon\prime}$ (right panel) for the LDOR quasi-equilibrium stability functions. For the computation of the SEE version the k-ω model parameters have been used. $Ri_{st} = 0.25$.

be chosen, since both, Ri_{cr} and Ri_{cr}^{SE} were too close to the value 0.25 (see Tab. 3.6 and Tab. 3.9).

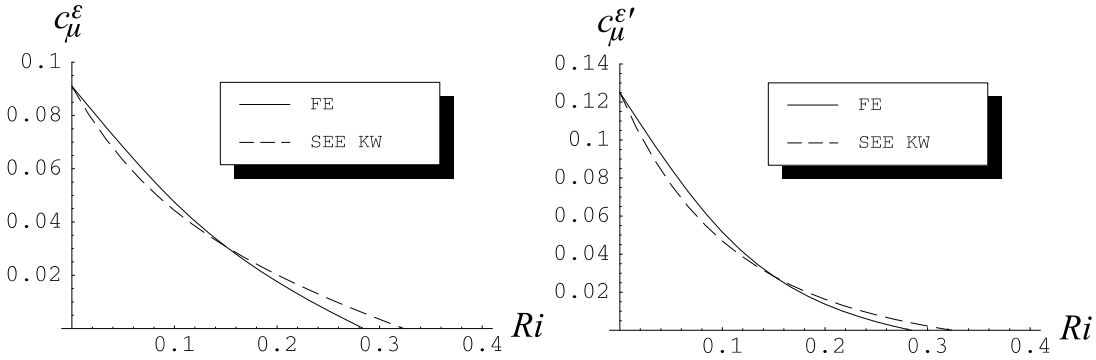

Figure 3.11: Same as in Fig. 3.10, but now with $Ri_{st} = 0.15$.

For the CHCD stability functions shown in Fig. 3.13, the differences between the FE and the SE versions are much larger: Distinct from SEE, the SE version does not approach the equilibrium value for $Ri \to 0$. In SE, this limit corresponds to homogeneously sheared turbulence not affected by buoyancy. Thus the values of c_μ^ϵ and $c_\mu^{\epsilon\prime}$ correspond to the value computed with α_M from Tab. 3.7 (also see Appendix A.1). $\nu_t^h = c_\mu^{\epsilon\prime}\frac{k^2}{\epsilon}$ for $Ri \to 0$

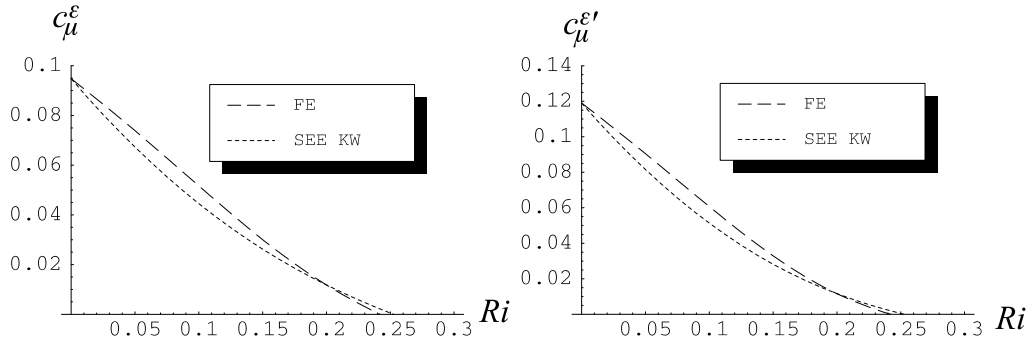

Figure 3.12: Same as in Fig. 3.10, but now for the KC quasi-equilibrium stability functions and $Ri_{st} = 0.2$.

then relates to the viscosity of a passive scalar as in the experiments of Tavoularis and Corrsin [254, 255]. Fig. 3.13 demonstrates particularly clearly, that the traditional critical Richardson number, Ri_{cr} (see Tab. 3.6), cannot be an important parameter in SE: The values of Ri_{cr}^{SE} indicate that turbulence in SE is predicted to be active for values much larger than Ri_{cr}. Again, both FE and SE stability functions coincide only for the single value $Ri = Ri_{st} = 0.25$.

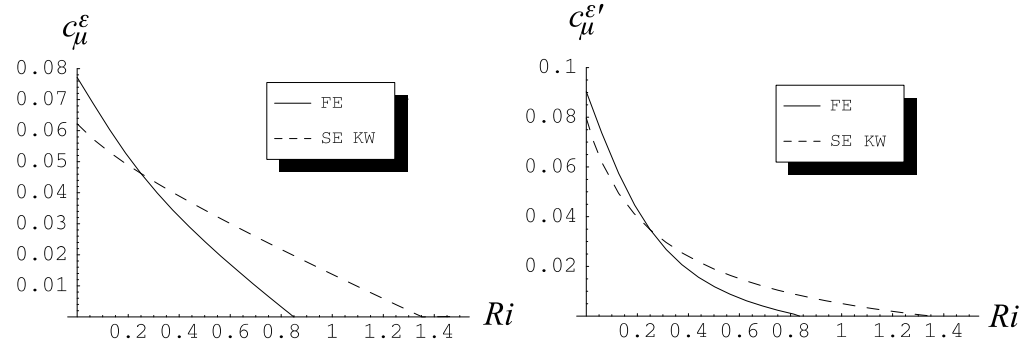

Figure 3.13: Same as in Fig. 3.10, but now for the FE and SE versions of the CHCD non-equilibrium stability functions.

The turbulent Prandtl number is the ratio of the turbulent diffusivities of momentum and heat as in

$$Pr_t = \frac{\nu_t}{\nu_t^h} = \frac{c_\mu^\epsilon}{c_\mu^{\epsilon\prime}} \quad . \tag{3.51}$$

The dependence of Pr_t on Ri is displayed in Fig. 3.14 for the FE and the SE/SEE versions of the stability functions. The value for passive stratification ($Ri \to 0$), Pr_{t0}, is in the interval $0.7 < Pr_{t0} < 0.85$ for all models. Pr_{t0} changes from FE ($Pr_{t0} \approx 0.85$) to SE ($Pr_{t0} \approx 0.78$) for the CHCD stability functions. These values are close to $Pr_{t0} = 0.79$ resulting from the DNS of GERZ ET AL. [86]. LAUNDER [146] tuned his second-order closure to $Pr_{t0} = 0.63$. On the other hand, the laboratory experiments of TAVOULARIS AND CORRSIN [254] suggested somewhat higher values of $1.06 < Pr_{t0} < 1.12$. The strong increase of Pr_t with increasing Ri is in agreement with all measurements and DNS (see, e.g., Figure 8 in GERZ ET AL. [86]). Only moderate Richardson numbers have been plotted, since it is known from DNS (GERZ ET AL. [86]) and LES (KALTENBACH ET AL. [134]) that Pr_t may become infinite near $Ri \approx 0.5$, where the heat flux becomes zero (and counter-gradient for even higher values of Ri). This trend would certainly not be reproduced by the simple models used here.

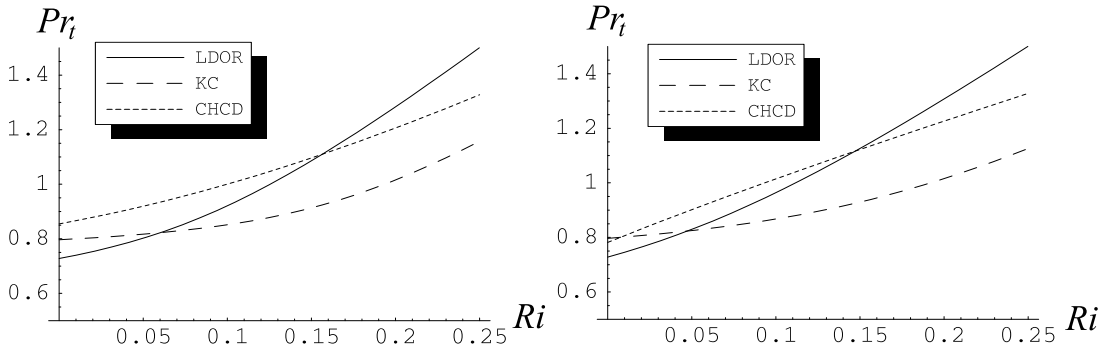

Figure 3.14: Turbulent Prandtl number, Pr_t, as computed with the FE versions (left panel) and the SEE (LDOR/KC) and SE (CHCD) versions (right panel) of the stability functions. SE and SEE results have been computed with the k-ω coefficients. Ri_{st} was chosen as in Fig. 3.10 - Fig. 3.13.

Turbulent Length-Scales in Stably Stratified Shear Flows

In stratified turbulence a number of different length-scales appear. The study of their interrelations opens up new vistas on the properties of stratified turbulence (DILLON [65], SCHUMANN [219], MOUM [179], BAUMERT AND PETERS [11]). Most prominent in the framework of two-equation models is the master length-scale, l, directly available in the Mellor-Yamada model, but also easily obtained from the other length-scale related variables via the relations $(3.7)_2$ and $(3.14)_1$. These relations also show that l is a dissipative scale by its nature.

The overturning length-scale of stratified laboratory flows is usually reported in terms of the so-called Ellison scale

$$L_E = -\langle \rho'^2 \rangle^{\frac{1}{2}} \left(\frac{\partial \rho}{\partial z} \right)^{-1} = \langle \theta'^2 \rangle^{\frac{1}{2}} \left(\frac{\partial \theta}{\partial z} \right)^{-1} \quad , \tag{3.52}$$

a scale that also can be computed from the ASM. Using (2.48) and $(2.49)_3$, the result is

$$L_E = \left(c^\theta c_\mu^{\epsilon\,\prime} \right)^{\frac{1}{2}} \frac{k^{\frac{3}{2}}}{\epsilon} \quad . \tag{3.53}$$

Then, with the help of $(3.14)_1$ it is easy to obtain the relation

$$\frac{L_E}{l} = \left(c^\theta c_\mu^{\epsilon\,\prime} \right)^{\frac{1}{2}} \left(c_\mu^0 \right)^{-3} \quad . \tag{3.54}$$

In SE, relation (3.54) can be expressed as a function of the Richardson number if (3.49) is applied.

The Ellison scale is very sensitive with respect to fluctuations caused by internal waves omnipresent in field measurements. There is another overturning scale better suited to measurements in the ocean and in lakes. This scale is based on the stable reordering of density fluctuation profiles and was introduced by Thorpe [267]. It is usually referred to as the Thorpe scale, L_T. Clearly, there is no straightforward way to obtain L_T from the model. Fortunately, the laboratory measurements of Itsweire et al. [123] and the DNS of Itsweire et al. [124] indicate that it is quite reasonable to simply assume $L_E \approx L_T$.

Baumert and Peters [11] used results from the investigations of Rohr et al. [208] and Ivey and Imberger [125] and claimed that

$$\frac{L_T}{l} \approx \frac{L_E}{l} = \frac{1}{c} \left(c_\mu^0 \right)^{-3} \quad , \tag{3.55}$$

with a value of $c \approx 2.8$. Baumert and Peters [11] established their analysis of turbulent length-scales computed by two-equation models partly on the basis of (3.55). However, there are two serious problems with this approach: First, as remarked by the authors themselves, it is not clear if c can really be considered a constant. Second, and more seriously, by using (3.55), Baumert and Peters [11] mixed up experimental results and model parameters, in order to study the behaviour of a model. Indeed, inspection of (3.54) and (3.55) shows that the models do not predict $c = \text{const}$ in general. Fig. 3.15 reveals that for different versions of stability functions, L_E/l is a strong function of Ri. This should be contrasted to the constant value of $\frac{L_E}{l} \approx 2.2$, which is obtained from (3.55) using a standard value of $c_\mu^0 \approx 0.55$.

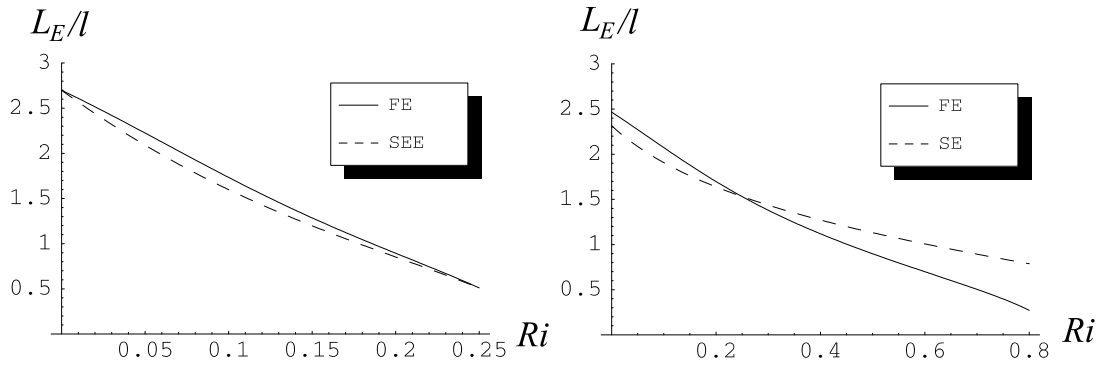

Figure 3.15: L_E/l for the FE and the SE/SEE versions of the LDOR (left panel) and CHCD (right panel) stability functions. $Ri_{st} = 0.25$ was used together with the coefficients of the k-ω model. Note the different ranges of Ri.

The scales at which vertical turbulent motions are likely to be affected by buoyancy has become famous by the name Ozmidov [186] scale. It is defined by

$$L_O = \left(\frac{\epsilon}{N^3}\right)^{\frac{1}{2}} \quad . \tag{3.56}$$

An interesting relation can be found from (3.53) and (3.56). Making use of $(2.54)_2$, it is easy to show that

$$\frac{L_E}{L_O} = \left(c^\theta c_\mu^{\epsilon\prime}\right)^{\frac{1}{2}} \alpha_N^{\frac{3}{4}} \quad . \tag{3.57}$$

In FE and SE, the scale relation (3.57) can be expressed as a function of the Richardson number only, if (3.48) and (3.49) are used. (3.57) extends the results of Baumert and Peters [11] in providing an *exact* analytical expression of the model behavior. The above authors used the empirical (and problematic) relation (3.55) and, in addition, another empirical relation for the turbulent Prandtl number (their equation (84)), to express L_E/L_O in terms of Ri. It will be interesting to see, how their findings deviate from the exact expression (3.57). Note, that the experiments of Rohr et al. [208] were conducted for turbulence in SE, and hence $c_\mu^{\epsilon\prime}(Ri)$ and $\alpha_N(Ri)$ in (3.57) should be derived also for SE.

Laboratory data of Rohr et al. [208] and the LES of Schumann and Gerz [220], obtained from turbulence in SE, support a simple power law of the form

$$\frac{L_E}{L_O} = 4.2 Ri^{\frac{3}{4}} \, , \tag{3.58}$$

which is valid up to (very roughly) $L_E/L_O \approx 1.2$. For larger Richardson numbers the data are not conclusive. Fig. 3.16 illustrates, how measured and modelled length-scales relate for several versions of stability functions. The FE versions of both, the LDOR

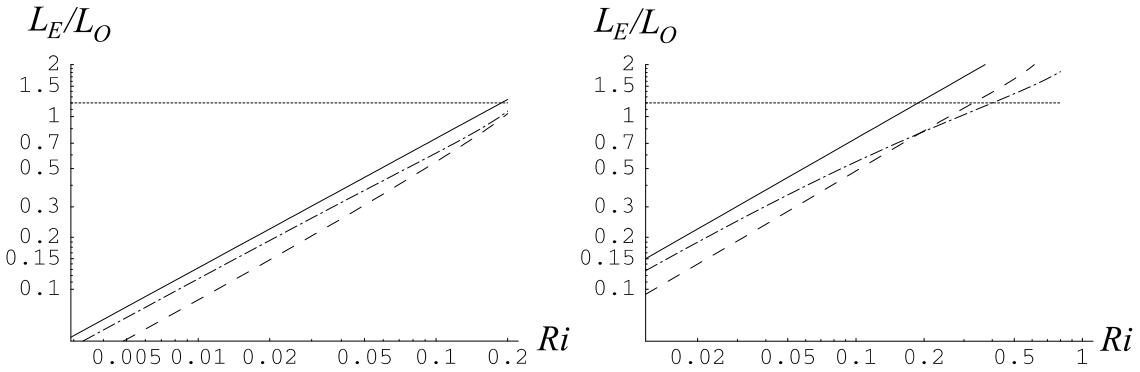

Figure 3.16: L_E/L_O for different versions of the LDOR (left panel) and the CHCD (right panel) stability functions. The line coding is as follows: — $4.2Ri^{\frac{3}{4}}$, - - - FE model, – · – · – SE/SEE model. The horizontal line marks the approximate range of validity of (3.58).

and the CHCD stability functions almost perfectly mimic the 3/4 exponent of the power law, but underestimate somewhat the factor in the scale ratio. The SE/SEE versions are closer to the measurements for small Ri, but tend to show a larger departure and undesired curvature for large values of Ri. The abrupt change in the power law exponent at $L_E/L_O \approx 1.2$ suggested by the data (and indicated by a horizontal line in Fig. 3.16) is not even rudimentarily reproduced by the models. Note, that this does not imply that the overturning scale is unlimited by the Ozmidov scale in other situations. In fact, it is shown in Section 4.1.3 that in FE the ratio L_E/L_O is a constant with a value near one (depending on Ri, see Tab. 4.1).

It has been remarked by several authors (Schumann [219], Kaltenbach et al. [134]) that stratified turbulence is a problem of multiple outer time-scales set by the shear frequency, M, and the buoyancy frequency, N. Thus, using a representative internal velocity scale, two length-scales can be defined, the shear length-scale, L_s, and the buoyancy length-scale, L_b, which can be written as

$$L_s = \frac{k^{\frac{1}{2}}}{M} \quad \text{and} \quad L_b = \frac{k^{\frac{1}{2}}}{N} \quad . \tag{3.59}$$

Other authors (e.g. Stillinger et al. [247], Kaltenbach et al. [134]) prefer using the r.m.s vertical velocity, $\sqrt{w'^2}$, instead of $k^{\frac{1}{2}}$, as the internal velocity scale. Results should, however, not be overly influenced by this choice. Schumann [219] and Kaltenbach et al. [134] pointed out that the dissipation roughly scales with L_s, but not with L_b.

The ratio of L_E to the buoyancy scale, L_b, can be found from combining (3.53), $(3.59)_2$

and $(2.54)_2$. The result

$$\frac{L_E}{L_b} = \left(c^{\theta} c_{\mu}^{\epsilon\prime}\right)^{\frac{1}{2}} \alpha_N^{\frac{1}{2}} \tag{3.60}$$

should be compared to $L_E/L_b \approx 1.6 Ri^{\frac{1}{2}}$, the approximate behaviour of the measured values for $Ri < 0.25$ (see BAUMERT AND PETERS [11]). Fig. 3.17 reveals that the model

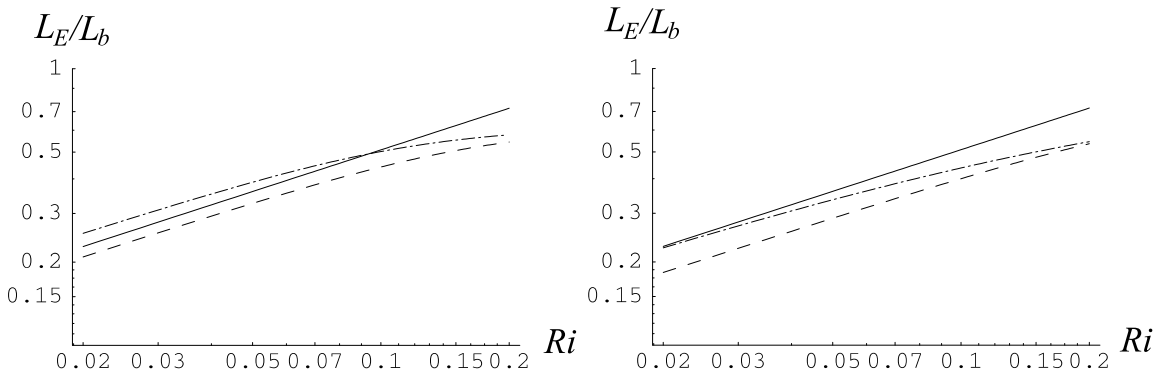

Figure 3.17: Same as in Fig. 3.16, but now for L_E/L_b. The line coding is as follows: — $1.6 Ri^{\frac{1}{2}}$, - - - FE, – · – · – SE/SEE.

behaviour is comparable to that in Fig. 3.16: The decay exponent is met almost perfectly by the FE versions of the stability functions, but the data are somewhat underestimated. The SE/SEE versions predict the data very well for small values of Ri, but exhibit deviations for high Ri.

Restrictions for the Parameters of Two-Equation Models

By using the canonical form of the two-equation models, simple relations between the parameters of different models can be derived by inspection of (3.29)–(3.33). A glance on Tab. 3.10 shows that the model coefficients are generally not far apart. It seems plausible that they are subject to similar restrictions.

In this context it was the important contribution of TENNEKES [257] to recognize that "on dimensional grounds, l cannot depend upon the shear because the shear is homogeneous and cannot impose a length-scale." Inspection of (3.34) reveals that this requires $c_{\epsilon 1} = 3/2$. Of course, an analogous argument is not valid for the influence of the stratification. In fact, the stratification is known to impose the only restriction on the length-scale in stratified flow, if the influence of boundaries is negligible. This is in accordance with the observation of SCHUMANN [219] that, if the value of $c_{\epsilon 1}$ is chosen far from $c_{\epsilon 1} = 3/2$, an unphysical increase of the dissipative length-scale under shear will result. With the

	$c_{\epsilon 1}$	$c_{\epsilon 2}$	$c_{\epsilon 3}$
Relation k-ω parameters:	$c_{\omega 1}+1$	$c^0_{\omega 2}+1$	$c_{\omega 3}+1$
k-ω 1988 values:	1.555	1.833	$f(Ri_{st})$
k-ω 1998 values:	1.52	1.8	$f(Ri_{st})$
Relation to MY-parameters:	$\frac{5}{2}-c_{l1}$	$\frac{5}{2}-c_{l2}$	$\frac{5}{2}-c_{l3}$
MY values:	1.6	2	1.6
Relation k-ϵ parameters:	$c^{\text{orig}}_{\epsilon 1}$	$c^{\text{orig}}_{\epsilon 2}$	$c^{\text{orig}}_{\epsilon 3}$
k-ϵ values:	1.44	1.92	$f(Ri_{st})$

Table 3.10: Relations of model coefficients of the canonical model expressed by (3.29) - (3.33).

coefficients used here, however, the exponential evolution of l in SE is controlled mainly by a balance between the first and the last term in (3.34).

It was Tennekes argument that tempted Baumert and Peters [11] to assume that the small differences between the parameters of different models were unimportant and that general results, valid for all models, could be derived from the canonical model. However, it has been shown in the preceeding sections that this is in fact not true: *It is precisely the small difference in model parameters that leads to large differences in model performance, a drastical example being the right panel of Fig. 3.8.*

3.4.6 Shear-Free Turbulence

In the preceeding section, two-equation models were shown to be isomorphic only in homogeneous turbulence, where the turbulent transport terms are zero. The structural difference of the models manifests itself only in the presence of turbulent transport, where the mapping from one model to another is known to introduce extra, so-called cross-diffusion terms. This section emphasizes the differences in model performance induced by the turbulent transport terms, which are modelled as diffusion terms in the standard down gradient form.

The essential influence of the turbulent diffusion terms can be investigated by considering the simple balance of turbulent dissipation and transport of turbulent kinetic energy in one coordinate direction. Using the Taylor scaling for the rate of dissipation, $\epsilon = Bk^{\frac{3}{2}}/l$,

the balance of kinetic energy simplifies to

$$\frac{\mathrm{d}}{\mathrm{d}z}\left(\nu_t \frac{\mathrm{d}k}{\mathrm{d}z}\right) = B\frac{k^{\frac{3}{2}}}{l} \quad . \tag{3.61}$$

In spite of its apparent simplicity, a balance of turbulent diffusion and dissipation is of great importance in geophysical situations: In lakes and oceans, e.g., the existence of a layer affected by wave breaking with a near balance of dissipation and diffusion of kinetic energy is now well established (see, e.g., Gemmrich and Farmer [85]). Stimulated by such observations, there have been some recent attempts to model the wave enhanced layer with differential turbulence closures (Craig and Banner [53], Craig [52], Burchard [25]). Since the wave affected layer is by far not the only region, in which the diffusive terms are important, this section focuses on the fundamental properties of two-equation models in the diffusive-dissipative balance.

Having wave induced mixing in mind, early laboratory set-ups by Rouse and Dodu [211], Cromwell [54], Turner and Kraus [274], and Turner [272] used grid stirrers to mimic wave breaking. These investigators were mainly interested in entrainment laws depending on a bulk Richardson number, like that in (3.1). Turner [273] summarized the knowledge available then.

Soon, however, it was recognized (Thompson and Turner [262], Linden [151]), that entrainment laws cannot reliably be formulated as functions of Richardson numbers depending only on bulk parameters. The local Richardson number based on turbulent parameters close to the interface was identified to be the most relevant parameter. As a consequence, a large number of publications appeared investigating the local Richardson number influence on entrainment processes (Hopfinger and Toly [111], Hannoun et al. [102], Hannoun and List [103], Nokes [184], Fernando [73], Briggs et al. [22]). Unfortunately, the entrainment turned out to depend on countless subtleties and Fernando [73] had to state that "it is clear that the present state of affairs does not allow us to arrive at any conclusion on the entrainment law". Thus, apparently little can be gained at the moment by comparing differential closures to entrainment laws.

If it is accepted, however, that the entrainment is correlated with turbulent quantities close to the interface, naturally the question arises, how these quantities decay with increasing distance from the stirrer (or the wave affected layer in open waters). A number of works were aimed to answer this question (Thompson and Turner [262], Hopfinger and Toly [111], Hannoun et al. [102], Briggs et al. [21]). However, it seems that only Briggs et al. [21] investigated (very briefly, though) the spatial decay of turbulent quantities as predicted by two-equation models. Since these models a very popular, a

more detailed investigation of this topic is necessary.

With the help of (3.61), first insight can be gained by using the plausible assumptions $\nu_t \propto k^{\frac{1}{2}} l$ and $\langle w' \frac{1}{2} u_i' u_i' \rangle = \nu_t \dfrac{\partial k}{\partial z} \propto k^{\frac{3}{2}}$ as suggested by the results of HANNOUN ET AL. [102]. Then (3.61) simplifies to

$$\frac{\mathrm{d}}{\mathrm{d}z} k^{\frac{3}{2}} = B \frac{k^{\frac{3}{2}}}{l} \,, \tag{3.62}$$

where the constants of proportionality have been absorbed in B. (3.62) can be integrated, if the mixing length is described as a function of z. A relation of the form $l = Lz$ (L being the constant of proportionality) suggested by many experiments (THOMPSON AND TURNER [262], HOPFINGER AND TOLY [111], HANNOUN ET AL. [102]) can be used. The spatial decay of k is then given by a simple power law of the form

$$k = k_0 \left(\frac{z}{z_0} \right)^{\alpha} \,, \quad \alpha = -\frac{2B}{3L} \,, \tag{3.63}$$

where k_0 is the kinetic energy at the position $z = z_0$.

Indeed, the existence of a power law for the decay of turbulent fluctuations has been confirmed by most authors (however, see NOKES [184]). Unfortunately, measurements did not allow for a very precise establishment of the decay exponent, α. Tab. 3.11 displays a range of $-3.0 < \alpha < -1.7$, with a value of $\alpha = -2.45$ computed from the DNS of BRIGGS ET AL. [21].

Measured decay rates:	α	L
THOMPSON AND TURNER [262]	-(3.0)	0.1
HOPFINGER AND TOLY [111]	- 2.0	0.17-0.33
NOKES [184]	-(1.7-3.0)	—
HANNOUN ET AL. [102]	-(2.0)	0.1
BRIGGS ET AL. [21]	- 2.45	—

Table 3.11: Decay exponent for the turbulent kinetic energy, α, and the constants of proportionality for the length-scale, L, in grid stirring experiments and DNS. The values in brackets have been calculated by assuming that the decay exponent for the horizontal velocity fluctuations is half of that for k.

In the unstratified, shear-free, but inhomogeneous case, all two-equation models simplify to a balance between diffusion and dissipation of the kinetic energy and of the length-scale determining variable. Under these conditions, (3.3), describing the WILCOX [293]

k-ω model, becomes

$$\frac{\mathrm{d}}{\mathrm{d}z}\left(\frac{1}{\sigma_k^\omega}\frac{k}{\omega}\frac{\mathrm{d}k}{\mathrm{d}z}\right) = (c_\mu^0)^4\omega k \;, \quad \frac{\mathrm{d}}{\mathrm{d}z}\left(\frac{1}{\sigma_\omega}\frac{k}{\omega}\frac{\mathrm{d}\omega}{\mathrm{d}z}\right) = (c_\mu^0)^4 c_{\omega 2}^0\omega^2 \quad . \tag{3.64}$$

Note, that the new WILCOX [294] version would have introduced the parameter function f_{c_μ} (defined in (3.4) and (3.5)) on the left hand side of (3.64). In this case, however, the equations become intractable by analytical methods. Nevertheless, a numerical solution can be found and this is discussed below.

With the same assumptions, the Mellor-Yamada model, expressed by (3.9), simplifies to

$$\frac{\mathrm{d}}{\mathrm{d}z}\left(c_k^l k^{\frac{1}{2}} l\frac{\mathrm{d}k}{\mathrm{d}z}\right) = (c_\mu^0)^3\frac{k^{\frac{3}{2}}}{l} \;, \quad \frac{\mathrm{d}}{\mathrm{d}z}\left(c_l k^{\frac{1}{2}} l\frac{\mathrm{d}kl}{\mathrm{d}z}\right) = (c_\mu^0)^3 c_{l2} k^{\frac{3}{2}} \quad . \tag{3.65}$$

For simplicity, it has been assumed, that walls are remote, and thus $F = 1$ can be assumed for the wall function appearing in $(3.9)_2$. Recalling that the wave affected layer is close to the surface, it is clear that this assumption does not hold in general. Chances are small that the wall function, F, which has been tuned to the logarithmic boundary layer will be of great benefit in shear-free situations. This again indicates that the presence of a wall function must be considered a large draw back of the Mellor-Yamada model.

Finally, the k-ϵ model (3.13) reduces to

$$\frac{\mathrm{d}}{\mathrm{d}z}\left(\frac{(c_\mu^0)^4}{\sigma_k^\epsilon}\frac{k^2}{\epsilon}\frac{\mathrm{d}k}{\mathrm{d}z}\right) = \epsilon \;, \quad \frac{\mathrm{d}}{\mathrm{d}z}\left(\frac{(c_\mu^0)^4}{\sigma_\epsilon}\frac{k^2}{\epsilon}\frac{\mathrm{d}\epsilon}{\mathrm{d}z}\right) = c_{\epsilon 2}\frac{\epsilon^2}{k} \quad . \tag{3.66}$$

Even with symbolic mathematical tools, it turned out to be impossible to obtain a complete analytical solution of the non-linear systems (3.64)–(3.66). However, recalling (3.63), it seemed promising to try a simple power law Ansatz of the form $k = Kz^\alpha$, $\epsilon = Ez^\beta$, $\omega = Wz^\delta$, $l = Lz^\sigma$ and $\nu_t = Nz^\gamma$ with constant factors and exponents. This method has already been used successfully by BRIGGS ET AL. [21]. If the power law Ansatz is inserted in (3.64)–(3.66), after some algebra the non-linear systems of differential equations reduce to linear systems for the exponents of the decay laws. The exponents and the model coefficients for the k-ω model have to obey the relations

$$0 = \alpha - 2\delta - 2 \;, \quad 1 = \frac{\sigma_\omega c_{\omega 2}^0}{\sigma_\omega^k}\frac{\alpha(2\alpha - \delta - 1)}{\delta(\alpha - 1)}; \tag{3.67}$$

for the Mellor-Yamada model they are

$$0 = \sigma - 1 \;, \quad 1 = \frac{c_k^l c_{l2}}{c_l}\frac{\alpha(\frac{3}{2}\alpha + \sigma - 1)}{(\alpha + \sigma)(\frac{3}{2}\alpha + 2\sigma - 1)} \;, \tag{3.68}$$

and for the k-ϵ model

$$0 = 3\alpha - 2\beta - 2 \;, \quad 1 = \frac{\sigma_\epsilon c_{\epsilon 2}}{\sigma_\epsilon^k} \frac{\alpha(3\alpha - \beta - 1)}{\beta(2\alpha - 1)} \quad . \tag{3.69}$$

Each system yields a quadratic equation for the decay exponent α. On physical grounds, one of the two roots can be discarded in all cases. Tab. 3.12 summarizes the relevant roots for the standard model coefficients. Also included are results in which the turbulent Schmidt numbers, σ_ω and σ_ϵ, appearing in (3.67) and (3.69) have been re-computed for a von Kármán constant $\kappa = 0.4$ by means of the log-layer compatibility relations (3.15) and (3.17), respectively. It has been remarked several times above that models should be compared only, if they are tuned to compute a common von Kármán constant, κ, in the logarithmic boundary layer.

The sensitivity of the new WILCOX [294] k-ω model to the parameter function f_{c_μ} was investigated by simply setting $f_{c_\mu} = 1$, but otherwise retaining the new parameter values. The difference between the decay exponents computed this way and the ones computed numerically with non-constant f_{c_μ} (see below) extracts the influence of f_{c_μ}. Tab. 3.12 re-

computed decay rates:	α	σ	γ
k-ω 1988 (orig.)	-2.53	1	-0.26
k-ω 1988 ($\kappa = 0.4$)	-2.39	1	-0.2
k-ω 1998 ($f_{c_\mu} = 1$)	-2.68	1	-0.34
Mellor-Yamada (orig.)	-2.87	1	-0.43
k-ϵ (orig., $\sigma_\epsilon = 1.2$)	-7.95	1	-2.98
k-ϵ (orig., $\sigma_\epsilon = 1.3$)	-4.97	1	-1.49
k-ϵ (orig., $\sigma_\epsilon = 1.4$)	-3.65	1	-0.83
k-ϵ ($\kappa = 0.4$)	-19.47	1	-8.74

Table 3.12: Decay exponents α for the turbulent kinetic energy, k, σ for the turbulent length-scale, l, and γ for the turbulent diffusivity, ν_t, as computed by different two-equations models.

veals that the decay exponents for the kinetic energy are in the range of the measurements in all cases, except for the k-ϵ model. In perfect accordance with the measurements, the turbulent length-scale, l, is computed to increase in proportion to the value of z for all models.

All models, except the k-ϵ model, are rather insensitive to small changes in model parameters. Thus, it seemed worthwhile to conduct a sensitivity analysis for this model

by expressing the decay exponent of the turbulent energy, α, as a function of the model parameters. (3.69) and (3.17) have been used to study the behaviour of α, if the von Kármán constant, κ, and the parameters $c_{\epsilon 2}$ and σ_k, respectively, are varied over a small, physically reasonable interval. Surprisingly, a singularity in the decay exponent α predicted by the k-ϵ model is revealed in Fig. 3.18: For certain parameter relations, α becomes infinite and, after crossing the singularity, it takes on values that are beyond the physically meaningful range.

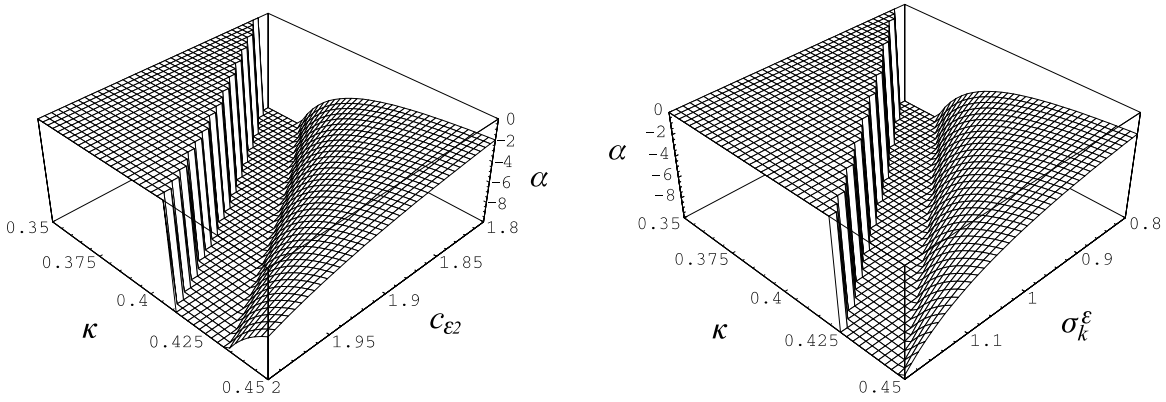

Figure 3.18: Sensitivity of the spatial decay exponent α for small changes of the parameters κ and $c_{\epsilon 2}$ (left panel) and κ and σ_k^{ϵ} (right panel) as computed by (3.69) and (3.17) for the k-ϵ model. The singularities are marked by a vertical surface, respectively. Only negative exponents have been displayed.

Conducting a similar sensitivity study for the k-ω model, Fig. 3.19 confirms that this model is not sensitive to small parameter changes and computed results are in the range of the measured values.

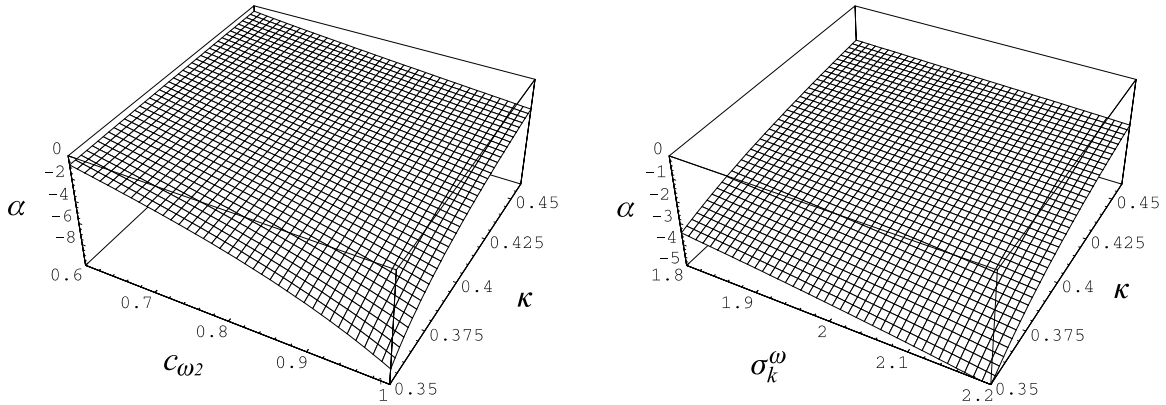

Figure 3.19: Sensitivity of the spatial decay exponent α for small changes of the parameters κ and $c_{\omega 2}$ (left panel) and κ and σ_k^{ω} (right panel) as computed by (3.67) and (3.15) for the k-ω model. Only negative exponents α have been displayed.

A closer investigation of the singularity of the k-ϵ model showed that for certain relations of the model parameters κ, $c_{\epsilon 2}$, and σ_k, the denominator of the polynomial expression determining α becomes zero. These relations are illustrated in Fig. 3.20. The figure reveals that the standard k-ϵ model predicts a singular α, if the von Kármán constant, κ is tuned to a value of $\kappa^{\text{crit}} \approx 0.387$. For lower values of κ, α becomes regular again, but takes on unphysical values. The value of κ^{crit} should be contrasted to the popular value of $\kappa = 0.35$ used in atmospheric sciences (see BUSINGER ET AL. [32]).

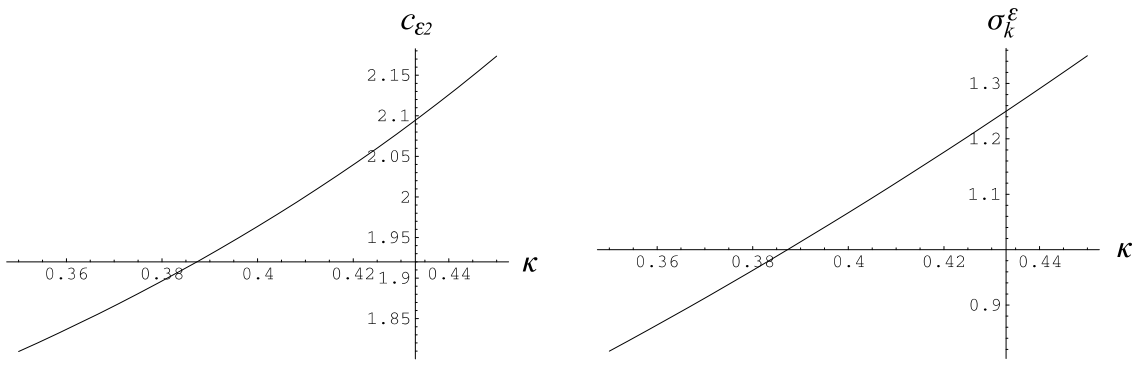

Figure 3.20: The k-ϵ model: Critical relations, at which the spatial decay exponent α becomes infinite, for the model parameters κ and $c_{\epsilon 2}$ (left panel) and for κ and σ_k^{ϵ} (right panel). Axis origin is at the standard values, respectively

As remarked above, a power law of decay probably does not embrace the complete set of solutions of the non-linear systems (3.64)–(3.66). The question, whether the power law solutions are in fact reproduced by the numerical models and whether singularities can really be identified, will be answered now. Fig. 3.21 displays numerical results for the decay of the turbulent kinetic energy, k, computed with the standard k-ϵ model, but with the parameter σ_ϵ varied between $1 < \sigma_\epsilon < 1.4$. Note, that for the standard model parameters a range of the von Kármán constant $0.35 < \kappa < 0.45$ corresponds to a range of $0.85 < \sigma_\epsilon < 1.41$. The critical value $\kappa^{\text{crit}} \approx 0.387$ corresponds to $\sigma_\epsilon^{\text{crit}} \approx 1.042$.

At a first glance, Fig. 3.21 contradicts the analytical results derived above: Seemingly, there is no evidence of a singularity or of a particularly unphysical behaviour in the decay of k. Moreover, the curves in Fig. 3.21 do not simplify to straight lines, if plotted on a double-logarithmic scale (not shown). This indicates that there is apparently no simple power law behaviour.

The apparent contradiction between analytical and numerical results can be resolved by introducing the notation of the *virtual origin*. It has been remarked by almost all authors conducting grid stirring experiments (HOPFINGER AND TOLY [111], NOKES [184],

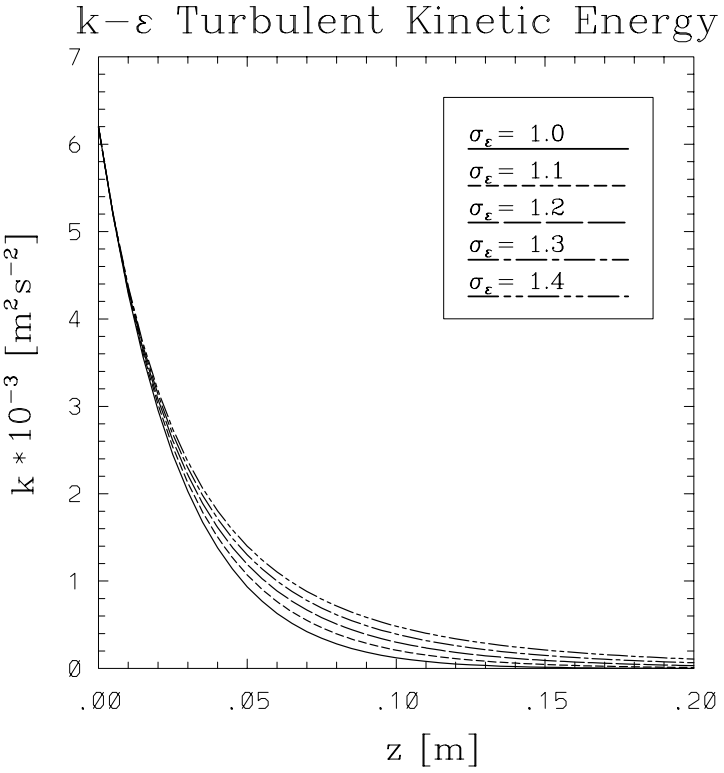

Figure 3.21: Decay of the turbulent kinetic energy, k, with distance, z, from the source of k at $z = 0$. The results have been computed with the standard k-ϵ model, but with varying parameter σ_ϵ. Values of k and ϵ at the source ($z = 0$) have been used in accordance with an experiment by HOPFINGER AND TOLY [111].

HANNOUN ET AL. [102]) or Direct Numerical Simulations (see BRIGGS ET AL. [21]) that the mid position of the oscillating grid (or the position of the source of k in DNS) is not the appropriate origin for the determination of the decay exponents. Of course, the same arguments apply also for the numerical results presented here: *The position of the source of k, which has been assigned the value $z = 0$ in Fig. 3.21, is not an appropriate choice for the origin of the decay laws.*

Different methods have been suggested to assess the appropriate position of the virtual origin. Here, the method of HOPFINGER AND TOLY [111], who defined the virtual origin as the point, where the integral scale of turbulence, l, becomes zero, is adopted. Fig. 3.22 displays numerical results for l using different values of the parameter σ_ϵ. In accordance with the analytical solution, a linear relation between the distance, z, and the length-scale, l can be observed. Note, that a linear relation is the only one not affected by the choice of the virtual origin. The position of the virtual origin, i.e. the position at which $l = 0$, varies strongly with the parameter σ_ϵ. Furthermore, for values $\sigma_\epsilon > \sigma_\epsilon^{\text{crit}}$ it is at $z < 0$ and for $\sigma_\epsilon < \sigma_\epsilon^{\text{crit}}$ it is at $z > 0$ (recall that $\sigma_\epsilon^{\text{crit}} = 1.042$). As illustrated in Fig.

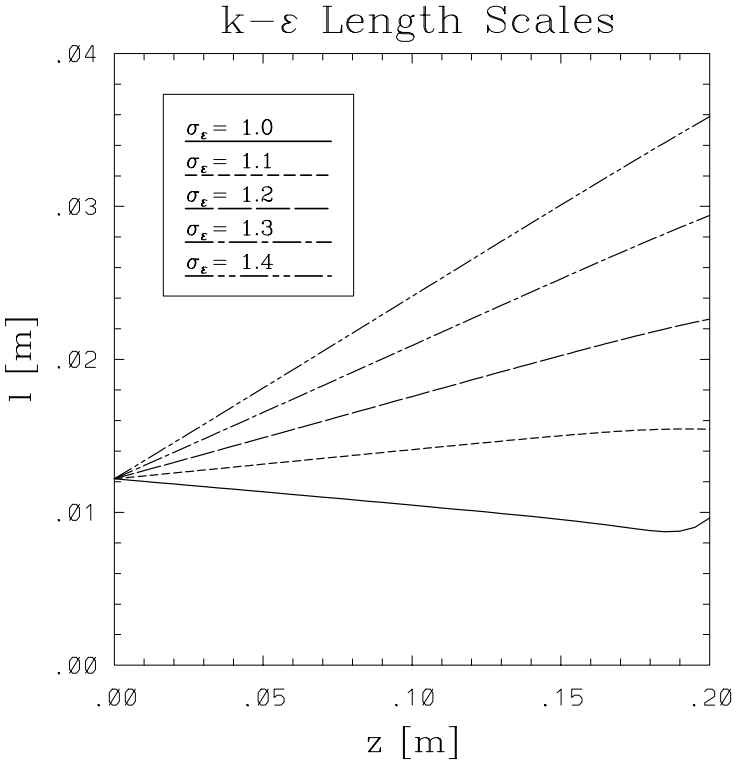

Figure 3.22: Same as Fig. 3.21, but now for the turbulent length-scale, l. The theoretical value for the transition from increasing to decreasing l is $\sigma_\epsilon^{\text{crit}} = 1.042$.

3.22, in the latter case the k-ϵ model predicts, in contrast to all measurements, that the turbulent length-scale, l, decreases with increasing distance from the source. At $\sigma_\epsilon = \sigma_\epsilon^{\text{crit}}$ the position of the virtual origin changes from $-\infty$ to $+\infty$.

It is hoped that, if the spatial decay of k is re-evaluated with an offset corresponding exactly to the virtual origin, a power law of decay will be recovered. That this is indeed the case, is illustrated in Fig. 3.23: Using the method outlined above, the spatial decay of k has been plotted on a double-logarithmic scale for different versions of the k-ϵ and the k-ω models. From Fig. 3.23 it is clear, that all curves are represented almost perfectly by straight lines. These lines start in each case at a value of z, which corresponds to their offset from the virtual origin, respectively. The computed slopes (marked by small numbers in the plot) agree very well with the values given in Tab. 3.12 considering the uncertainty in finding the exact position of the virtual origin.

The above arguments show that the numerical model perfectly reproduces the analytical results. Thus, the power law solution of the non-linear systems (3.64)–(3.66) is identical to the numerical results. It should be added that the numerical solution of the complete Wilcox [294] k-ω model (recall that no analytical solution could be found for this case)

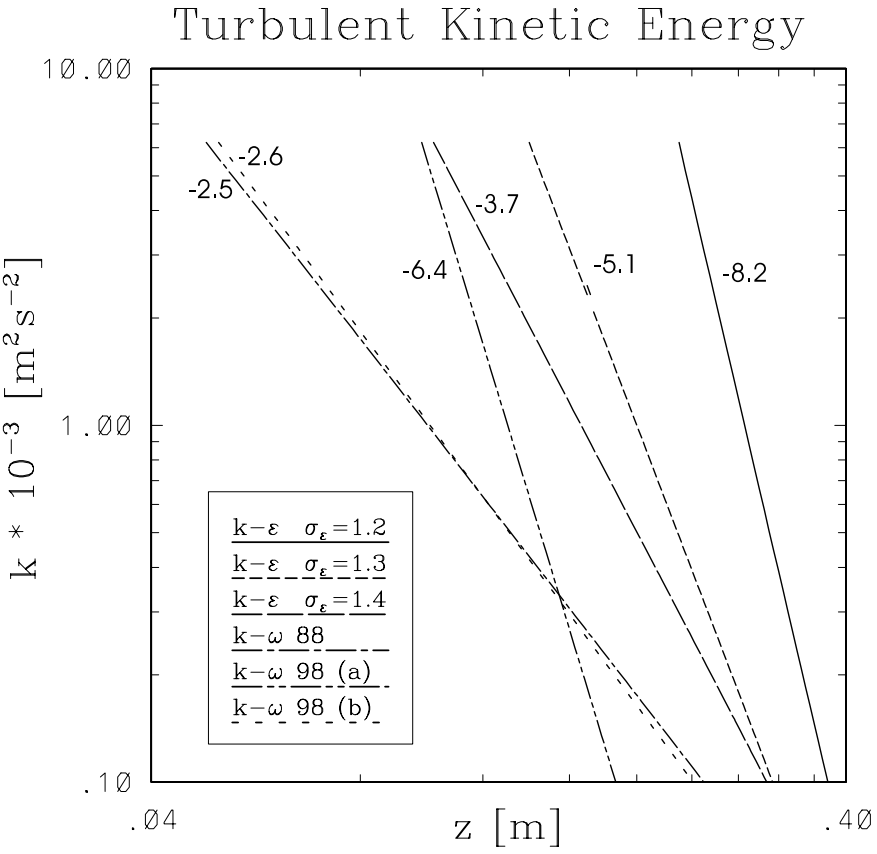

Figure 3.23: Doubly logarithmic representation of the numerically computed spatial decay of the turbulent kinetic energy, k, for the standard k-ϵ model (with different values of σ_ϵ) and for different versions of the k-ω model. k-ω 88 relates to the WILCOX [293] model, k-ω 98 (a) to the complete WILCOX [294] model, whereas k-ω 98 (b) stands for the same model with $f_{c_\mu} = 1$. Numbers indicate the slope of the curves estimated from a straight line fit.

predicts a decay exponent of $\alpha \approx -6.4$. This value is not in the range of the measurements and it can be concluded that the parameter function f_{c_μ} introduced in (3.5) has a strong, but undesired effect in shear-free situations.

Some concluding remarks seem appropriate. In this section it has been demonstrated that the only meaningful method of interpreting laboratory and numerical results for shear-free decay experiments is by referring to a virtual origin. If this method is used, numerical calculations agree perfectly with simple analytical power law solutions. However, it has also become evident that the standard k-ϵ model computes a decay rate, that is far too high. Moreover, for slightly different, but physically reasonable and popular parameter values, the decay rates computed by this model cross a singularity and become unphysical. In this case the turbulent length-scale, l, decreases with increasing distance from the source, a behaviour that is contradicted by all measurements. Since $\nu_t \propto k^{\frac{1}{2}} l$ this leads

also to an unphysical decay of the turbulent diffusivity. In contrast to that, the standard versions of the k-ω model and the Mellor-Yamada model predict decay rates that are fully in the range of the measured values and insensitive to small changes in the model parameters. Taking the drawbacks related to the wall function of the Mellor-Yamada model into consideration, the results discussed in this section indicate a clear superiority of the k-ω model of Wilcox [293] compared to all other two-equation models introduced in this chapter.

Chapter 4

Applications

In this chapter a number of applications of the two-equation models introduced in Section 3 will be presented. The chapter starts with a model validation by comparing model predictions for three standard flows: A plane Couette flow, a barotropic channel flow, and the stratified shear-entrainment experiment of Kato and Phillips [137]. Besides this, the prerequisites for the following section are prepared.

The validation also includes an investigation of the relative performance of the two-equation models used in this chapter: The k-ω model in its traditional form from 1988 (Wilcox [293]), the same model in its revised form from 1998 (Wilcox [293]), and the k-ϵ model in its standard form. The Mellor-Yamada model is not included, because the ambiguous definition of its wall damping function was considered to be a too serious impairment of an objective model comparison[1].

The main section consists of an application of the k-ω and the k-ϵ models to the seiche-induced boundary layer of a small lake (Umlauf and Lorke [282]). This part of the chapter owes much to Drs. A. Wüest and A. Lorke from the EAWAG, Switzerland, who kindly gave me access to their very recently measured and still unpublished data in the seiche-induced bottom boundary layer of Lake Alpnach, Switzerland. Their unique data set made it possible to present here (for the first time, it is believed) a comparison of modelled and measured turbulent quantities in the oscillating bottom boundary layer of a lake. These results will be contrasted to the much better explored tidally induced boundary layers in the ocean.

[1] Excellent comparisons between the k-ϵ model and the Mellor-Yamada model can be found in Burchard et al. [31] and Burchard [24].

4.1 Validation

The numerical models presented in this work are based on a new, object-oriented structure (see Section 6); besides this, they use non-standard boundary conditions and a different type of boundary cells (see Section 5). To demonstrate, that the numerical method and the model implementation are correct, in this section a brief validation of the respective model performance for three standard flows is executed: A turbulent plane Couette flow, a pressure-gradient driven, open barotropic channel flow, and the entrainment experiment of KATO AND PHILLIPS [137] shall be considered.

All models have been tuned to compute a common von Kármán constant of $\kappa = 0.4$ by using the consistency equations (3.15) and (3.17). Close to a rigid wall all models compute the well-known solution

$$\frac{u}{u_*} = \frac{1}{\kappa} \ln \frac{z + z_0}{z_0} \,, \tag{4.1}$$

where the wall roughness length, z_0, has been assigned a value of $z_0 = 10^{-3}$m for all runs (see Appendix A.1). For comparison, this asymptotic solution has been included in some of the plots shown below (see respective legends). For the Couette flow and the channel flow, the results presented in this section correspond to steady-state solutions for large times. In the case of the open barotropic channel flow and the entrainment experiment, no-flux boundary conditions for all quantities have been used at the free surface.

4.1.1 Plane Couette Flow

The structure of the plane turbulent Couette flow is well established by numerous experiments (cf. SCHLICHTING AND GERSTEN [217]): Apart from the viscous sub-layers, not resolved here, it consists of two logarithmic boundary layers and a small transition region in the centre.

The non-dimensional profiles displayed in Fig. 4.1 correspond to the steady-state solutions computed by several two-equation models. The left panel of this figure demonstrates that all models reproduce the structure of the plane Couette flow. Close to the walls, the profiles approach their asymptotic forms according to (4.1). Note, that on the scale of this panel the profiles computed by the different models are indistinguishable.

The turbulent length-scale, l, displayed on the right panel of Fig. 4.1 has been computed by using the formulae $(3.7)_2$ for the k-ω and $(3.14)_1$ for the k-ϵ model. This scale is seen

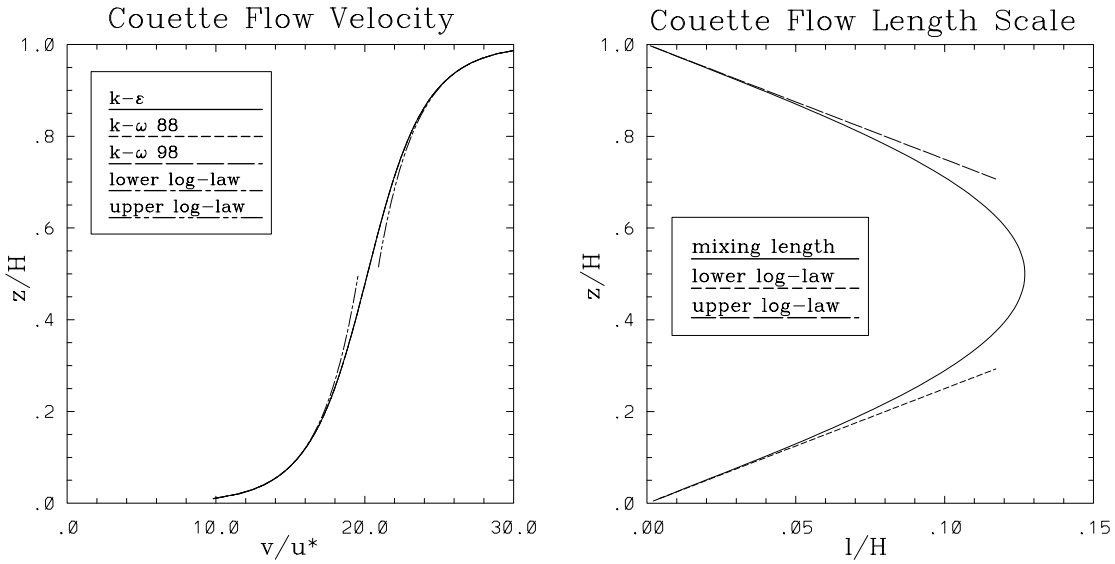

Figure 4.1: The mean velocity, v, (left panel) and the turbulent length-scale, l, (right panel) as functions of the distance from the bottom, z, in a shear-driven turbulent Couette flow for different models. The variables have been made dimensionless with the channel depth $H = 5$ m and the friction velocity $u_* = 6 \cdot 10^{-3}$ m/s. The wall roughness length is $z_0 = 10^{-3}$ m. All models have been tuned to compute a von Kármán constant of $\kappa = 0.4$. The asymptotic law-of-the-wall relations have also been included (see legends).

to approach exactly its asymptotic value $l = \kappa(z + z_0)$ close to the wall. As with the velocity profiles, the curves computed by different models cannot be distinguished and thus only the k-ϵ model result has been plotted here.

4.1.2 Pressure-Driven Channel Flow

Pressure-driven, barotropic channel flows with free surface have been investigated in detail by numerous researchers (see Schlichting and Gersten [217]). Baumert and Radach [12] demonstrated that their k-ϵ model (which is almost identical to that used here) could reproduce the measurements of several authors fairly well. They pointed out, however, that the slight asymmetry of the measured turbulent viscosity (not shown here) is not predicted by the standard model. Here, the results of Baumert and Radach [12] are assumed to be correct and their computations shall not be repeated. Merely, the differences computed by different types of two-equation models will be considered. Fig. 4.2 shows that, in contrast to the Couette flow, the predicted profiles of the velocity and the turbulent length-scale are not entirely identical for different models. Close to the wall, however, all models approach the asymptotic log-layer form. A comparison with Figure 1

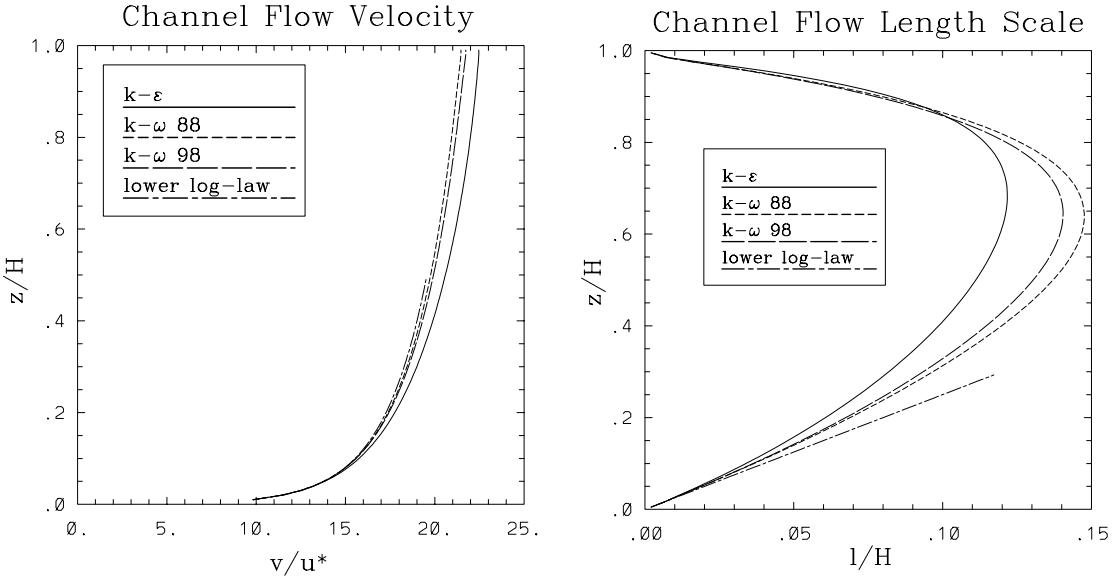

Figure 4.2: Same as in Fig. 4.1, but now for a barotropic channel flow driven by a pressure-gradient of $\frac{1}{\rho}\frac{\partial p}{\partial x} = -7.2 \cdot 10^{-6}$ m/s^2, which yields a value of $u_* = 6 \cdot 10^{-3}$ m/s at the bottom as in the plane Couette flow.

of Baumert and Radach [12] reveals that the scatter in the measurements of different authors does not allow for a conclusive decision, which of the models would best predict this channel flow.

Also in contrast to plane Couette flow, where $k/u_*^2 = 1/(c_\mu^0)^2$ is a constant (not shown), in the barotropic channel flow (Fig. 4.3) k/u_*^2 is seen to be a linearly decreasing function of z. Clearly, this behaviour is due to the presence of a pressure-gradient and only very close to the lower wall the asymptotic value $k/u_*^2 = 1/(c_\mu^0)^2 \approx 3.333$ is assumed. Fig. 4.3 also demonstrates that all models predict nearly identical profiles of k.

The influence of the non-constant k-distribution in the barotropic channel flow can also be conceived in Fig. 4.4, which displays the budget of the turbulent kinetic energy according to (2.11). The figure illustrates that this budget consists of a perfect balance between shear production and dissipation for the plane Couette flow, whereas for the barotropic channel flow there is also a small contribution due to the divergence of the turbulent transport. Kinetic energy is shown to be transported from the lower part of the channel to the upper part. For positions larger than $z/H \approx 0.8$, where the shear production becomes rather small, the divergence term dominates the budget of k. It has been shown in Section 3.4.5 that two-equation models are only isomorphic, if the transport terms are negligible. Hence, the small differences in the predicted profiles of Fig. 4.2 and Fig. 4.3

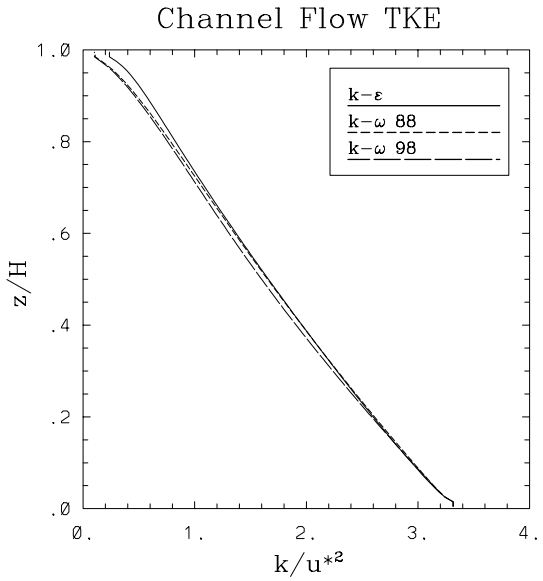

Figure 4.3: Profiles of the turbulent kinetic energy, k, in the open barotropic channel flow as predicted by different models. Variables have been made non-dimensional with the channel height, H and with the square of the friction velocity u_*^2. All other parameters are as in Fig. 4.2.

are likely due to the different influence of the turbulent transport terms for $z/H \gtrsim 0.8$ in different models.

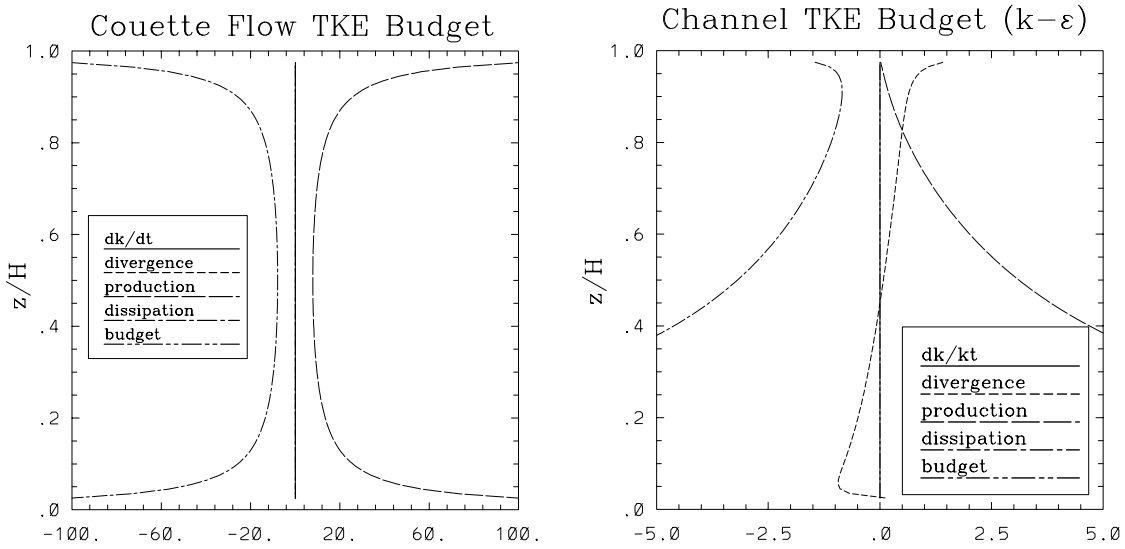

Figure 4.4: Terms contributing to the budget of the turbulent kinetic energy, (2.11), as computed by the k-ϵ model. Profiles of the budget are shown for the plane Couette flow (left panel) and the barotropic channel flow (right panel). The budget terms have been made dimensionless with the dissipation scale u_*^3/H. Parameters are as in Fig. 4.1 and Fig. 4.2. The term "budget" in the legends refers to the sum of all budget terms, which clearly should be zero and fall directly on the ordinate axis. Note the different scales!

It is also illustrated in Fig. 4.4 that for both, the plane Couette flow and the barotropic channel flow, the models compute the sum of all budget terms to be exactly zero. This can be taken as another indication for the correct discretization and implementation of the model equations.

4.1.3 Wind-Driven Entrainment

One of the most essential requirements for a turbulence model used in oceanography and physical limnology is the correct prediction of the mixing layer depth[2] (MLD). As discussed in Section 3.2, a great amount of research has been devoted to this topic, the results, however, being not entirely conclusive until today.

An important contribution to the understanding of mixing layer deepening was the experiment of Kato and Phillips [137] (KP) describing the entrainment of a turbulent mixing layer, driven by a constant surface stress, into a linearly stratified fluid. KP proposed an entrainment law of the form (3.1), scaled with $U = u_*$. However, later investigations of Price [195] and Thompson [261] showed, that their experiments were affected by sidewall friction and that the scaling with u_* was not appropriate. Having an instability mechanism in mind, Price [195] suggested to scale with the difference between the vertically integrated bulk velocity in the mixing layer and the velocity below it. This idea, expressed as $U = \Delta U$ in (3.1), traces back to the work of Pollard et al. [192]. Price [195] showed that it leads to an entrainment law of the form

$$E = \frac{u_e}{\Delta U} = \frac{1}{2} Ri_v^{\frac{1}{2}} Ri_\tau^{-\frac{1}{2}} \,, \tag{4.2}$$

where

$$Ri_v = \frac{g\,\delta\rho\,h}{\rho_0(\Delta U)^2} \quad \text{and} \quad Ri_\tau = \frac{g\,\delta\rho\,h}{\rho_0 u_*^2} \quad . \tag{4.3}$$

Recall, that E is defined as the dimensionless entrainment function, h as the depth of the mixing layer, $\delta\rho$ as the difference between the vertically integrated density in the mixing layer and the density just below it, and ρ_0 as some reference density.

For linear stratification, $\delta\rho$ can be expressed in terms of the initial buoyancy frequency, N_0, leading to

$$Ri_\tau = \frac{1}{2}\frac{N_0^2 h^2}{u_*^2} \quad . \tag{4.4}$$

[2]The term "mixing" layer is used here instead of the more common term "mixed" layer to emphasize, that the layer in not completely mixed.

It is seen that Ri_τ increases quadratically with increasing MLD.

PRICE [195] demonstrated the existence of a constant bulk Richardson number $Ri_v \approx 0.6$ over a wide range of Ri_τ. With this assumption (and using the definition $u_e := dh/dt$), (4.2) constitutes a simple differential equation for the MLD that can be integrated to yield

$$h = (2Ri_v)^{\frac{1}{4}} u_* \, (t/N_0)^{\frac{1}{2}} = 1.047 \, u_* \, (t/N_0)^{\frac{1}{2}} \quad \text{with } Ri_v = 0.6. \tag{4.5}$$

An equation of this form has also been suggested by THOMPSON [261]. Remarkably, the same result can be obtained by simply considering the self-similarity of this entrainment experiment (cf. KUNDU [143], MELLOR AND STRUB [167]). However, in all cases an equation of the form (4.5) can only be found, if $Ri_v = \text{const.}$ is assumed for all times. Unfortunately, the physical basis of this bulk Richardson number criterion is not easy to justify. As pointed out by KUNDU [142, 143], the requirement $Ri_v = \text{const.}$ is equivalent to $Ri = \text{const.}$ at the bottom of the mixing layer, if self-similarity is taken into account. However, this author also remarked that other criteria like $Ri_f = \text{const.}$ would have led to very similar results. In this section a new, unifying interpretation of the physical processes at the bottom of the mixing layer is suggested solely in terms of the steady state Richardson number, Ri_{st}, defined in (3.45).

Almost all authors who modelled mixing layer deepening with one- or two-equation models of the MELLOR AND YAMADA [169] type (e.g. HASSID AND GALPERIN [106], GALPERIN ET AL. [81] , MARTIN [160], RICHARDSON ET AL. [201]) had to employ a constraint of the form

$$l < c_{\lim} \frac{q}{N} \qquad \text{with} \quad q = \sqrt{2} k^{\frac{1}{2}} \tag{4.6}$$

to obtain a reasonable mixing length at the bottom of the mixing layer. Using the definition of the Ozmidov scale (3.56) and expressing the dissipation in terms of k and l according to $(3.11)_1$, (4.6) leads to a constraint on the ratio of the mixing length, l, to the Ozmidov scale, L_O, according to

$$\frac{l}{L_O} < \left(\frac{c_{\lim}}{\sqrt{2} c_\mu^0} \right)^{\frac{3}{2}} = 1.57 \cdots 1.7 \, , \tag{4.7}$$

if the value $c_{\lim} = 0.53$ (suggested by HASSID AND GALPERIN [106]) and the values for c_μ^0 implied by the ASMs introduced above are used.

Very recently, however, BURCHARD [24] pointed out that the restriction (4.6) is only necessary because the MELLOR AND YAMADA [169] model uses a model coefficient c_{l3} in (3.9) that does not allow for a turbulent state of Full Equilibrium (FE). If this coefficient is adjusted to yield a reasonable steady state Richardson number Ri_{st}, (4.6) is automatically

satisfied at the bottom of the mixing layer. It has been argued already by Burchard and Bolding [28] that Ri_{st} is the most important parameter affecting the predicted MLD. In accordance with their findings, the left panel of Fig. 4.5 confirms, that the MLD[3] is almost exclusively determined by Ri_{st}: Both, the non-equilibrium ASM of Canuto et al [38] (CHCD) and the quasi-equilibrium model of Luyten et al. [156] (LDOR) lead to almost identical MLDs, provided Ri_{st} is the same. The right panel of Fig. 4.5 reveals

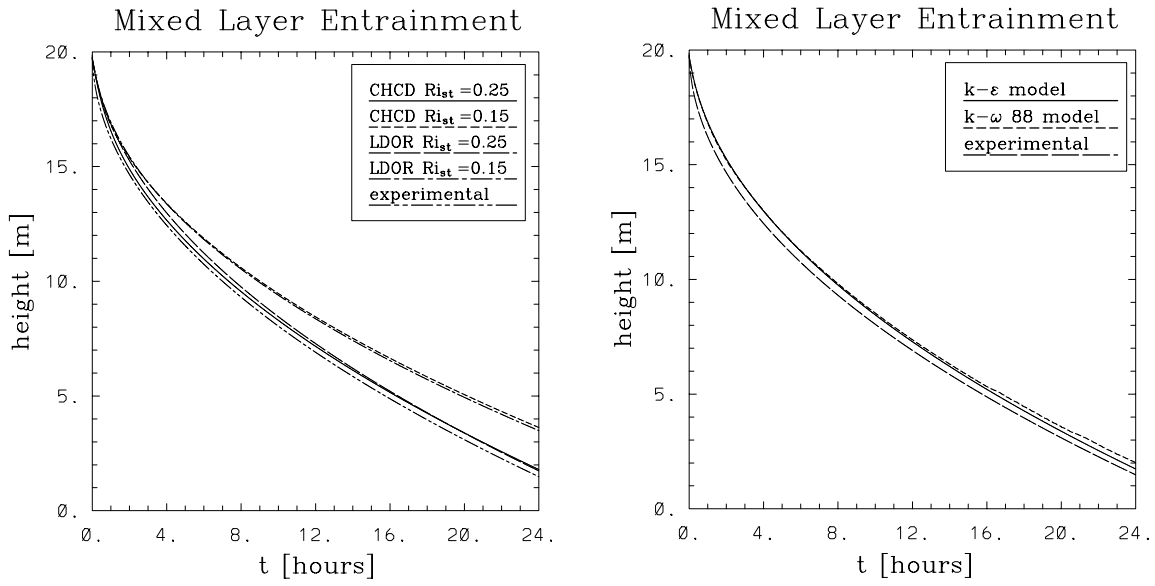

Figure 4.5: Left panel: MLD for shear-driven entrainment as computed by the k-ϵ model with the ASMs of Canuto et al [38] (CHCD) and Luyten et al. [156] (LDOR). The models have been tuned to different values of Ri_{st}. Right panel: Same as left panel, but now for the k-ϵ model and the k-ω model with $Ri_{st} = 0.25$ and the ASM of LDOR. The empirical relation suggested by Price [195] is also included. ($N^2 = 10^{-4}\mathrm{s}^{-2}$, $u_* = 6 \cdot 10^{-3}\mathrm{m/s}$.)

that the findings of Burchard and Bolding [28] can also be generalized to the new buoyancy extended k-ω model: For $Ri_{st} = 0.25$ the MLDs computed by the k-ϵ model and the k-ω model satisfactorily reproduce the data of the KP experiment.

The left panel of Fig. 4.6 demonstrates, that at the bottom of the mixing layer $Ri \approx Ri_{st}$, irrespective of the ASM. This explains, at least partly, why Ri_{st} is the key parameter in mixing layer simulations. With the LDOR model and for $Ri_{st} = 0.25$, the Richardson number levels off faster with increasing distance from the interface. This effect is most likely related to the fact that $Ri_{st} = 0.25$ is close to $Ri_{cr} = 0.28$ (taken from Tab. 3.6),

[3]The MLD is defined in this case as the depth, where the criterion $k > 10^{-5}\ \mathrm{m}^2\mathrm{s}^{-2}$ is first violated. It is almost identical to other criteria that consider, e.g., the depth of the strongest density gradient. The criterion used here emphasizes that the layer is actively "mixing" and can also be used for unstratified entrainment experiments.

at which turbulence is completely suppressed in FE. In contrast, for the CHCD model the critical Richardson number $Ri_{cr} = 0.85$ is much higher and the profile of Ri is not affected. According to the right panel of Fig. 4.6, both ASMs compute comparable

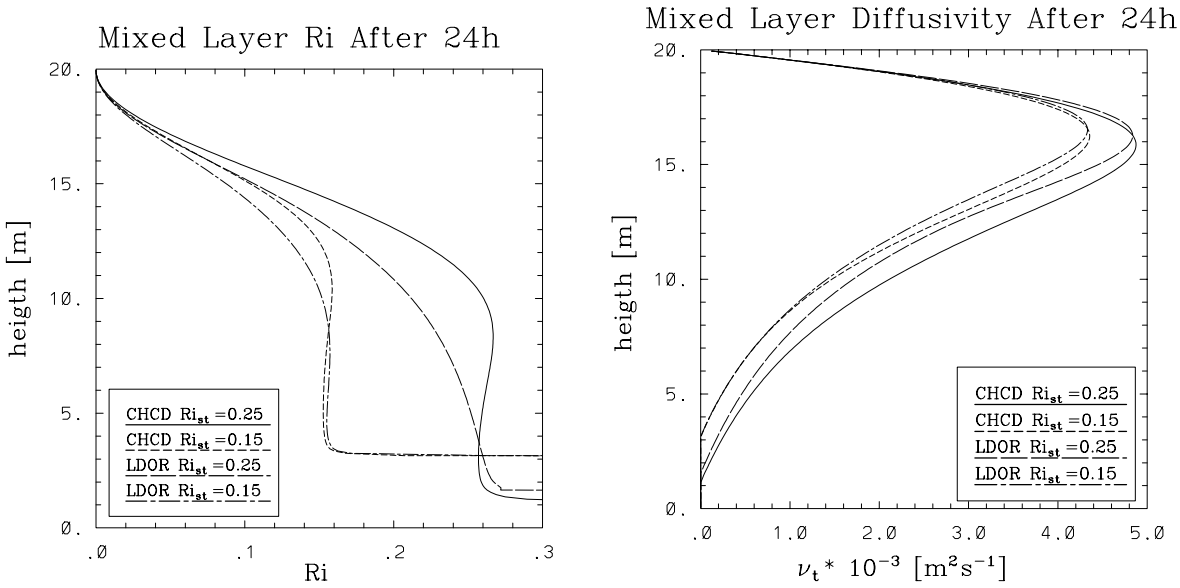

Figure 4.6: Left panel: Ri as a function of height after 24h entrainment as computed by the k-ϵ model. Right panel: Same as left panel, but now for the turbulent diffusivity of momentum, ν_t. Parameters and abbreviations as in Fig. 4.5.

turbulent diffusivities, if the models are tuned to the same Ri_{st}. However, for the reason explained above, for $Ri_{st} = 0.25$, the LDOR model computes a somewhat suppressed turbulent diffusivity at the bottom of the mixing layer compared to the CHCD model.

It is also instructive to look at the budgets of the turbulent kinetic energy, k, as displayed in Fig. 4.7. It is obvious, that for both, the LDOR and the CHCD model, the rate term and the turbulent transport term play only a marginal role (even though the latter is somewhat more pronounced with the LDOR model). From this fact two important conclusions can be drawn:

- Since the only structural difference between the two-equation models used here is the representation of the turbulent transport terms, they will compute very similar results, if used with the same ASM (see Fig. 4.5, left panel).

- The equilibrium $P+G = \epsilon$ is a necessary condition for FE (see Section 3.4.5). Since this condition is satisfied over the whole mixing layer and $Ri = Ri_{st}$ at its bottom, turbulence must be in a state of FE there.

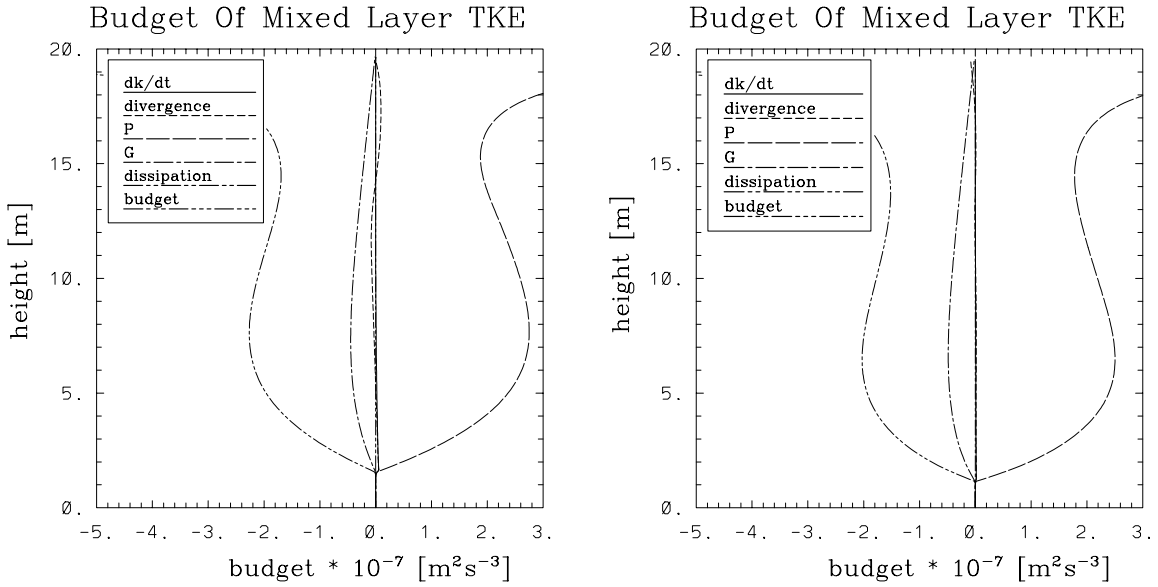

Figure 4.7: Same as Fig. 4.6, but now for the terms contributing to the budget of k in the mixing layer. "Divergence" denotes the divergence of the turbulent transport of k, "budget" the sum of all terms (which has to be zero). Left panel: k-ϵ model with the ASM of LDOR and $Ri_{st} = 0.25$. Right panel: k-ϵ model with the ASM of CHCD and $Ri_{st} = 0.25$.

The last conclusion can be used to resolve the question of KUNDU [143] discussed at the beginning of the section, whether $Ri_v = \text{const.}$, $Ri_f = \text{const.}$ or $Ri = \text{const.}$ is physically most relevant for self-similarity of the problem: *Self-similarity is achieved because turbulence at the bottom of the mixing layer is in a state of Full Equilibrium (FE).* According to (3.45) in FE we have $Ri = \text{const.} \Rightarrow Ri_f = \text{const.}$ As shown by KUNDU [143] the conditions for similarity then also require $Ri_v = \text{const.}$ Only in this case, the conditions $Ri_v = \text{const.}$, $Ri_f = \text{const.}$, and $Ri = \text{const.}$ are equivalent.

To see, how the constant c_{lim} in (4.6) and Ri_{st} are related in FE, consider the relation

$$\frac{l}{q}N = \frac{(c_\mu^0)^3}{\sqrt{2}}\frac{k}{\epsilon}N = \frac{(c_\mu^0)^3}{\sqrt{2}}\sqrt{\alpha_N}\,, \tag{4.8}$$

which can easily be obtained, if $(3.14)_1$ is applied. Now, according to (3.48), in FE the buoyancy parameter α_N is only a function of Ri_{st} (an illustration is given in Fig. 3.3). Hence, lN/q and by means of (4.6) also c_{lim} are only functions of Ri_{st}. Moreover, using relation (3.57), the ratio L_E/L_O is also only a function of Ri_{st} (see Section 3.4.5). Tab. 4.1 summarizes the results. From this table it is seen that for the ASM of LDOR a steady state Richardson number somewhat lower than $Ri_{st} = 0.225$ yields approximately the value of $c_{\text{lim}} = 0.53$ also suggested by HASSID AND GALPERIN [106]. This is very close to $Ri_{st} = 0.25$, which has been shown to agree best with the MLD of the KP experiment.

For both values, the ratio L_E/L_O is somewhat larger than one.

Ri_{st}	0.15	0.175	0.20	0.225	0.25
L_E/L_O	0.78	0.90	1.04	1.21	1.46
$c_{\lim}$	0.28	0.34	0.43	0.55	0.78

Table 4.1: Relation between the steady state Richardson number, Ri_{st}, the constant $c_{\lim}$ of (4.6), and the ratio L_E/L_O for the ASM of LDOR.

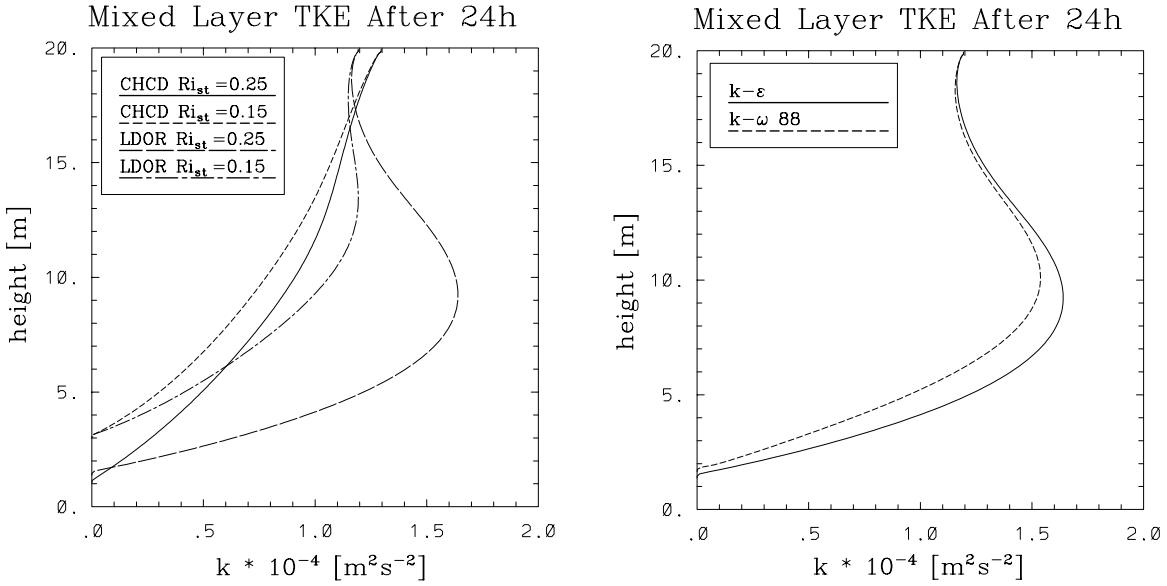

Figure 4.8: Left panel: Same as Fig. 4.6, but now for the turbulent kinetic energy, k. Right panel: Same as left panel, but now for the k-ϵ model and the k-ω model with $Ri_{st} = 0.25$ and the ASM of LDOR.

Note, that the conclusions drawn above do not imply that all ASMs compute the same turbulent structure in mixing layers if adjusted to the same value of Ri_{st}: Fig. 4.8 clearly shows that the profiles of k computed from different ASMs can be very different. The LDOR model predicts a maximum of k in the lower part of mixing layer that is hard to interprete physically. Unfortunately, KP did not measure any turbulent quantities and there seem to be no other experiments which could be used to verify or contradict such a profile. The CHCD model, in contrast, computes a smooth decrease of k with increasing depth. The small differences in the values of k at the upper boundary result from the different values of the Bradshaw constant, c_B, predicted by the LDOR and the CHCD model in the logarithmic boundary layer (see Appendix A.1).

4.2 Modelling a Seiche-Induced Oscillating Boundary Layer in a Lake

Mixing in the interior of oceans and lakes is known to be weak and intermittent. The current state of knowledge is, that turbulence occurs in an extensive number of turbulent patches with low dissipation rates, small vertical displacements, and consistently negligible mass flux, $\langle \rho' w' \rangle$ (Imberger [117]). This author also estimates an average value for the turbulent diffusivity of all turbulent patches of around $\nu_t \approx 10^{-7}$ m^2/s. A value of this order can also be deduced from the dissipation rate measurements of Wüest et al. [299] in a small Swiss lake. This value is at least an order of magnitude smaller than the net value $\nu_t^{\text{net}} \approx 10^{-6}$–$10^{-5}$ m^2/s, found by tracer experiments of numerous authors using different methods (Imboden and Emerson [121], Robarts and Wart [203], Wüest et al. [299], Goudsmit et al. [92]).

The same discrepancy between tracer experiments and microstructure measurements has been puzzling oceanographers for a long time. Finally, more than two decades ago, Armi [6, 7] pointed out that bottom currents in the deep ocean were in many cases energetic enough to produce a well mixed turbulent bottom boundary layer. He set forth that a combination of mixing at the boundaries of the ocean and lateral advection might be disguised in form of the high measured net (or better apparent) vertical diffusivity. It is very likely that a comparable mechanism is of importance also in lakes. Indeed, this assumption has obtained considerable support from an interesting tracer experiment in a small lake, recently published by Goudsmit et al. [92]: A tracer cloud released far from the boundaries of this lake at first showed a vertical diffusivity in perfect agreement with parallel microstructure measurements. However, a soon as the tracer cloud touched the bottom boundary layer, the basin-wide diffusivity of the tracer increased by an order of magnitude. This carefully conducted experiment was an explicit proof of the importance of boundary mixing, but it could not clarify, what kind of mixing mechanisms occurred at the boundary.

From the classical works of C. H. Mortimer it is known, that in lakes the bottom currents are most often caused by different types of (generally Coriolis force affected) internal oscillations or seiches. Periods usually observed range between several hours and a few days and the bottom speed seldom exceeds 10 cm/s (Mortimer [177]; Hutter [115], Bäuerle [9], Lemmin and Imboden [149], Münnich et al. [181]). Imberger [117] demonstrated that, even though the seiche-induced bottom currents are much weaker compared to the ocean, the high value of the net diffusivity could be directly related to

the action of internal seiches.

There are several other bottom mixing mechanisms that can be important in stratified fluids (see THORPE [268], GARRETT [82, 83], IMBERGER AND IVEY [119]). The mixing caused by the breaking of internal waves at sloping boundaries (see DE SILVA ET AL. [62]) is most notable in this context. Near the thermocline, the intrusion of mixed water from the boundaries into the lake interior is a phenomenon also sometimes observed (see GLOOR ET AL. [90]). However, all these effects cannot be parameterized by the one-dimensional two-equation models used here, and hence the discussion is confined to the dynamics of boundary layers near the deepest part of a lake, where the effect of sloping boundaries is small.

The first investigations of the turbulence structure in the bottom boundary layer of a continental shelf were published by CALDWELL AND CHRISS [33]. These authors found strong evidence for the existence of a viscous sub-layer of a couple of millimetres thickness below a logarithmic boundary layer. However, a closer investigation of the same site, published a couple of years later by the same authors (CHRISS AND CALDWELL [47, 48]), indicated that observations in oceanic boundary layers were somewhat different from the standard laboratory flow experiments over hydrodynamically smooth surfaces: They found that the form drag and the non-local influence of larger roughness elements had to be taken into account. Most interesting in the context of this work was their demonstration that multiple roughness scales can generate velocity profiles with multiple logarithmic regions above each other. It will be shown below that some of their findings can be explained by only considering the dynamical behaviour of currents and turbulence in non-stationary bottom boundary layers with a single roughness length.

Later measurements of velocity profiles on the deep sea floor by GUST AND WEATHERLY [95] and the dissipation measurements in the boundary layer performed by DEWEY AND CRAWFORD [63] corroborated the fact, that it is unreliable to obtain estimates of the bottom stress by simply fitting a logarithmic profile to velocity measurements. These findings will be confirmed by the current work, however with completely different arguments considering the dynamical behaviour of the boundary layer. Even though the importance of the pressure-gradient and rate terms in the equations describing non-stationary boundary layers are well documented (see YAGLOM [300], SLEATH [227]) only few oceanographers have taken this fact into account, a noticeable exception being SOULSBY AND DYER [230].

A number of applications of differential turbulence closures to oceanic boundary layers have been reported. VAGER AND KAGAN [284] conducted a theoretical investigation of

unstratified rotating tidal flows with a one-equation model. Weatherly and Martin [289] applied the zero-equation (level 2) model of Mellor and Yamada [168] to a steady-state turbulent boundary layer and investigated the effects of stratification and bottom slope. Zero-equation models do not predict a phase-lag between the velocity shear and the turbulent quantities, known to be important in tidally accelerated flows (see Baumert and Radach [12]). Besides this, they are known to compute unstable and unphysical diffusivity profiles as shown by Burchard and Baumert [27]. Applications of one- and two-dimensional two-equation models with simple ASMs to laboratory and stratified real-world tidal flows have been reported by Smith and Takhar [228, 229]. Thomas and Takhar [260] modelled the turbulent boundary layer induced by long non-linear waves with a k-ϵ model. A complete second-order closure was used by Richards [200] for their theoretical investigation of the stratified, rotating and oscillating boundary layer. No comparison to measurements was included, though. One of the few comparisons of measured and modelled tidal currents was conducted by Baumert and Radach [12]. With their standard k-ϵ model, they were able to explain the essential physics of tidal flows, most remarkably the characteristic tidal time-lag between the current and the turbulent kinetic energy at the flow reversal. Two-equation models have also been very successfully compared to near bottom dissipation rate measurements in the Irish Sea over several tidal cycles by Burchard et al. [31]. To my knowledge, no investigations of this kind have ever been reported for the oscillating bottom boundary layer in a lake. Apparently, there exist also no continuous time series of microstructure measurements of the turbulent dissipation for a complete seiche period. This work presents results that fill the gap.

Oscillating boundary layers of industrial relevance have also been modelled. Shima [224] could excellently reproduce several laboratory and DNS results with his second-order low Reynolds number model. Jakirlić [127] compared several other low Reynolds number second-order closure schemes and came to a similar conclusion.

It can be summarized that differential closure schemes are a powerful tool for the description of oscillating boundary layers. Even though some aspects of such flows are known to be only reproducible with expensive low Reynolds number second-order closure models, the essential physics of tidal flows are captured by simple two-equation models. It will be shown in the following that this is also true for the seiche-induced boundary layers in lakes.

4.2.1 The Measurements

Measurements of turbulent quantities in the bottom boundary layer of lakes are difficult to perform. The rate of dissipation is several orders of magnitude smaller compared to tidal flows in the ocean and the vertical extent of the boundary layers seldom exceeds a few meters. Because of instrumental restrictions, no such measurements in lakes have been realized until recently. The data available for this work were gathered by the EAWAG, Switzerland. Apparently, they include the first reported measured dissipation rate profiles in a seiche-induced bottom boundary layer of a lake, that have a temporal resolution allowing for the construction of a dissipation rate time series over a whole seiche cycle.

The measurements have been conducted in Lake Alpnach, a small lake in Switzerland, on 16./17. Mai 2000. Lake Alpnach is a relatively shallow (max. depth is 34 m), almost completely isolated side-basin of Lake Lucerne (see Fig. 4.9). In summer, the mountain

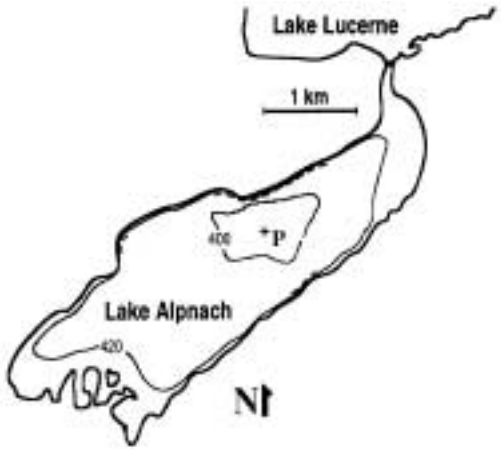

Figure 4.9: Geometry and bathymetry of Lake Alpnach (Switzerland). "P" denotes the approximate position of the measuring site, where the depth is close to the maximum depth of 34 m.

and valley breezes along the nearby mountains result in a predominantly dial wind that blows parallel to the major axis of the lake. Under such conditions, internal seiching of the first and, remarkably, second vertical (and first horizontal in both cases) mode and corresponding deep-water currents are excited in this lake. Observed periods are about 8 hours for the first vertical and about 24 hours for the second vertical mode (for details see Münnich et al. [181], Gloor et al. [91, 89]).

The data set comprises high-resolution ADP velocity measurements at different heights above the sediment, temperature profiles, and a great number of temperature microstructure profiles for one complete seiche period.

Boundary layer velocities, averaged over moving intervals of one hour, are displayed in Fig. 4.10. This figure illustrates that during the period of the measurements, time series of the velocity can be approximated rudimentarily by a simple cosine curve. The seiche period is somewhat less than 24 hours, indicating the excitation of the second vertical mode (the corresponding eigenvalue problem for continuous stratification has been solved numerically by MÜNNICH ET AL. [181]). However, as modulations of the simple cosine

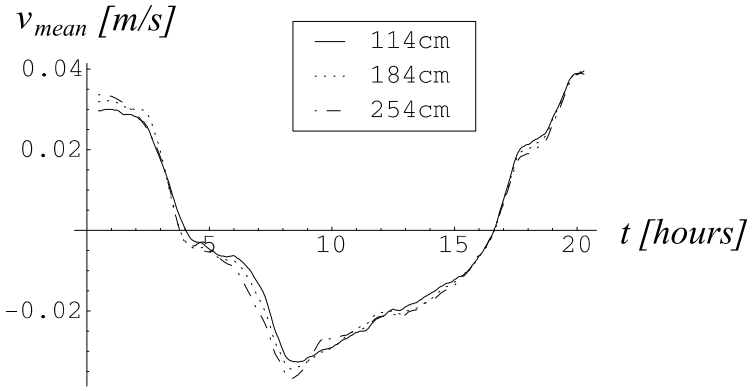

Figure 4.10: Measured averaged velocities in the main direction of the basin for one seiche period at different heights above the sediment.

curve, there appear episodes of very high time rates (e.g. between 1 and 4 hours) and episodes with almost constant velocities (e.g. between 4 and 6 hours and between 17.5 and 19 hours). It is not clear, if these distinctive features are due to the non-linearity of the long internal wave, due to laminarization effects as described in SHIMA [224] or due to the superposition of different internal wave modes and other influences. There is no conclusive indication for a phase-shift in the velocity records at different heights as suggested, e.g., by SOULSBY AND DYER [230], however a small phase-shift can be deduced from single velocity profiles (see below).

A typical temperature profile during the measuring period is given in Fig. 4.11. Only the lower part of the water column is resolved. It can be seen that near the bottom there is a well-mixed boundary layer of approximately 3m thickness. Earlier publications (GLOOR ET AL. [91, 90])) reported a thickness of 2-7 m with an average of 4-5 m. It is also known that the thickness can vary considerably within a few hours solely because of the reversible redistribution of water masses by the internal seiching motion. The observed time-scale of decay of the well-mixed layer at the deepest part of the lake is 10-20 days, after the seiching motion ceases (see GLOOR ET AL. [91, 90]).

An investigation of the high resolution temperature profiles (not shown) revealed that in the turbulent boundary layer the buoyancy frequency, N, is at least one order of magni-